PIEZOELECTRIC ENERGY HARVESTING FROM ROADWAY

By

ABBAS FADHIL JASIM

A dissertation submitted to the

School of Graduate Studies

Rutgers, The State University of New Jersey

In partial fulfillment of the requirements

For the degree of

Doctor of Philosophy

Graduate Program in Civil and Environmental Engineering

Written under the direction of

Dr. Hao Wang

And approved by

New Brunswick, New Jersey

May 2018

ABSTRACT OF THE DISSERTATION

Piezoelectric Energy Harvesting From Roadway

by ABBAS FADHIL JASIM

Dissertation Director:

Dr. Hao Wang

Energy harvesting technologies have attracted much attention as an alternative power source of roadway accessories in different scales. Piezoelectric materials, which have been widely used in sensor technologies due to their cost-effectiveness, are capable of producing electrical energy from mechanical energy. Therefore, piezoelectric transducers can be designed to harvest the wasted mechanical energy generated under wheel loading that can be stored in an electronic capacitor or integrated with sensors for in-situ road condition monitoring.

This dissertation aims to develop a novel design of a piezoelectric transducer with optimized geometry for energy harvesting under vehicular loading in the roadway. The novel Bridge transducer with layered poling is designed to increase the piezoelectric coefficient and the relative dielectric permittivity, which produces much higher energy than traditional transducers. Finite element analysis (FEA) was conducted to predict the generated energy output and the resulted mechanical stress in the lead zirconate titanate (PZT) transducer. The results of the optimization analysis indicate that the optimized geometry parameters can generate the maximum energy output within the stress failure

criteria. Later, an energy harvester module that contains multiple stacked transducers, 64 novel transducers, was fabricated and tested under single pulse and cyclic loading events. The main objectives of this part were to evaluate the energy output and fatigue behavior of the piezoelectric energy harvester using laboratory testing and numerical simulation. The analysis results showed that two different material failure models need to be considered in relation to mechanical failure of the Bridge transducer, namely tensile and shear failure. This emphasizes that the optimum design of energy module should consider the balance of energy output and fatigue life that are affected by the fabrication of a single Bridge transducer and the packaging design of the energy module.

To take into account the nature of the energy harvester-pavement interaction and to achieve better computation efficiency, the effect of this interaction on pavement responses was studied using a decoupled approach. First, a 3D pavement model was built, and then the pavement responses under the tire contact stresses were calculated. The effects of energy harvester-pavement interaction at different locations, horizontally and vertically, were also analyzed. The results show that the maximum power output of the energy harvester module is around 122mW at a vehicle speed of 65mph and 3 inches embedded depth. Furthermore, embedding the energy harvesting module below 3 inches from the pavement surface is the best location to maximize both power output and service life.

Finally, to reveal the potentials of some important technologies for harvesting energy from a pavement network, a case study is discussed, which uses the New Jersey roadway network as the example for analysis. The potential of electrical energy generation for thermoelectric and piezoelectric (cymbal and novel bridge design)

technologies were considered. Based on available energy harvesting technologies, a thermoelectric-based pipe system covering the entire New Jersey roadway network may potentially collect 20.11 GWh electrical energy per day, while a piezoelectric transducer system may collect around 3.74 and 10.01MWh of electrical energy per day for cymbal and novel bridge transducer designs, respectively.

DEDICATION

To my wife, Israa Al-Saadi, for all her endless support and encouragement along the way.

Abbas Fadhil Jasim

ACKNOWLEDGMENT

Al hamdu lillaahi rabbil ‘alameen, who gave me the knowledge, wisdom and courage to complete this research work. May Allah make this work useful for me and for others in the future (Aamin).

After this, I would like to say a special thanks to my supervisor, Dr. Hao Wang who provided me with knowledge and guidance, motivated me in crucial periods, and encouraged me at each and every moment during this research work. His continuous involvement and invaluable suggestions have been remarkable. Dr. Wang has been a great academic advisor during the pursuit of my Ph.D. He has always been ready to discuss with me and share his spectacular view of the question. Over the last five years, I have learned a lot, and I have enjoyed working with him.

I am also grateful to the members of my graduate committee: Associate Professor Hao Wang, Professor Ali Maher, Professor Yook-Kong Yong, and Professor Ahmad Safari for their encouragement and valuable suggestions on my research.

My special thanks are extended to the Center for Advanced Infrastructure and Transportation (CAIT) at Rutgers University and the U.S DOT University Transportation Center (UTC) Program for their support of research.

I am also grateful for Dr. Greg Yesner in the Material Engineering Department, who fabricated the energy harvesting modules and established the electric circuits that made my work possible.

I want to thank my colleagues and friends at the Department of Civil and Environmental Engineering for their friendly and continuous support during the completion of this work. They will always be remembered for the wonderful times we spent together during my stay at Rutgers University, New Jersey.

My deep appreciation goes to my wife Israa, who has always been supportive and enduring of all the ups and downs of my life in graduate school. Also, I am very grateful to my family in Iraq for all their love, support, and encouragement through all the years of my life.

Last but not least, a special thanks to my sponsor, The Higher Committee For Education Development in Iraq (HCED), who brought me to the US to attend graduate school and supported me at Rutgers University. I would not have had the opportunity to receive my education in the US as well as the career opportunities that lie ahead without the sacrifice of my government.

Abbas Fadhil Jasim

TABLE OF CONTENTS

LIST OF TABLES

LIST OF FIGURES

LIST OF ABBREVIATIONS

A	Surface area of PZT ceramic element (m^2)
C	Capacitance of the material (Farads)
D	Electric displacement tensor (charge/area)
DC	Direct Current
d_{ij}	Piezoelectric charge constant (pC/N)
E	Electric field (V/m)
FEA	Finite Element Analysis
g_{3i}	Piezoelectric voltage constant of PZT (10^{-3} V m/N)
k	Electromechanical coupling factor
L_c	Total width and length of Piezoceramic (mm)
LCOE	The levelized cost of electricity
LED	Light-Emitting Diode
L_i	Inner length of the end cap (mm)
L_o	Length of the cavity base (mm)
n	Number of segments between electrodes
N	The lifetime for constant amplitude σ cycling
P_3	Piezoelectric polarization at the 3rd axial direction
PVDF	Polyvinylidene Fluoride
PZT	Pb (Lead) Zr (Zirconate) Ti (Titanate)
RAINBOW	Reduced and Internally Biased Oxide Wafer
S	Strain tensor
S^E_{ij}	Elastic Compliance tensor at the constant E condition (10^{-12} m^2/N)
T, T_i	Stress tensor (MPa)
t_c	Thickness of metal cap (mm)
TEG	Thermoelectric Generator
THUNDER	Thin-layer composite unimorph ferroelectric driver and sensor
t_i	Height of the cavity (mm)
t_p	Thickness of PZT strip (mm)

U_E	Stored electric energy (Joule)
V	Electric potential (voltage)
V_0	Electric potential at open circuit (voltage)
V_3	Electric potential at the 3rd axial direction (voltage)
W_1	Work done by the external force in short circuit condition
W_2	Recovered work during unload period in open circuit condition
ε_o	The permittivity of free space (8.85 x 10^{-12} Farad / m)
σ	Stress amplitude (MPa)
λ_{max}	Energy transmission coefficient
ε_{33}^{T}	Dielectric constant in the 3rd axial direction
$C_{ij}^{E} = (S_{ij}^{E})^{-1}$	Stiffness matrix
ε_{m}^{s}	Relative dielectric constant at constant strain
ε^{T}	Permittivity of ceramic material at the constant stress condition (Farad / m)

CHAPTER 1 INTRODUCTION

1.1 BACKGROUND

Energy harvesting is a promising technique that can help solve the global energy problem without depleting natural resources. New knowledge and innovations in the areas of material science, mechanics, and sensor systems offer revolutionary solutions for preserving transportation infrastructure condition and developing green energy technologies. Energy harvesting technologies capture unused and wasted energy and convert it into a more usable form. Solar, wind, hydro, thermo, and kinetic energy are the common energy sources that can be used for energy harvesting. In recent years, researchers have begun to harvest electrical energy from the ambient environment using different techniques, such as piezoelectric, thermoelectric, electromagnetic, and photovoltaic energy harvesting (Davidson and Mo 2014).

Roadway pavement is designed to carry millions of vehicles passes during its service life, wherein it is subject to considerable stress, strain, deformation and vibration from moving vehicles. These energies are dissipated in the pavement as wasted energy, leading to increased risks of pavement damage. Piezoelectric materials, which have been widely used in sensor technologies due to their cost-effectiveness, are capable of producing electrical energy from mechanical energy. Therefore, piezoelectric transducers can be designed to harvest the wasted mechanical energy generated under wheel loading that can be stored in an electronic capacitor or integrated with sensors for in-situ road condition monitoring. The collected energy can be also used for traffic signals, electrical signs, lighting, and roadside safety features.

The piezoelectric transducer can be further developed into a live sensor in the pavement structure that tracks axle loads for traffic monitoring and measures pavement responses for condition monitoring. In the future, there is a potential to integrate traffic monitoring, condition assessment, and energy harvesting into one sensor bed. It is believed that this will create a new paradigm for building the next generation of smart and sustainable pavement infrastructure with longevity and multi-functionality.

1.2 PROBLEM STATEMENT

Roadways are one of the major civil infrastructures that play an important role in connecting communities, and moving people. Traditionally, roadway is regarded as the structure platform to carry traffic loading. Innovative research is needed to explore the potential for harvesting energy from live-loading on roadway using smart materials technology. In the recent years, a number of studies have attempted to take advantage of the available mechanical energy potential in the pavement and convert it into a usable electrical energy using piezoelectric materials. Harvesting energy from pavements by piezoelectricity is a new research field with opportunities and challenges.

Previous researchers have investigated different energy harvester designs made of piezoelectric material for stress-based or vibration-based energy harvesting from roadway or bridge. It is concluded that the generated energy output is usually small for a single piezoelectric transducer. In order to generate the energy that is applicable for energy storage or direct use, multiple sensor arrays under repeated traffic loading are needed. However, the effects of field condition and traffic variables on the generated energy out of piezoelectric materials are not fully understood due to the lack of comprehensive investigation. Furthermore, the mechanical properties of piezoelectric transducer materials, such as ceramic and epoxy, are limiting the functional life of transducer due to applied mechanical stresses. Therefore, it is important to expand the current concept of piezoelectric energy harvesting system and develop an energy harvester module that can produce the greater energy in the life-cycle of piezoelectric transducer.

On the other hand, the energy harvester module is embedded in the pavement, which may cause stress concentration due to its rigid module. Previous studies usually assumed the generated stress on the piezoelectric transducer and also neglected the impact of energy harvester on pavement deterioration for simplicity. Therefore, investigation is needed to take in to account the integrity between the energy harvester and pavement material considering the interaction between pavement structure, traffic loading, and transducer design.

1.3 RESEARCH OBJECTIVE AND SCOPE

New knowledge and innovation in the fields of material science, mechanics, and sensor systems could offer revolutionary solutions for preserving transportation infrastructure and developing green energy technologies. The main objective of this research is to develop new piezoelectric energy harvester module using finite element analysis that can produce large potential energy during pavement service life and study the optimum placement of energy harvester in the pavement. To achieve this objective, the following research tasks are conducted:

1. Develop a novel Bridge transducer design of piezoelectric transducer with the optimized geometry for energy harvesting in the roadway under vehicular loading. The novel design includes layered poling to increase the piezoelectric coefficient and the relative dielectric permittivity.
2. Evaluate the performance of energy harvester module that contains multiple stacked transducers with respect to the amount of sensor arrays and the material selection of module box using the combination of laboratory investigation and finite element simulation.
3. Analyze the effect of energy harvester module on pavement responses using finite element modeling. The model incorporates tire loading conditions and appropriate material characterizations for each pavement layer.
4. Analyze the energy conversion efficiency, fatigue life, and integrity with pavement material of energy harvester module under vehicular loading. The results will provide a basis for optimizing the installation of energy harvester in the pavement to maximize the amount of total energy harvested in a cost-effective way.
5. Check the feasibility of the developed energy harvesting module and compare the results with some available energy harvesting technologies from roadways.

The research outcome will lead to the development of smart pavements with multifunction and contribute to the generation of renewable electrical energy from waste energy. This could benefit the transportation community at large by providing a green energy solution.

1.4 DISSERTATION OUTLINE

This dissertation is divided into seven chapters. The first chapter introduces the problem statement, objective, and methodology of the dissertation. The second chapter summarizes previous research on three main topics; piezoelectric materials, pavement responses and modeling, and fatigue failure. Also, chapter two provides an extensive literature review, which will describe the previous studies conducted on existing energy harvesting from the transportation infrastructure.

The third chapter describes the analysis and optimization process of a novel piezoelectric transducer for energy harvesting from roadway and some comparison with some traditional transducers.

The fourth chapter describes the developed 3-D FE energy harvester module, optimized new shape based on available materials, and evaluation of the final module based on appropriate material characterizations. In addition, the effect of casing material of the energy harvesting module was investigated in this study.

The fifth chapter presents an analysis of thin asphalt pavement responses utilizing nonlinear anisotropic modulus of the base layer with/without the energy harvester module. This chapter also analyzes the fatigue life and placing strategy of the whole energy harvester module in pavement.

The sixth chapter presents a feasibility analysis on the current energy harvesting module compare to all other technologies using Geographic information technology (GIS). Using the information collected from the literature, a case study is presented based on the New Jersey roadway network, to mathematically assess and compare the potentials of some significant energy-harvesting technologies for use in pavements.

Finally, Chapter 7 summarizes the key findings and conclusions of the dissertation and provides recommendations for future research to explore the potential of energy harvesting technologies in roadway.

CHAPTER 2 LITERATURE REVIEW

The objective of this chapter is to review energy harvesting techniques that are used for pavements and highways and identify limitations and advantages of different techniques. The review includes four different sections: energy harvesting, piezoelectric material, pavement material and loading, and fatigue failure of sensor. The first section provides general information regarding the use of energy harvesting technology. The second part of the literature review summarizes previous applications of the piezoelectric transducer for energy harvesting in pavements, available methods of energy harvesting, piezoelectric transducer technology, sensor basics and performance, including transducer designs, and critical factors affecting energy harvesting efficiency. The third part describes mechanistic analysis of pavement responses under tire loading. The last part introduces fatigue failure concept, factors affecting on fatigue, fatigue theories will be discussed in the fourth part of this chapter.

2.1 ENERGY HARVESTING

2.1.1 Introduction to Energy Harvesting

The discovery of green energy resources, renewable and sustainable is the most critical challenge in this world with regard to the sustainable development of human civilization (Wang 2008). The petroleum, coal, hydraulic, natural gas, and nuclear energy are the most common energy resources that used for the power these days. Recently, many researches are being started for the discovery of alternative energy resources, including solar, geothermal, biomass, nuclear, wind, and hydrogen energy (Wang 2008; Truitt and Mahmoodi 2012).

The numbers of trucks and vehicles that operate on roads have an adverse impact on our infrastructure systems and environment. Examples of their adverse impact on the environment are evidenced in air pollution incidences and the global warming phenomenon. This high traffic caused high dissipation of energy wasted on pavement due to deformation. Many agencies have drawn attention to the importance of reducing greenhouse gas emissions on civil and road infrastructures. Hendrowati *et al.* (2012) mentioned that about 10%–16% of fuel energy is used to drive the cars, to allow them resist road friction and air drag. Most researchers in the energy field are seeking to develop new sources of energy for future use. Energy harvesting is one of the most important techniques used to capture available global energy without reducing natural resources (Andriopoulou 2012).

Energy harvesting technologies can be defined as applications that capture and utilize wasted energy to convert it into a usable form. Williams and Yates (1996) defined energy harvesting as the process of obtaining the energy from surrounding systems and converting it into usable electricity. Energy harvesting, energy scavenging, power harvesting and electricity scavenging are the four terms that are commonly used to describe the process (Lu *et al.* 2014).

In recent years, researchers have begun to harvest electricity from the environment using different techniques, such as piezoelectric, thermoelectric, electromagnetic, and photovoltaic energy harvesting. Many researchers focused on the energy harvesting technology as a new source of clean energy and as a power supply of electronics in an enclosed environment. They proposed different energy harvesters to be used for converting ambient energy into serviceable electrical energy (Kim *et al.* 2011; Dutoit *et al.* 2005).

Voigt *et al.* (2003) made a comparison of the output power of four energy harvesting technologies: thermoelectric, electromagnetic, piezoelectric, and photovoltaic technology. The main conclusion of Voigt et al. study is that the peak productivity of photovoltaic technology is much greater than others. However, its energy productivity can be maximized only under direct sunlight during a certain period of a day. The productivity is limited under low illumination conditions, such as during a cloudy day or in a tunnel. Other than photovoltaic technology, under certain conditions, piezoelectric energy harvesting is the most productive one

2.1.2 Energy Harvesting Technologies in Transportation Infrastructure

The most common sources of energy harvesting are:

1. Mechanical energy – vibration and mechanical stress and strain
2. Thermal energy – waste energy from furnaces, heaters, and friction
3. Light energy – natural and artificial light
4. Electromagnetic energy –inductors, coils, and transformers
5. Other sources of Natural energy such as wind, water flow, ocean currents, and the sun

Among the energy converting technologies, the four energy harvesting technologies that draw most attention include photovoltaic (PV), thermoelectric (TE), electromagnetic (EM), and piezoelectric (PE). These four technologies will be discussed in this section. Dutoit *et al.* (2005) provided a comparison of the energy productivity of these four technologies in terms of power density. In this study, the PV technology showed much greater energy potential than the others, as shown in Figure 2.1.

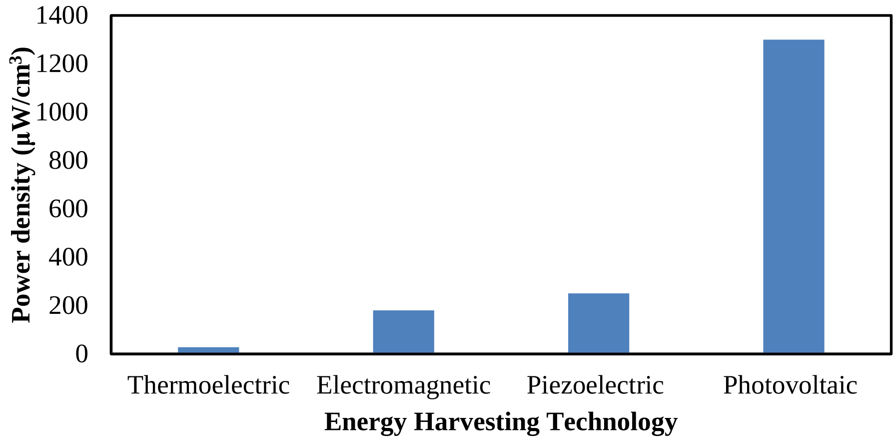

Figure 2.1 Comparison of the output power of four energy-harvesting technologies (after Dutoit et al. 2005)

Many efforts have recently been made to evaluate the opportunity to use roads and highways to generate energy. Several approaches have been investigated by which to harvest solar energy from asphalt pavements. In addition to the produced heat inside the pavement layers, Kang-Won and Correia (2010) studied the capturing of thermal energy from the temperature gradient through the pavement. They also investigated the feasibility of using solar cells, or photovoltaic technologies, as systems to harvest solar energy by embedding such cells into the pavement infrastructure. One challenge in the solar energy system is that thin-film solar cells are difficult to use on pavement surfaces because high mechanical load cycles due to traffic loading and environmental conditioning could cause early corrosion and wear (Kang-Won and Correia 2010). For this reason, the researchers are developing new thin-film solar cells that can meet the requirements for use on road surfaces (Andriopoulou 2012).

In addition to using PV technology to capture energy from pavement layers, there are other applications such as noise barriers. The application of photovoltaic to noise barriers (PVNB) is increasing across miles of motorways and railway tracks in the world (Nordmann and Clavadetscher 2004). This technology is one of the most efficient applications of PV technology and provides noise protection to surrounding areas. Nordmann *et al.* (2000) studied the potential of PVNB infrastructure technologies for six European countries. The authors observed that these technologies generated 800 MWh of electricity with an expansion potential to 680 GWh of electricity per year. Such technology could be a primary contributor to the growing green energy along railways and highways.

The main disadvantage of photovoltaic technology is that it depends on weather conditions during the daytime. PV technology energy productivity can be maximized only under direct sunlight during a particular period of the day. Productivity is also limited under low lighting conditions such as cloudy days or inside tunnels.

A thermoelectric generator (TEG) is the main part of a TE technology system, which harvests energy from the thermal change of the pavement infrastructure (Wu and Yu 2012). TEGs exploit the temperature differences between pavement layers, which can generate an electricity based on thermoelectrical principles. The major disadvantage of this technology is low efficiency, but using novel materials for TEG manufacturer could improve the efficiency. Wu and Yu (2012) studied the application of TE units on the surface of pavement and tried to optimize the modules' design. A TE module creates a connection between the lower part of the module and the subgrade soil, using highly thermally conductive materials, which guarantees a considerable temperature difference between the upper and bottom surfaces of the module. Highly thermally conductive materials are used to expedite heat transfer and thus to increase electricity production.

In electromagnetic energy harvesting, a magnetic field converts mechanical energy to electrical energy. A coil attached to an oscillating mass traverses a magnetic field that is established by a stationary magnet. The coil travels through a varying amount of magnetic flux, inducing a voltage according to Faraday's law (Zhang *et al.* 2014). The other advantageous ways involve moving the magnetic structure (which is inherently massive) and keeping the coil fixed (Beeby *et al*. 2006), therefore increasing the power output and making the electrical connections more reliable. Significant research has been done on both Microelectromechanical systems (MEMS) scale (El-Hami *et al.* 2001; Wang *et al.* 2007; Sardini and Serpelloni 2011) and on a macro scale (Zuo *et al.* 2010; Cassidy *et al.* 2011) to improve the performance of electromagnetic energy harvesting. Its applications to civil infrastructure such as bridge structures can also be found in the literature (Sazonov *et al.* 2009; Chen and Liao 2010).

However, according to Priya (2007) theoretical calculations, the energy density of piezoelectric energy harvesting devices is 3–5 times higher than that of electrostatic and electromagnetic devices (Kim *et al.* 2011). Based on Figure 2.2, piezoelectric energy harvesting is the most productive type. Piezoelectric transduction appears to be most encouraging technology, given that it has the widest power density versus voltage envelope, as shown in Figure 2.2 (Cook-Chennault *et al.* 2008; Papagiannakis *et al.* 2016).

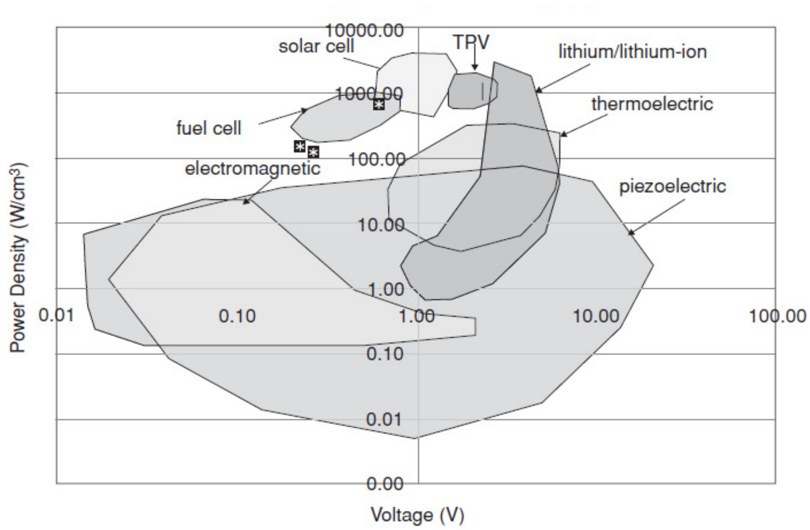

Figure 2.2 Various energy harvesting technologies using power density versus voltage relationship (after Cook *et al*. 2008**)**

The piezoelectric energy harvester is found in different forms, but the essential form is that of a cantilever beam structure with piezoelectric layers attached to the beam with a mass at its unattached end, since the mass at the end can provide higher strains for a given input force. The cantilever beam can produce voltage from the piezoelectric layer that varies with time and strain, effectively producing different AC signals. Piezoelectric energy harvesting produces relatively higher voltage and power density levels than the electromagnetic and electrostatic systems. The particular application will determine which type of piezoelectric material is used; these materials often have different properties. Kim *et al.* (2009) mentioned that piezoceramic lead zirconate titanate, known as PZT, is widely used in many designs of energy harvesters.

Some energy harvesters utilizing piezoelectric technology have proposed various mechanisms of energy conversion. Roundy *et al.* (2003) proposed a piezoelectric energy harvester to harvest energy from vibration. After that, Jeon *et al.* (2005) designed an energy harvester with thin piezoceramic films mounted on a cantilever beam. They found that a 170 μm × 260 μm beam-shaped energy harvester could generate about 1 μW of average power. The cantilever beam transfers the vertical force to the mounted films, which are deformed transversely, whereby electric potential is created.

2.2 PIEZOELECTRIC TRANSDUCERS FOR ENERGY HARVESTING

2.2.1 Theory on Piezoelectric Effect

Piezoelectric materials generate an electric charge when subjected to mechanical stress, and change dimensions when an electric field is applied across the material. These are known respectively as the direct and the inverse piezoelectric effect (Cobbold 2006). The effect is observed in a variety of materials such as quartz, dry bone, polyvinylidene fluoride (PVDF) and lead zirconate titanate (PZT). PZT is one of the most commonly used piezoelectric ceramics today and it is also the piezoelectric material used in the simulations in this dissertation.

The piezoelectric effect only occurs in anisotropic materials (Auld 1981), which implies that a piezoelectric crystalline material must have a noncentrosymmetric structure. However, an isotropic material can change dimensions when an electric field is applied, but there will be no generated charge when the material is subjected to mechanical pressure. This is caused by a small nonlinear effect known as the electrostrictive effect, while the piezoelectric effect is linear (Yang 2004).

Initially, the dipoles in PZT are polarized in random directions resulting in little to no polarization of the material as a whole, and thus little to no piezoelectric effect. This problem can be addressed by poling. In the poling process the material is heated to above its Curie temperature, causing the PZT to form a centrosymmetric lattice structure and lose all polarization, as seen to the left in Figure 2.3. Then a high electric field is applied across the material, and the temperatures are lowered while the field is still applied. This forces the polarization in the unit cells to align to the exterior field, resulting in a strong polarization of the bulk material.

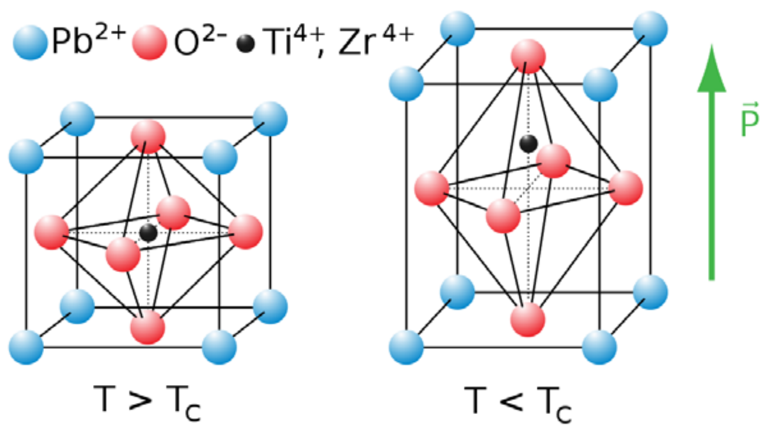

Figure 2.3 Crystal Structure of PZT, above and below its Curie temperature (Source: Wikimedia Commons)

A piezoelectric material is described by the electromagnetics and mechanics laws. It is important to get an overview of the relevant laws of both domains before attempting to combine them. In electrical engineering, a piezoelectric material is a polarizable dielectric (Carcangiu *et al.* 2015). Hence, the electrical behavior of the material is as described in Equation 2.1.

$$\begin{bmatrix} D_1 \\ D_2 \\ D_3 \end{bmatrix} = \epsilon_0 \begin{bmatrix} E_1 \\ E_2 \\ E_3 \end{bmatrix} \begin{bmatrix} P_1 \\ P_2 \\ P_3 \end{bmatrix}, \ \nabla . D = 0 \tag{2.1}$$

Where, D is the electric displacement field [C/m^2], ε is the vacuum permittivity, E is the electric field [V/m] and P is the polarization density. The second equation defines the material as a dielectric, i.e. no free charges. The index convention is the same as with the first three values in the stress and strain vectors.

The mechanical properties of piezoelectric material can be described as a linear-elastic material assuming only small deformation. Consequently, it follows the generalized Hooke's law, as seen in Equation 2.2.

$$\begin{bmatrix} T_1 \\ T_1 \\ T_1 \\ T_1 \\ T_1 \\ T_1 \end{bmatrix} = \begin{bmatrix} c_{11}^E & c_{12}^E & c_{13}^E & c_{14}^E & c_{15}^E & c_{16}^E \\ c_{21}^E & c_{22}^E & c_{23}^E & c_{24}^E & c_{25}^E & c_{26}^E \\ c_{31}^E & c_{32}^E & c_{33}^E & c_{34}^E & c_{35}^E & c_{36}^E \\ c_{41}^E & c_{42}^E & c_{43}^E & S_{44}^E & c_{45}^E & c_{46}^E \\ c_{51}^E & c_{52}^E & c_{53}^E & S_{54}^E & c_{55}^E & c_{56}^E \\ c_{61}^E & c_{62}^E & c_{63}^E & S_{64}^E & c_{65}^E & c_{66}^E \end{bmatrix} \begin{bmatrix} S_1 \\ S_2 \\ S_3 \\ S_4 \\ S_5 \\ S_6 \end{bmatrix} - \begin{bmatrix} e_{11} & e_{21} & e_{31} \\ e_{12} & e_{22} & e_{32} \\ e_{31} & e_{23} & e_{33} \\ e_{14} & e_{24} & e_{34} \\ e_{15} & e_{25} & e_{35} \\ e_{16} & e_{26} & e_{36} \end{bmatrix} \begin{bmatrix} E_1 \\ E_2 \\ E_3 \end{bmatrix} \tag{2.2}$$

The piezoelectric effect is, as previously mentioned, a linear effect. This implies that Equations 2.2 and 2.1 can be expanded with a linear term to include said effect. For instance the stress in a piezoelectric material expressed by the strain and electric field can be seen in Equation 2.2, while the electric displacement field represented by the strain and the electric field can be seen in Equation 2.3. These equations give a mathematical expression for the inverse and direct piezoelectric effect, respectively.

$$\begin{bmatrix} D_1 \\ D_2 \\ D_3 \end{bmatrix} = \begin{bmatrix} e_{11} & e_{12} & e_{13} & e_{14} & e_{15} & e_{16} \\ e_{21} & e_{22} & e_{23} & e_{24} & e_{25} & e_{26} \\ e_{31} & e_{32} & e_{33} & e_{34} & e_{35} & e_{36} \end{bmatrix} \begin{bmatrix} S_1 \\ S_2 \\ S_3 \\ S_4 \\ S_5 \\ S_6 \end{bmatrix} - \begin{bmatrix} \epsilon_{11} & \epsilon_{12} & \epsilon_{13} \\ \epsilon_{21} & \epsilon_{22} & \epsilon_{23} \\ \epsilon_{31} & \epsilon_{32} & \epsilon_{33} \end{bmatrix} \begin{bmatrix} E_1 \\ E_2 \\ E_3 \end{bmatrix} \tag{2.3}$$

The superscripted E's in Equation 2.2 indicates that the values of the stiffness matrix were measured while the electric field across the material was constant. Similar superscripts exist to show constant electric displacement field, stress or strain. A permittivity matrix, ε, has also been introduced to replace the vacuum permittivity and the polarization vector. Moreover, it has been necessary to include the e-coefficients. These are one of four sets of piezoelectric coefficients used to relate the mechanical (S and T) and the electrical variables (E and D). All these relations are listed in their abbreviated form in Equations 2.4 giving four different sets of piezoelectric parameters.

$$\left.\begin{array}{c} D = eS + \epsilon^S E \\ T = c^E S - e^t E \\ D = dT + \epsilon^T E \\ S = s^E T + d^t E \\ E = -gT + (\epsilon^T)^{-1} D \\ S = s^D T + g^t D \\ E = -hS + (\epsilon^S)^{-1} D \\ T = c^d S - h^t D \end{array}\right\} \tag{2.4}$$

The superscripted *t* in some of these equations indicate that the matrix is transposed, while the s-matrix is the compliance matrix of the material, is the inverse of the stiffness matrix. Each of these sets of parameters gives a mathematical description of the direct and the inverse piezoelectric effect in the upper and lower equation respectively and is sufficient to describe the material. Each of the four sets is also related to each other. Hence it is possible to change from one set of parameters to another if it should become necessary.

Equations 2.2 and 2.3 contains a large number of independent variables, 63 in total. However, this number is significantly reduced when including the symmetry in PZT. The poling process turns PZT into a transversely isotropic material with a rotational symmetry around the direction of polarization, usually defined as the x3-direction (Yang 2004). One of the parametric sets for such a material can be written as seen in Equations 2.5 and 2.6, showing that the number of independent variables has been reduced to 10.

$$\begin{bmatrix} T_1 \\ T_1 \\ T_1 \\ T_1 \\ T_1 \\ T_1 \end{bmatrix} = \begin{bmatrix} c_{11}^E & c_{12}^E & c_{13}^E & 0 & 0 & 0 \\ c_{21}^E & c_{22}^E & c_{23}^E & 0 & 0 & 0 \\ c_{31}^E & c_{32}^E & c_{33}^E & 0 & 0 & 0 \\ 0 & 0 & 0 & S_{44}^E & 0 & 0 \\ 0 & 0 & 0 & 0 & c_{55}^E & 0 \\ 0 & 0 & 0 & 0 & 0 & c_{66}^E \end{bmatrix} \begin{bmatrix} S_1 \\ S_2 \\ S_3 \\ S_4 \\ S_5 \\ S_6 \end{bmatrix} - \begin{bmatrix} 0 & 0 & e_{31} \\ 0 & 0 & e_{32} \\ 0 & 0 & e_{33} \\ 0 & e_{24} & 0 \\ e_{15} & 0 & 0 \\ 0 & 0 & 0 \end{bmatrix} \begin{bmatrix} E_1 \\ E_2 \\ E_3 \end{bmatrix} \tag{2.5}$$

$$\begin{bmatrix} D_1 \\ D_2 \\ D_3 \end{bmatrix} = \begin{bmatrix} 0 & 0 & 0 & 0 & e_{15} & 0 \\ 0 & 0 & 0 & e_{24} & 0 & 0 \\ e_{31} & e_{32} & e_{33} & 0 & 0 & 0 \end{bmatrix} \begin{bmatrix} S_1 \\ S_2 \\ S_3 \\ S_4 \\ S_5 \\ S_6 \end{bmatrix} - \begin{bmatrix} \epsilon_{11} & 0 & 0 \\ \epsilon_0 & \epsilon_{22} & 0 \\ 0 & \epsilon_{32} & \epsilon_{33} \end{bmatrix} \begin{bmatrix} E_1 \\ E_2 \\ E_3 \end{bmatrix} \tag{2.6}$$

Where $c_{66}^E = (c_{11}^E - c_{12}^E)$.

Piezoelectric materials are exceptional for energy harvesting applications because of their ability to resist large amounts of strain (Anton and Sodano 2007). There are two methods by which to increase the amount of produced electrical ene9rgy. The first is to increase the strains, which provide more mechanical energy converted into electrical energy. The other method of increasing the amount of harvested energy is to use the coupling mode more efficiently. Another important factor must be considered, which is the mode selected to maximize conversion efficiency. Two possible coupling modes exist, the d_{31} mode and the d_{33} mode. Both modes depend on material poling and applied force direction. The mode defined as d_{31} mode when the material is subjected to force perpendicular to the poling direction, whereas the material is subjected to force in the same direction as the poling direction in the d_{33} mode. The d_{33} mode provides a higher electromechanical coupling when compared with the d_{31} mode, using typical piezoelectric materials. The d_{31} mode has been frequently used coupling mode, but the d_{31} mode yields a lower coupling coefficient, k, than the d_{33} mode (Anton and Sodano 2007). The two modes are presented in Figure 2.4.

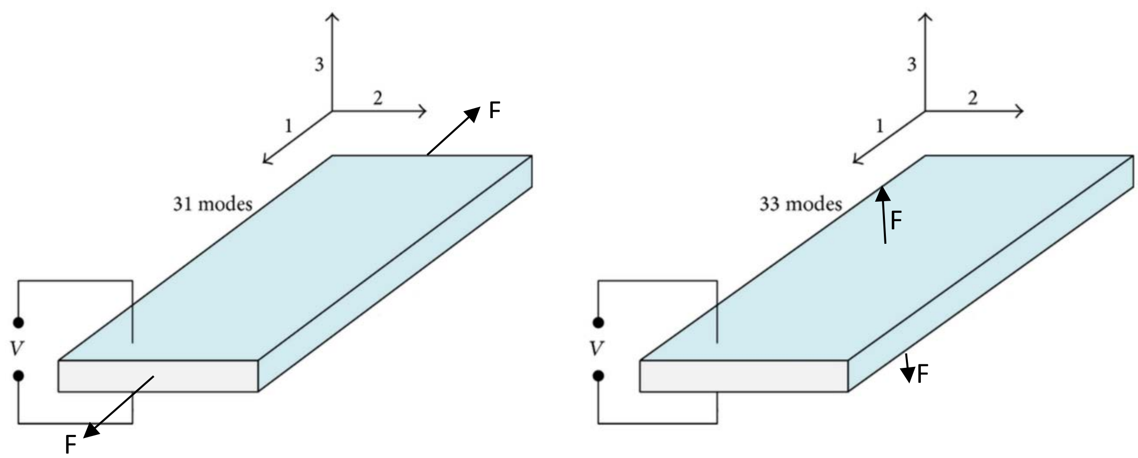

Figure 2.4 Piezoelectric materials modes (d_{33} and d_{31}) (after Roundy et al. 2003)

This was proven in testing three forms of piezoelectric material by(Baker *et al.* 2005). It was found that while a d_{33} mode piezoelectric stack was more robust than a cantilever beam of an equal volume (and had a greater coupling coefficient), application of a given force resulted in two orders of magnitude less power than was produced by the cantilever beam (Anton and Sodano 2007; Priya and Inman 2009). This can be explained by the mechanical properties of the stack configuration – the stack has a high physical stiffness which makes induction of strain in the material less simplistic.

Therefore, the conclusion reached was that a stack configuration would be appropriate in an environment in which durability was required or high forces were commonplace, such as in large operating machinery or in an industrial manufacturing facility. The better robustness would be important in such an application and the power output, although lower than that from a cantilever, would be acceptable. In a situation involving smaller forces and where vibrations were on a much smaller magnitude, a d_{31} cantilever would be more the efficient configuration. This conclusion was in agreement with that of another study that reported that a system's resonant frequency was lower when operated in the d_{31} mode; a lower resonant frequency implies that in a natural environment, the system is more likely to be driven at resonance, which will result in a greater power output (Roundy *et al.* 2003).

2.2.2 Selection of Piezoelectric Transducer Material

Piezoelectric material, steel, and epoxy were the three primary materials used in the transducer. Elastic material properties were used for the PZT, metal cap, and epoxy. Piezoelectric materials have excellent potential when it comes to mechanical energy conversion because they exhibit a good electromechanical coupling effect (Li *et al.* 2011). Piezoelectric materials can be classified into the following categories: single crystalline material (e.g., quartz), piezoceramics (e.g., lead zirconate titanate [PZT]); piezoelectric semiconductors (e.g., ZnO_2), polymer (e.g., Polyvinylidene fluoride [PVDF]), piezoelectric composites, and glass ceramics (e.g., $Li_2Si_2O_5$, Ba_2TiSiO_6). These different types of piezoelectric materials have different piezoelectric and mechanical properties (Uchino 2009).

All of the above materials show piezoelectric properties. Some materials are naturally occurring (e.g., quartz), while others are engineered to display the properties (Swallow *et al.* 2008). The most common piezoelectric materials are polymers (PVDF) and ceramics (PZT). Polymer materials are soft and flexible, while piezoelectric ceramics are rigid. In addition, polymer has lower dielectric and piezoelectric properties than ceramics. Lead zirconate titanate (PZT) is a frequently studied ferroelectric material due to its extremely wide field of application as a piezoelectric material.

The stored electric energy under a low-frequency pavement load can be calculated using Equation 2.7 (Zhao *et al.* 2012):

$$U_E = \frac{1}{2}PEAt = \frac{1}{2}V_o^2\frac{s_r^T s_o A}{t} \tag{2.7}$$

where U_E is the electric energy storage in the piezoelectric device, P is the polarization caused by the vehicle load, E is the inner electric field, V_o is the electric potential in an open circuit, A is the area of PZT, t is the thickness of PZT, and s_r^T is the relative dielectric constant of PZT.

From Equation 2.7, the density of stored electric energy can be obtained using Equation 2.8:

$$U_E = \frac{1}{2}PE = \frac{1}{2}dgT^2 \tag{2.8}$$

where d is the piezoelectric strain constant, g is the piezoelectric voltage constant, and T is the external stress. From Equation 2.8, it can be concluded that U_E is related to (d·g) value if external stress is a constant. Thence, the PZT materials with a high (d·g) value are improved for energy harvesting.

Steel, brass, or aluminum can be used for transducer end caps. Chua *et al.* (2014) concluded that a steel end cap can generate higher electric potential under linear force compared to an aluminum end cap. Steel was chosen as the cap material because the yield strength of steel is higher than that of either brass or aluminum, allowing the loading of a higher force on the transducer (Kim *et al.* 2004). In addition, steel produces less displacement, and therefore it is capable of enduring loading with higher force on the transducer compared to aluminum (Li *et al.* 2014).

Usually, metal end caps were attached to the piezoelectric ceramic using epoxy. Epoxy is a durable glue material that provides a high level of bonding properties between two surfaces. Physically, epoxy systems comprise two essential components, namely a resin and a hardener. Sometimes there is a third component, an accelerator, but this is less common.

2.2.3 Available Piezoelectric Transducers Technology

During the past few years, a significant amount of research has been performed on the control of flexible structures through smart sensors and actuators (Dehart and Griffin 1991; Ha *et al.* 1992; and Tzou and Ye 1996). Lead titanate zirconate (PZT) is the most used piezoceramic in various solid solutions. This is because of its high degree of orientation and spontaneous polarization, combined with a high permanent polarization and high dielectric constant (Pan and Yoshikawa 1996). In general, piezoelectric material are used widely in transducers manufacturing. Many of those transducers can be used to harvesting energy from the surrounding environment, such as the Cymbal (Dogan 1994), multilayer (*Heinzmann et al. 2002*; Uchino 2009), Bridge Zhao *et al.* 2010, Moonie (Dogan,1994), THUNDER (THin layer UNimorph DrivER and sensor) (Mossi *et al.* 1998), RAINBOW (Reduced and INternally Biased Oxide Wafer) (Haertling 1991), MFC (Macro-Fiber Composite), and Bimorph (Roundy *et al.* 2003).

There are two types of PZT transducers that can be used to harvest energy from the ambient environment: vibration-based and stress-based. Bimorph, Unimorph, Polyvinylidene fluoride (PVDF) and MFC based cantilever are widely accepted to harvest the energy from the surroundings vibration (Roundy 2005). Cymbal can also used as a vibration energy harvesting device (Kim *et al.* 2004; Kim *et al.* 2005; Kim *et al.* 2006). On the other hand, the mechanical energy in the pavement is mostly caused by the stress of moving vehicle (stress driven). It can be harvested by converting it into electric alternating current using piezoelectric transducers, such as multilayer, Moonie, Bridge, Cymbal, THUNDER, RAINBOW, etc. In pavement, the energy source is driven by stress more than vibration.

The multilayer transducer was developed in 1970's and is composed of thin layers of PZT (Uchino 2009). If the piezo-ceramic consists of one layer, it is called a single layer technology and if the piezo-ceramic component includes some active piezoceramic layers, we speak of a multi-layer technology. In general, multilayer transducer contains any number of piezo layers that may be stacked on top of one another. Knowing that, increasing the volume of piezoceramic increases the energy that may be delivered to a load. Furthermore, as the number of layers grows, so does the difficulty of accessing and wiring all the layers. A multilayer transducer structure is shown in Figure 2.5.

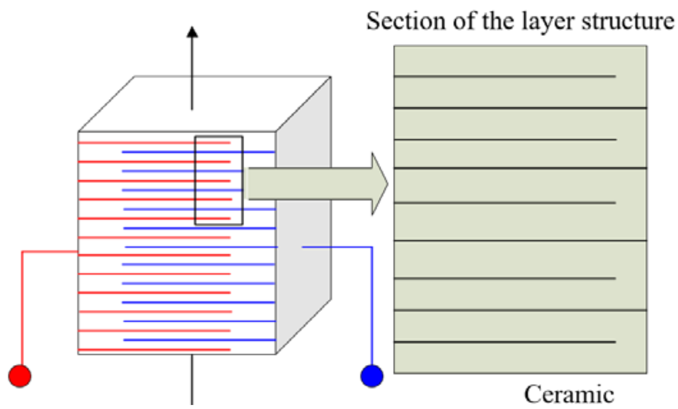

Figure 2.3 Configuration and sectional diagram of a monolithic multi-layer piezo-ceramic actuator

Moonie was constructed using brass metal end caps with shallow internal cavities, which were bonded to a piezoelectric ceramic disk (Sugawara *et al.* 1992; Xu *et al.* 1991). The cavity is used between the PZT ceramics and thick metallic electrode to convert a portion of the z-direction stress into a large radial and tangential stress of opposite sign (Xu *et al.* 1991). The Cymbal transducer is a developed version of upon Moonie to reduce the stress concentrated in the PZT disk and improve displacement (Dogan, 1994). It consists of a piezoelectric ceramic disk sandwiched between two metal end caps. The applied vertical load on the end cap causes radial stress in PZT disk, the stress of which will generate an electric field due to the piezoelectric effect. Furthermore, the traditional Bridge transducer had the same dimensions as the Cymbal, except its length and width are equal, square piezoceramic. Moonie and Cymbal structures are shown in Figure 2.6.

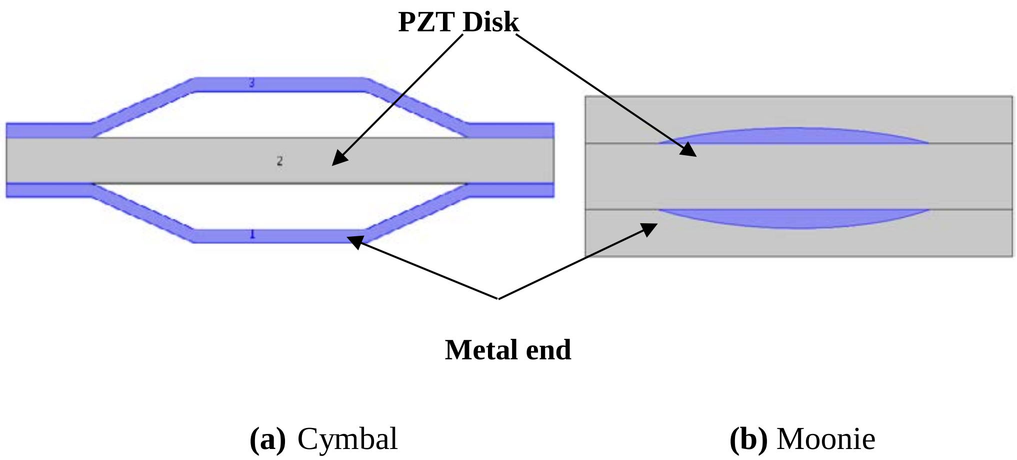

Figure 2.4 Cymbal and Moonie structure

RAINBOW is composed of two main components; PZT and oxygen reduced layer. A RAINBOW ceramic is a uniform structure with an integral electrode that is fabricated to place an internal compressive stress bias on the piezoelectric element (Ashley 1995; Furman *et al.* 1994). However, RAINBOW is brittle because of its brittle components, therefore it is not robust enough to ensure the vehicle load. RAINBOW is a pre-stressed transducer, see Figure 2.7.

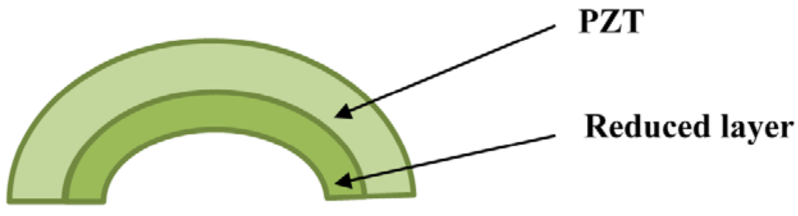

Figure 2.5 RAINBOW structure

THUNDER as a type of piezoelectric actuator/sensor was developed at NASA Langley Research Center in 1994 (Pinkerton and Moses 1997). THUNDER is composed of a ferroelectric material which is prestressed against a foundation material (glass, metal, etc.). This new piezoelectric device is based on a piezoelectric ceramic wafer attached to a metal backing using a polyimide adhesive (Siochi *et al.* 1995). An electrode lead zirconate titanate (PZT) wafer is sandwiched between two layers of adhesive film surrounded by a thin metal shim on top and a thicker shim on the bottom (Bryant 2007). In general, THUNDER is composed of three layers; aluminum at the top, PZTin the middle and stainless steel at the bottom, with epoxy between all three. Figure 2.8 shows the THUNDER structure.

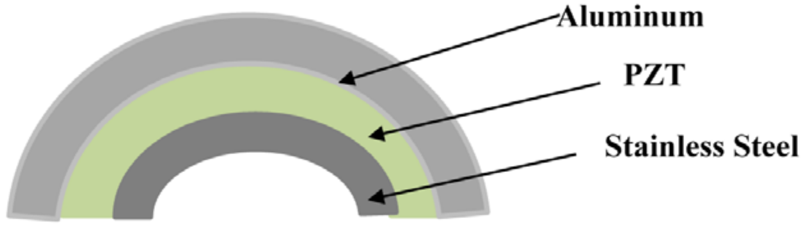

Figure 2.6 THUNDER structure

MFC was developed at NASA Langley Research Center in the later 1990's (Wilkie *et al.* 2000; High and Wilkie 2003). MFC is a composite shape made of PZT fiber, epoxy, and an integrated electrode as shown in Figure 2.9. The MFC is an actuator that uses piezo fibers and interdigitated electrodes to capitalize on the higher g_{33} piezoelectric coupling coefficient, allowing it to produce higher strain and force than the typical monolithic PZT (Sodano *et al.* 2004a). Zhao *et al.* (2012) found that the MFC has acceptable efficiency, whose electromechanical coupling factor (k) is 0.24 and energy transmission coefficient (λ_{max}) is 0.10 under a horizontal stress. In addition, they found that the storage electric energy of MCF is very small and the stiffness is very low.

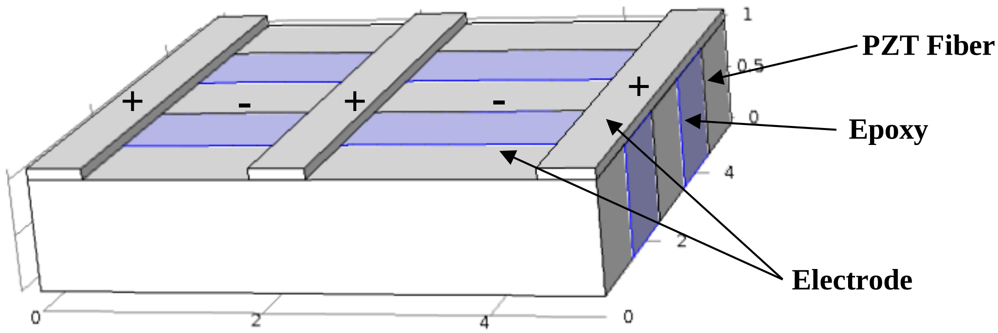

Figure 2.7 MFC Structure

2.2.4 Application of Piezoelectric Energy Harvesting in Civil Infrastructure

Highway pavements are exposed to energy-potential resources from vehicle vibrations and traffic loading strains during their service lives. These resources could be potentially converted into some usable sorts of energy such as electric power. Piezoelectric materials and other such smart materials are capable of converting mechanical energy such as that in ambient vibrations into electrical energy (Hill *et al.* 2013; Ali *et al.* 2011). Research has shown that smart materials show promise for improving the potential uses, maintenance, and longevity of physical infrastructure systems. Some other researches such as Szary (2009) developed a novel , high voltage and durable weigh-in-motion (WIM) sensor.

Advancements in sensing technology have enabled a new generation of smart structures, machines, and materials to be developed. The application of energy harvesting to civil infrastructures, especially in bridges and pavement, has been studied because it provides an encouraging way to supply power. Many portable electrical devices are capable of exploiting power harvesting techniques that are not reliant on conventional methods such as batteries. This is of benefit as the operating lifetime of batteries is somewhat limited. Indeed, the requirement for remote power sources for such portable devices (which may include electronics powering by walking or structural health monitoring equipment) has driven work into energy harvesting. Energy harvesting's underlying principle is that the operating environment itself provides the required energy; research into the technique has focused on enabling and developing techniques for extracting this energy – that is, the harvesting itself. While there are many potential harvestable energy sources, such as mechanical, chemical, solar and thermal (or, indeed, combinations of these), there has been much recent research demonstrating the feasibility of the use of piezoelectric devices as the source of the power. This has been reflected in patents including the devices for this purpose.

In the theoretical work of Umeda *et al.* (1996), electrical energy was generated by the impact of a falling ball on a plate to the underside of which a PZT wafer was attached. The energy produced was modeled using an equivalent circuit. Meanwhile, there are a number of studies in which energy harvesting is compared to the battery technology currently in common use. Goldfarb and Jones (1999) analyzed the efficiency of a linearized model of a PZT stack as a means of generating power. The authors demonstrated that the piezoelectric material's hysteresis resulted in the efficiency being dependent on the input force's amplitude, while the efficiency rose to its greatest value in a region of much lower frequency than the stack's resonant frequency. With force inputs transverse and parallel to a piezoelectric generator's poling direction, Clark and Ramsay (2000) demonstrated that the d_{31} mode was particularly advantageous in the conversion of applied pressure to working stress in the process of generating power. They further reported that a micro electromechanical system (MEMS) device can be powered by a 1 cm^2 piezoelectric wafer in the microwatt range.

A lumped element circuit model of (Kasyap *et al.* 2002), in which PZT's dynamic performance characteristics were represented in multiple energy domains has been verified experimentally using a one-dimensional beam structure. Peak power efficiencies in the order of 20% were shown. Several means of increasing the power output to theoretical levels for piezoelectric generators were considered by Gonzalez *et al.* (2001). As PZT both generate significantly less power than is required for most realistic electronic applications and generate power too slowly to charge power storage devices for many applications, Sodano *et al.* (2004) investigated methods for the storage of the energy piezoelectric devices produce. A nickel metal hydride battery was found to increase the output power level of stored energy that had been generated by a PZT generator, as well as increasing the time for which the energy could be stored, compared to the performance of a capacitor for the same purposes. The simultaneous combination of structural damping with the harvesting of electrical energy was reported by Lesieutre *et al.* (2004). The energy was harvested from a mechanically loaded piezoelectric structure by a full bridge rectifier, in combination with a battery, a step-down converter, a filter capacitor and a switching D.C.-D.C. step-down converter. Two modes of operation are possible with such a system. In the first, the converter is placed between the battery and rectifier; this is used at higher excitation levels. The second mode is used at lower excitation levels differs from the first in that the battery is directly charged by the rectifier.

Baldwin *et al.* (2011) focused on investigating the application of piezoelectric technology within the structure of highway bridges using sixteen piezoelectrics (PZT-5A). The PZT were constructed with a thickness of 2 mm in squares 7.24 cm x 7.24 cm in dimension. The piezoelectric wafers were fastened to the steel shims of a six-layer bridge bearing and the steel shims were separated by using 60-durometer rubber sheets. Cyclic force loading (square wave) was applied on the built prototype and mean load, load amplitude, and loading frequency were the experimental variables for the study. The experimental output, prompt power output and total energy harvesting, were measured based on the voltage drops across 480-ohm load resistors connected to the PZT outputs. In their study, the highest amount of energy of 1.253×10^{-6} W·hr was achieved using a load frequency of 1.5 Hz with load amplitude of 17.8 kN and mean load value of 44.48 kN. Although this was a successful experiment from a technical standpoint, the results were disappointing in that the devices were unable to generate enough energy to drive a modest electrical load.

A different approach was taken by Peigney and Siegert (2013), at the University Paris-Est, and concentrated on the potential energy harvested from vibrations within a bridge structure. The researchers designed a cantilever type prototype of piezoelectric harvester. The prototype consisted of a steel plate with dimension of 40 ×220× 0.8 (length× width× depth) mm, two bimorph piezoelectric patches attached on the clamped end side of top and bottom surface of the steel plate. To tune the resonant frequency of the oscillator, a concentrated mass with the weight of 12 gr was located on the steel plate. By conducting a field study on a bridge, the researchers found that the pipe that is fixed beneath the bridge has higher levels of vibration than other bridge parts. Therefore, they decided to attach their prototype to that pipe to achieve higher level of vibration. This prototype specifically targeted one of the bridge’s transverse bending modes at a frequency of 14.5 Hz and the results showed that the maximum power of 0.03 mW can be generated from peak traffic intensity. To use this amount of energy, the researchers recommended using output energy to power wireless health monitoring sensor nodes with low cycle duty. Siegert and his group also developed a model for piezoelectric harvester under random excitations and claimed that the model is comparatively consistent with the experimental results.

Having first been seen in the years around 1980, Structural Health Monitoring (SHM) was subsequently applied both in the aerospace environment in relation to the space shuttle’s development and in civil engineering, where it was used with regard to bridges. SHM comprises both passive sensing monitoring (used to identify the force-time history as well as the location of external sources such as acoustic emissions or impacts) and active sensing monitoring (which is used to identify location and magnitude of damage that is already present). Detecting damage by an SHM method is also possible using a smart layer, which is additionally beneficial in that it enables a highly loaded structure’s hot spots’ to be observed over time.

One example of the use of SHM in crack detection was the excitation and detection of Lamb waves using a smart layer with a PZT-sensing element (Lin and Chang

1998); the researchers positioned the transducers at a number of discrete locations on the smart layer. Hurlebaus (2002), meanwhile, used PVDF-sensing elements and bulk waves in detecting possible delaminations and changes in thickness. In this work, the smart layer of Hurlebaus and colleagues contained a network of distributed piezoelectric polymers; they covered the smart layer's full surface with their PVDF polymer. In order to test their system on an aluminum plate (1.5 cm deep and 15 x 15 cm transversally), they created a test 'defect' by grinding out some sections of the plate's base were milled out to a depth of approximately 2 mm The smart layer was attached to the upper face of the plate, opposite the defect, using a couplant ratio notched/perfect plate material.

There has been a great deal of research into the ways in which highway bridges behave. Considerable uncertainty regarding the application to the dynamic situation of a moving load transiting the highway bridge persists and the effect is, as yet, accounted for in terms of a relationship. In one report, the conditions were limited in order to simplify the situation and enable the beams' vibration under a dynamic load to be analyzed numerically (Sridharan and Mallik 1979). The assumptions used in this work were a constant velocity and restricting the period of analysis to that for which the beam was acted on by the moving load. Wilson and Barbas (1980) researched the non-dimensional dynamic response histories for the specific situation of continuous, undamped, Euler-Bernoulli beam resting on evenly spaced, equal elastic, undamped, discrete supports. They found that the responses were dependent on the ratio of support stiffness to beam stiffness and the constant force loads' distributions (the constant force loads being a load speed parameter with no dimension). A commercially available software package, ADINA (Automatic Dynamic Incremental Non-linear Analysis) has a load arrival time option. It was used by Saadeghvaziri (1993) to demonstrate a highway bridge being crossed by a moving load can be analyzed by a general purpose finite element package.

In the Virginia Tech University, Xiong (2014) conducted a comprehensive research on energy harvesting for roads with using piezoelectric materials. Several prototypes were fabricated and embedded in the pavement in order to investigate their performance in terms of electricity production (Xiong 2014). Some samples were placed within the pavement at different locations include a smart road and parking lot at VTTI, and a weigh station on I-81 at Troutville, VA to measure the output voltage and current under real traffic loads. Design-7 (AD7) test results showed that the output power is extremely varied because of wandering of vehicles. A later version was designed to take advantage of the whole load caused by vehicles with maintained width and depth but with twice the length to reduced losses to these factors.

Xiong *et al.* (2012) tested most of their energy harvesters in the field and laboratory. They installed some of their energy harvesters in the field and tested them over approximately eighteen months without performing any maintenance. The field tests result on the assembly design number 3 (AD3) didn't provide enough power to be measured. This energy harvester probably was failed during installation and compaction process. The mean power of the remaining units indicated that each energy harvester, built in Virginia Tech, is able to generate 3.1 mW from per vehicle. Further testing were conducted to compare Virginia Tech products to the Innowattech's harvester against cost efficiency. Finally, they claimed that their products cost fewer than the energy harvesters made by Innowattech Company and the total output energy significantly depended on the total axles of vehicle.

Finally, efficiencies of piezoelectric materials can range from 20-30 percent for some devices and as low as 10-15 percent for low cost devices (Hill *et al.* 2013). Devices used for roadway harvesting are designed for low cost and therefore lie toward the lower end of the spectrum. Piezoelectric energy harvesting modules in road infrastructure would be placed beneath an adequate layer of asphalt and will not affect pavement quality at the surface. The driver will experience no reduction in pavement smoothness quality. Regarding the environmental aspect of piezoelectric materials, the embedded devices will not increase the fuel efficiency of passing vehicles and thus do not contribute to an increase in the emissions of greenhouse gasses. The piezoelectric devices themselves do not emit any greenhouse gasses. These devices can, for all practical purposes, be considered "green" and not environmentally hazardous.

2.3 MECHANISTIC ANALYSIS OF PAVEMENT RESPONSES

2.3.1 Multilayer Elastic Theory versus Finite Element Method

A closed-form solution for calculating the strains, stresses and displacements for a two-layer pavement system was first proposed by Burmister in 1944 (approximate). He subsequently expanded the scope of his solution to cover three layered pavements (Burmister 1945); this is his layered theory. As the layered theory is easily solved, it is suitable for calculating the response of layers of pavement to the loading due to vehicular traffic. Representing flexible pavements as homogeneous masses is inappropriate as they are layered systems. Therefore, several assumptions have been reported as being necessary to make the use of layered elastic theory appropriate (Huang 1993).

Firstly, every layer of the pavement is isotropic, homogeneous, and linearly elastic. The elastic modulus of each layer is E and the Poisson ratio v. The second assumption is that all the materials are both laterally infinite and weightless. Thirdly, the pressure, q, over the pavement is uniform over a circular area of radius a. The fourth assumption is that the subgrade is assumed to be infinitely thick with a constant modulus while the other layers are considered to have a finite thickness. Finally, it is assumed that at each interface between layers, continuity exists in terms of stress and strain and no shearing stress exists as a result.

Advances in computing technology has enabled the generalization of the layered theory to systems with multiple layers and Huang (1993) has listed many pieces of software used for this purpose. These include BISAR, EVERSTRESS, WESLEA, JULEA, KENLAYER and ELSYM.

Viscoelastic materials are those which exhibit both viscous properties and elastic properties and include asphalt concrete (AC). AC, when subjected to direct stress such as that resulting from the loading from trucks and other vehicle displays both elastic and viscous characteristics as well as time-dependent strain (Yin *et al.* 2007). In addition to the time-dependent strain, related to the viscous properties and increasing with time (albeit it at a lower rate), such stress also causes instantaneous strain, which is associated with the elastic property. Typically, the loading rate, time and loading history determine the mechanical response of asphalt pavement; viscoelastic materials additionally act in a way that is a function of their temperature at the time the load is applied and the period of time for which it is applied.

There have been several methods used in evaluating the response of viscoelastic materials such as AC to moving loads. Elliott and Moavenzadeh (1971) utilized a linear viscoelastic theory that was also built on by Chou (1969). While Elliot and Moavenzadeh looked at circular loads, Chou and Larew approximated the response of multilayered pavements to moving point loads. Meanwhile, Huang (1973) investigated viscoelastic pavements using the approximate collocation method. In doing this, the Dirichlet series assumption was utilized for the viscoelastic modulus, the moving load was modeled by a stationary load whose magnitude varied with time.

Further developments in the capability of software have enabled further advancements in the theory of viscoelasticity. The VESYS constitutive models, BItumen Stress Analysis in Roads (BISAR 3.0) (a program accounting for different bonding conditions at the interfaces between pavement layers) and CIRCLY (which facilitated the modeling of loading horizontally), added the ability to describe viscoelastic materials to the basic layered theory. It must be noted that such changes to the original theory are appropriate only when based upon other valid assumptions. The Viscoelastic Road Analysis (ROAD) software is a viscoelastic multilayer software that calculates pavement responses through consideration of the original model of Burger applied to circular loads (Hopman, 1996).

The complexity of the multilayered pavement problem is reflected in the non-simplistic nature of any mathematical description of the structures’ behavior, in particular, the combination of pavement geometries and physical properties and variations in the loading (for example, their spatial and temporal variations). It is possible to model the response in a more manageable way by considered the pavement structure as being composed as a number of smaller elements. This is based on the assumption that analyzing the response of each subsection individually and then combining the responses of all the individual elements appropriately approximates the response of the structure as a whole. Determining the response of these smaller elements – or finite elements (FEs) is much more straightforward than doing so for the system as a whole.

FE models have been used in the analysis of pavements responses, the first ones used for this purpose being two-dimensional finite element (2D FE) models, which were either plane strain models or axisymmetric models. The former type of 2D FE model assumed that the strain acts only in the *x*-*y* plane and the strain in the *z*-direction was zero; this assumption is valid for long structures that are subjected to loads that act only in the *x*-*y* plane. The axisymmetric FE, meanwhile, is similar but rather than being based on a linear, plane model, it is based around a circularly symmetric model. Analysis within this model is based on a unit radian as opposed to the unit out-of-plane depth that is used in the plane strain model, and assumes that the pavement loading is circular on the pavement surface and that the pavement is formed by horizontal layers of homogeneous material arranged in planes. Various software solutions for performing axisymmetric FE analysis are available, one of the most popular of which is the ILLI PAVE package.

A fuller description of the behavior of pavements is provided by three-dimensional finite element (3D FE) analysis; as Zaghloul and White (1993) described, such analysis requires significant computing power and advanced algorithms. With such advanced capabilities, many aspects of pavement performance may be modeled using 3D FE analysis. For example, more complex structural properties of the pavement such as infinite foundations, discontinuities in (or even the movement of cracks through) the pavement or its nonlinear and viscoelastic properties may be modeled to determine the response to loads. Similarly, the effects of changes in the loading may be accounted for – these may include irregular imprint area from vehicles' tires or stress in the pavement that is not constant across the application area. Other aspects that might be modeled are the coupled temperature effect, dynamic analysis or quasi-static analysis, de-bonded or bonded interface and many others. While 3D FE can be an expensive and complex analysis tool to run, it is versatile and vital in investigating the behavior of pavements, enabling the simulation of the conditions at the interfaces between layers, the nonlinear characteristics and the effects of any non-uniformity in the loading from vehicles' tires.

2.3.2 Pavement Material Characterization

Dependent on design factors and, in particular, the means by which loads are distributed to the subgrade, pavements may be classified into one of two types. Rigid pavements comprise concrete slabs in addition to base and subgrade, the slabs being either reinforced concrete or cement concrete. In flexible pavements, meanwhile, the layers above a subgrade are the surface of bituminous or asphaltic material and aggregates over a compacted granular material. There are several strata in the structure – subgrade (the deepest), subbase, base and AC (the most superficial). Typically, the subgrade strength determines the pavement thickness, while the higher strength materials are utilized in the less deep layers.

2.3.2.1 Viscoelastic Asphalt Concrete Layer

It is necessary to model the components of pavement to analyze the responses of the pavement in detail. According to Wang *et al.* (2013), the simple analysis provided by elastic theory is inadequate for evaluation of the temperature dependence or frequency (and so time) dependence of the pavements, despite being acceptably accurate for asphalt concrete. Introducing a consideration of viscosity into the model enables the impact of uniaxial loading on viscoelastic materials to be investigated and may be informative. Many texts on viscoelasticity describe rheological models, which simulate the plastic flow of solids (for example,Flügge (1975) and Christensen (2012))– one means of describing such viscous flow such that both elastic and viscous properties under deformation are accounted for.

Two forms of relaxation are associated with the generalized viscoelasticity theory. One is structural relaxation (Zheng and Zhang 2014) and describes the time-dependency. Several models of viscoelasticity are in existence, each differing slightly in the arrangement of the structures used to model the phenomena. The generalized Maxwell model simulates a viscoelastic material using the series of springs and dashpots shown in Figure 2.10.

The relaxation shear modulus function can be approximated as shown in Equation 2.9 a Prony series.

$$\tau_{(t)} = G + \sum_{m=1}^{N} G_m \exp(\frac{-t}{\tau_m}) \tag{2.9}$$

Where, τ_m is the relaxation time of the spring-dashpot pair in the mth Maxwell branch and G_m is a factor representing the spring's stiffness in the same Maxwell branch. The instantaneous shear modulus is as shown in Equation 2.10.

$$G_o = G + \sum_{m=1}^{N} G_m \tag{2.10}$$

Equation 1 may be expressed in an alternative way, as shown in Equation 2.11:

$$\tau_{(t)} = G_o \left[\mu_o + \sum_{m=1}^{N} G_m \exp(\frac{-t}{\tau_m})\right] \tag{2.11}$$

where the values $\mu_m = G_m/G_o$ are such that Equation 2.12 hold:

$$\sum_{m=0}^{N} \mu_m = 1 \tag{2.12}$$

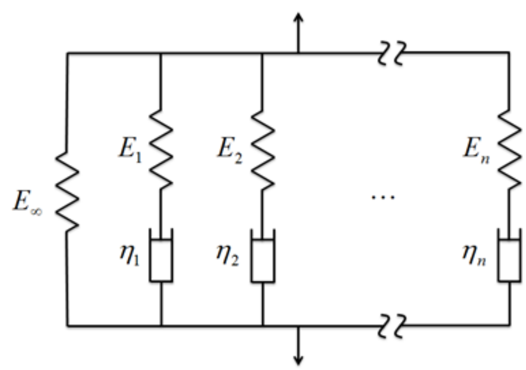

Figure 2.8 Schematic generalized Maxwell solid model

A strong dependence on temperature can be seen in many materials' viscoelastic properties. For these materials, an assumption that they are Thermo rheologically simple (TRS) is often made. A TRS material is one in which a change in temperature results in a change in the time scale for relaxation – that is, if the temperature changes, the relaxation time, □$_m$, is modified by a shift function, $a_T(T)$, to become $a_T(T)$□$_m$. There are various shift functions used, one of the most frequently employed being the Williams-Landel-Ferry (WLF) shift function:

$$\log(a_T) = \frac{-C_1(T-T_o)}{C_2+(T-T_o)} \tag{2.13}$$

where the temperature corresponding to the shift factor is T, T_0 is reference temperature, and C_1 and C_2 are regression parameters.

2.3.2.2 Nonlinear Cross-Anisotropic and Anisotropic Aggregate Behavior

Uzan (1992) and Tutumluer (1995) have demonstrated that the aggregate orientation and the nature of granular media result in direction-dependent (that is, anisotropic) and stress-dependent dependence in unbound layers of aggregate. Aggregate orientation is a function of loading conditions, compaction methods and shape; in granular base layers, a combination of wheel loading and compaction result in a specific form of directional dependence – cross-anisotropy (Wang 2013).

In 1997, Tutumluer and Thompson reported a shear stiffness of approximately 20% to 35% of the vertical stiffness and a horizontal stiffness of just 3% to 21% of the vertical stiffness in the granular layer for a certain group of aggregates. The dilative performance seen under the load of wheel and the impact of residual stress induced by compaction is accounted for well by nonlinear-anisotropic modeling. Adu-Osei *et al.* (2001) reported that to determine the cross-anisotropy and stress sensitivity of granular media, the International Center for Aggregate Research (ICAR) developed a Systems Identification (SID) approach and a robust modulus testing protocol.

A triaxial test system was employed to model in work to determine the dynamic stresses on a sample and, in particular, to investigate the impact of anisotropic, stress-dependent aggregate behavior (Tutumluer and Seyhan 1999). A novel procedure for investigating the impact of loading with moving wheels, in which variable confining pressure (VCP) was used in repeated load triaxial tests was designed by Seyhan *et al.* (2005). Through these "stress path tests," the researchers reported some findings. In all stress states, the vertical moduli tended to be higher than the horizontal moduli. The positive stress tests tended to give higher vertical moduli that the negative tests. Further, they found that the in-plane Poisson's ratios were higher than the equivalent values out-of-plane; the negative stress path tests resulted in the highest ratios both in- and out-of-plane.

A considerable quantity of research has shown anisotropy to be an important factor in accurate modeling the response of pavements. FE estimates were shown to be in better agreement with field measurements of sub-base and unbound base layers when based on anisotropic models (Masad *et al.* 2006; Oh *et al.* 2006). Tutumluer *et al.* 2003 and Park and Lytton 2004) reported that stress distributions in an unbound base layer were strongly affected by the nonlinear anisotropic modulus. They also found that that modulus reduced horizontal tension in the deeper part of the base layer. GT_PAVE, an axisymmetric FE program predicted the magnitudes and trends in the pavement responses more accurately when anisotropic and nonlinear representations of the granular base layer were used (Kwon *et al.* 2009). They reported that this was the case both for the control low volume, flexible pavement section, and the geogrid reinforced pavement section.

Therefore, as empirical methods of pavement design are replaced by more sophisticated procedures in which mechanistic elements are introduced, it is crucial that the resultant models are reflect measured data as closely as possible. To this end, it is vital that mechanistic-empirical (M-E) models incorporate nonlinear anisotropic granular behavior in the pavement response model.

Equation 4-13 shows the resilient modulus of unbound material (that is, the ratio of the deviatoric stress to that part of the axial strain that is recoverable from the triaxial load tests) (Huang 1993). Of the numerous models that have been suggested to include the impact of the stress level on this resilient modulus, the most frequently employed is the two-parameter bulk stress model This is a nonlinear elastic model and is also known as the $k-\theta$ model, as described by Hicks and Monismith (1971). A term representing the octahedral shear stress was added to the two-parameter bulk stress model (Uzan 1992); this is thought to account for the dilation effect resulting when a large principal stress ratio is applied to a pavement element directly under a wheel load. Uzan also added atmospheric pressure to the model for the purposes of normalization.

$$M_r = \frac{\sigma_d}{\varepsilon_r} \tag{2.14}$$

Where, σ_d is the deviatoric stress and ε_r is the recoverable strain.

A model in which the resilient modulus is the same in all directions is known as an isotropic model; a cross-anisotropic model differs in that the vertical and horizontal directions exhibit different material properties, in terms of the Poisson's ratio and resilient modulus. Research has shown that cross-anisotropic behavior is seen in the granular base layers of pavements as a result of applied wheel loading in the vertical direction and of compaction (Tutumluer 2009). If the plane of isotropy is taken to be the horizontal plane (that is, the 1-2 plane), Equation 2.15 describes the constitutive stress-strain relation for cross anisotropy (Zienkiewicz and Taylor 2000). It can be seen that five parameters of a material are required to define such a cross-anisotropic material. They are: E_1, E_3, G_{13}, v_{13}, v_{12} and v_{31}.

$$\begin{Bmatrix} \sigma_{11} \\ \sigma_{22} \\ \sigma_{33} \\ \sigma_{12} \\ \sigma_{13} \\ \sigma_{23} \end{Bmatrix} = \begin{bmatrix} D_{1111} & D_{1122} & D_{1133} & 0 & 0 & 0 \\ & D_{2222} & D_{2233} & 0 & 0 & 0 \\ & & D_{3333} & 0 & 0 & 0 \\ & Sym & & D_{1212} & 0 & 0 \\ & & & & D_{1313} & 0 \\ & & & & & D_{2323} \end{bmatrix} \begin{Bmatrix} \varepsilon_{11} \\ \varepsilon_{22} \\ \varepsilon_{33} \\ \varepsilon_{12} \\ \varepsilon_{13} \\ \varepsilon_{23} \end{Bmatrix} \quad (2.15)$$

$$\text{with} \begin{Bmatrix} D_{1111} = D_{2222} = E_1(1 - v_{13}v_{31})\lambda \\ D_{3333} = E_3(1 - v_{12}v_{12})\lambda \\ D_{1122} = E_1(v_{12} - v_{31}v_{13})\lambda \\ D_{1133} = D_{2233} = E_1(v_{31} - v_{12}v_{31})\lambda \\ D_{1212} = G_{12} = E_1/(2(1 + v_{12})) \\ D_{1313} = D_{2323} = G_{13} \\ \lambda = 1/(1 - v_{12}^2 - 2v_{13}v_{31} - 2v_{12}v_{13}v_{31}) \end{Bmatrix}$$

where:

E_1 is the modulus in the isotropy plane and E_3 is the modulus normal to the isotropy plane,

v_{xy} is the Poisson ratio for strain in direction y resulting from stress in direction x,

G_{13} is the shear modulus in the 1-3 plane and

E_1 / E_3 = v_{13} / v_{31}.

2.3.2.3 Subgrade Modulus

In general, stress-softening behavior is seen in fine-grained soil, as the modulus decreases when stress is increased. When this soil is acting as a subgrade, this behavior is particularly critical in the presence of a reasonably high-stress level – for example, in a thin asphalt pavement. Equation 4-18 shows the nonlinear, stress-dependent model employed to describe the thickness of the subgrade; it can be seen to be similar to the model fort the granular base layer if the k_2 component is set to zero. As previously done by Kwon *et al.* (2009), the values of the coefficients k_1 and k_3 were estimated using the bilinear model proposed by Thompson and Robnett (1976).

$$M_R = k_1 p_a (\frac{\tau_{oct}}{p_a} + 1)^{k_3} \tag{4.18}$$

The California Bearing Ratio, or CBR, of the subgrade in the thin section of asphalt pavement was used to derive an approximate value of the subgrade's linear elastic modulus, using Equation 2.16. This equation, taken from the AASHTO MEPDG (ARA, 2004), enabled comparison of results from the nonlinear and linear subgrade models.

$$M_R = 2555(CBR)^{0.64} \tag{2.16}$$

Where, M_R is the subgrade resilient modulus [psi] and CBR is its California Bearing Ratio [%].

2.3.3 Traffic Loading on Pavement

The response of pavements to the loading under the weight of vehicles is affected by a complex combination of important factors. These include the physical structure of the pavement itself, the pressure to which the vehicle tires are inflated, the temperature profile and how often the pavement is loaded by what size of vehicles. This response has been subject to research in recent times.

The effective loading time is an important factor when attempting to characterizing any form of asphalt. In order to determine the value of this parameter at any point within a layer of asphalt, it is necessary to evaluate the effective loading time when stress is applied to it. This has been done in a number of ways in the literature.

Barksdale (1971) reported that the geometry of the pavement does not affect the duration or shape of the loading time pulse. However, as depth within the pavement increases, the shape does change from a sinusoidal pulse close to the pavement surface to a virtually triangular shapeless superficially. In addition to these findings, which were based on elastic theory and the finite element (FE) method, the width of the compressive stress pulse was expressed as a function of pavement depth and vehicle speed, a chart relating the pulse duration to these two factors was produced. However, the loading times are not inversely proportional to the speed of a vehicle, as factors such as inertia forces and effects due to viscosity must be accounted for (these factors being taken from the AASHO Road Test).

A relationship between both the depth profile of the pavement and the pulse times of the stresses in three directions and the loading time was proposed by Brown (1973). The loading time itself was derived from elastic layered theory and taken to be the average of these pulse times. According to the publication, if t is the loading time [s], v is the vehicle speed [km/h] and d is the pavement depth [m], the relationship between the three factors as shown in the following equation:

$$\log(t) = 0.5d - 0.2 - 0.94\log(v) \tag{2.17}$$

Brown’s work yielded a loading time value slightly under half that of Barksdale.

A year later, McLean (1974) produced a chart plotting an applied square’s pulse width as a function of the pavement depth profile and the speed of the vehicle. Both sinusoidal and triangular pulses have longer pulse times that square waves.

The National Cooperative Highway Research Program employed a more basic technique based on Odemark’s method of equivalent thickness and the 45° influence zone method. In it, the frequency and loading time of the applied load was computed as a function of speed and the pavement’s cross-sectional structure. The time, *t*, for which a moving vehicle applies its load, from NCHRP 1-37A (Moulthrop and Witczak, 2014; Moulthrop and Witczak 2011) is defined according to Equation 2.18:

$$t = \frac{L_{eff}}{17.6\,V_s} \tag{2.18}$$

Where, t is the loading time [s], L_{eff} is the effective length [in] and v_s is the vehicle speed [mi/h].

Figure 2.11 graphically shows illustrated of effective length concept within pavement system Determination by MEPDG.

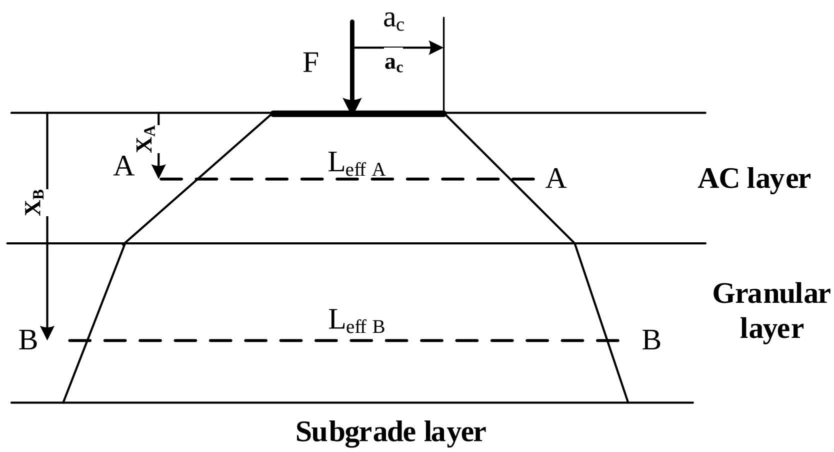

Figure 2.9 Illustration of the concept of effective length within a two-layered pavement system. by MEPDG (After Moulthrop and Witczak 2011)

In tests at the Virginia Smart Road (Loulizi *et al.* 2002), measurements of compressive stress pulses were made at depths of 59.7 cm and 4 cm, the vehicles traveling at 72 km/h, 40 km/h 24 km/h and 8 km/h. Having been measured using pavement instruments, the pulses were normalized to their static equivalents. The researchers discovered that once normalized, a moving vehicle's compressive stress pulse could be modeled by a haversine function or a normalized bell-shaped curve (Equation 2.22).

$$y(t) = sin^2(\frac{\pi}{2} + \pi.\frac{t}{d}) \tag{2.21}$$

Where, *d* is the pulse duration [s]

$$y(t) = e^{-t^2/s^2} \tag{2.22}$$

where , *s* is the standard deviation determining the shape of the curve.

Barksdale's results Barksdale 1971 showed comparable to trends to those calculated by curve fitting to measured data in terms of the impact depth and load speed had on the loading time. The calculated loading time values were dependent on the approximations used in the curve fitting (and so on the type of curves used – bell-shaped or haversine). Loulizi *et al.* (2002) reported that, while the resilient modulus testing used a standardized loading time of one-tenth of a second, fitting a haversine function suggested that using a value one-thirty of this more accurately reproduced field conditions.

The alternative of calculating the effective loading time is to detect the change in the slope of the vertical stress pulse from the FE method over time. Vertical compressive stress is complicated neither by strains due to changes in the direction of motion nor by strains due to the viscoelastic properties of the HMA layers (Wang *et al.* 2015). It is for this reason that the vertical stress was the parameter chosen for the calculation of pulse duration.

2.4 FATIGUE ANALYSIS

2.4.1 Fundamentals of Fatigue

For mechanical structures, one of the most common failure mechanisms is fatigue. When the material structure is constantly subjected to cyclic load, loading and unloading, it is called material fatigue. This load magnitude is smaller as compared to the material’s ultimate stress. Within each cycle, the stress magnitude is not enough to cause failure using the single cycle (Bhat and Patibandla 2011). For failure, there is a need for various cycles. There would be failure under fatigue since the metal behavior under the cyclic load would be different from the monotonic load. Additionally, for cyclic load, new cracks may form which does not take place under the static monotonic load. The crack would grow till its critical size when the material is subjected to operating load and finally causes rupture.

It is essential to note that the fatigue crack would grow at the stress level which is much below the metal's tensile strength. The applied load and component geometry determines the rate of the crack growth. At times, the crack does not grow or it might develop over a slow pace causing a high fatigue life for the component in the case of lower applied stress as compared to the metal fatigue limit (Bhat and Patibandla 2011). Fatigue cracks may only be accepted if thorough information is provided regarding the fracture mechanics and its critical or allowed crack size. The cracked structure present in a monotonic load has two possibilities which are unsafe and safe crack.

Compared to static failure, fatigue failure is more complicated as various other factors are involved. The fatigue life is usually defined as the number of loading cycles till failure occurs.

2.4.2 Classification of Fatigue

Load effect and environment are the two classifications of fatigue. Corrosive environments, water, and effective temperatures are the environmental factors involved. The fatigue failure results vary based on the different environmental conditions.

The rate determines the fatigue present under high temperature. As compared to the environment, the load effect has a much higher effect. Crack initiation is promoted by the corrosive and aqueous environmental and the crack growth rate increases even though the crack tip blunting and environmental product accumulation closure at the crack tip causes the dip crack growth rate to quite an extent. The environments are required to enhance growth rate of the crack. When there are high temperatures, in most of the metals, the fatigue resistance decreases with an increase in the crack growth rate caused by the creep effect.

The stress level determines the fatigue stress effect classifications as Low Cycle Fatigue (LCF) ($1 \leq N \leq 10^3$) and High Cycle Fatigue (HCF) ($N > 10^3$) (Shigley 2011). For the nonferrous metals, the 10^7 cycles and sometimes 5×10^8 cycles are used for the high-cycle fatigue tests (Campbell 2008). If the stress level is low and the form of material is primarily elastic, then the fatigue is referred to as the high cycle type. If the stress level is high enough to cause plastic deformation, the fatigue would be referred to as the low cycle type. For this case, there is a low need for the number of cycles for the fracture. The strain-based fatigue includes cycle and low fatigue since the stress is not as useful and the material strain provide enough description.

There are various factors responsible for affecting fatigue life and some are related to the material used and some to the loading condition. The fatigue failure result is controlled by the loading condition. Fatigue life is reduced by the multi-axial loads as compared to the uniaxial loads unless there is pure torsional loading. Fatigue life is also influenced by the mean stress. Negative mean stress increases fatigue life and the positive tensile mean stress would reduce it. For high-cycle or low-strain fatigue regime, the influence of mean stress is quite significant (Bhat and Patibandla 2011). The type of load cycles may be variable amplitude or constant. There are pre-determined constant amplitude load cycles used for the fatigue test in the rotating machines. The common kinds of load cycles are mentioned in Figure 2.12.

The manufacturing process, geometry, and microstructure of different materials is different. There is low yield strength for the large grains metals and reduced fatigue limit. The same can be stated vice versa. The fatigue properties become much more appropriate when there are higher temperatures and the coarse-grained metal can be observed. The fatigue properties are improved through the crack growth barriers like impurities, grain boundaries, precipitates and others. The fatigue life is also influenced by the phase transformations which take place during the cyclic loading.

Using the testing phase, the material geometry plays a vital role. Crack initiation is facilitated and stress risers are experienced due to discontinuities like notches, holes, and joints. The notched component would have a higher fatigue life as compared to the un-notched component when similar loads are subjected.

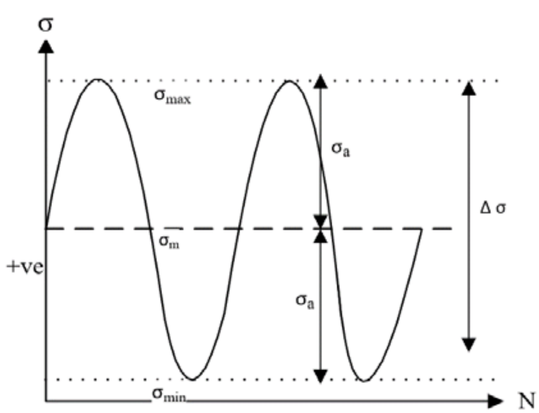

(a)

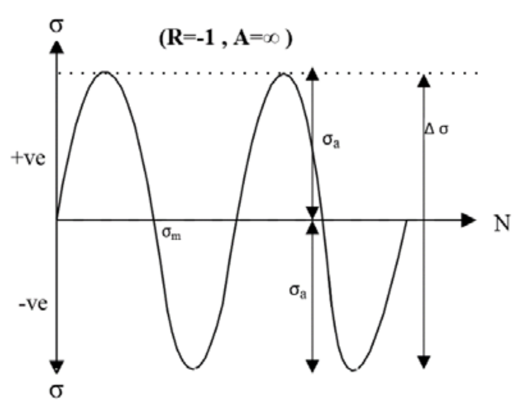

(d)

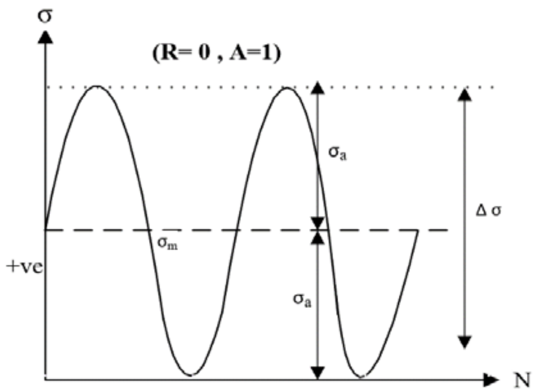

(b)

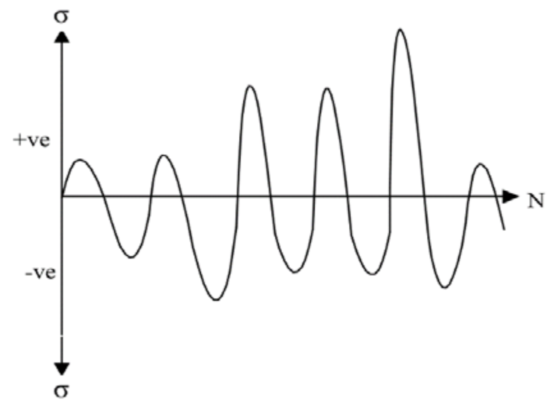

(e)

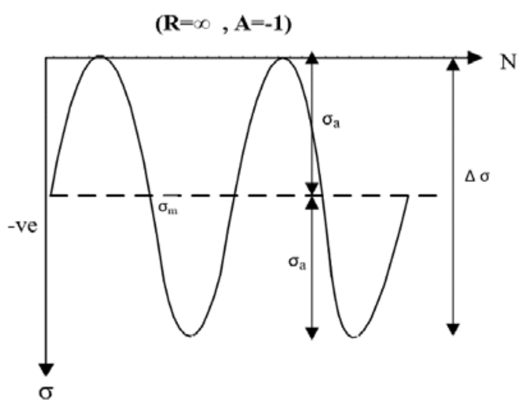

(c)

Stress range = $\Delta\sigma = \sigma_{max} - \sigma_{min}$

Alternating stress = $\sigma_a = \frac{\Delta\sigma}{2} = \frac{\sigma_{max}-\sigma_{min}}{2}$

Mean stress = $\sigma_m = \frac{\sigma_{max}+\sigma_{min}}{2}$

Also there are two ratios frequently used in presenting fatigue data are:

Stress ratio R = $\frac{\sigma_{min}}{\sigma_{max}}$

Amplitude ratio A = $\frac{\sigma_a}{\sigma_m}$

Figure 2.10 Types of Fatigue Cycles

(a) Constant amplitude cycles ,general fluctuating stress (non-zero mean): **(b)** Constant amplitude repeated stress: **(c)** Constant amplitude cycles zero to min: **(d)** Constant amplitude completely reversed stress: **(e)** Variable amplitude cycles

Finally, the fatigue properties are lower during the transverse direction in the manufacturing process and higher when the rolling, extrusion and forging direction is assumed. The crack initiation chances are reduces and fatigue properties are enhanced when processes like cold rolling, shot peening or other heat or hardening treatments take place to carry out the compressive residual stresses. Fatigue life is decreased due to rough surfaces caused by manufacturing processes like punching, machining, rolling, extrusion, forging, drawing, forming and others. The crack initiation sites for rough surfaces are higher as there are filled with asperities and are uneven. The asperities are minimal in the ground and polished surfaces providing an outstanding high fatigue life (Bhat and Patibandla 2011).

2.4.3 Fatigue Failure Criteria for Fluctuating Stress

When reversed stress (zero mean, $\sigma_m = 0$) is present for the machine element, the rotating-beam test provides the endurance limit. This is attained after the relevant factors are included. The situation is different and the fatigue failure criteria is required when the mean (or midrange) is non-zero. If the alternating stress component (σ_a) vs. the mean stress component (σ_m) are plotted, it would be possible to differentiate between the scenarios of fluctuating stress (Figure 2.13).

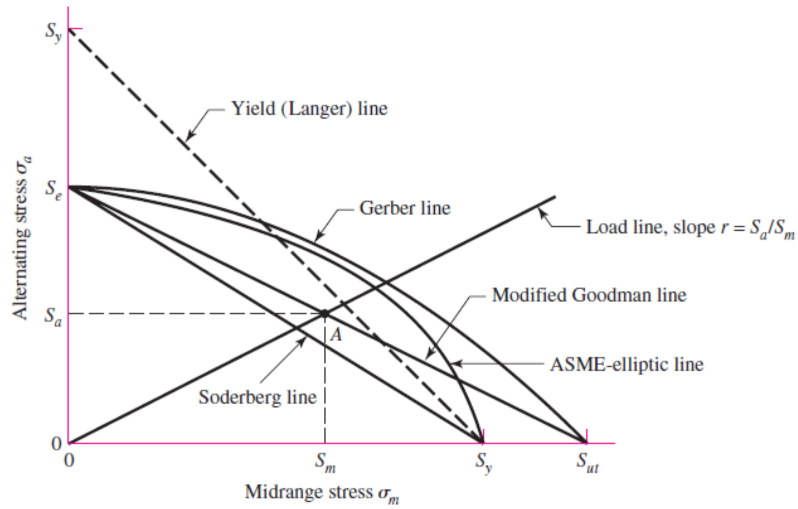

Figure 2.11 Fatigue diagram showing various criteria of failure (After Shigley 2011)

The complete reverse fluctuating stress has been denoted by $\sigma_m = 0$ and $\sigma_a \neq 0$ and static stress by $\sigma_a = 0$ and $\sigma_m \neq 0$. There would be two extremes, complete static or reversed where the combination of σ_m & σ_a would be stated.

There are mathematical models present which provide the mean stress effect predictions upon the stress amplitude. They use the fully reversed bending data like Goodman and Garber, Yield (Langer), Soderberg and ASME-elliptic. Out of these, the most accurate models are the Goodman and Graber for failure line prediction. The linear model was presented by Goodman and the parabolic model by Gerber.

2.4.4 Fatigue Life Prediction

2.4.4.1 Constant Amplitude Load

The initiation of fatigue failure within microscopic cracks was brought forward by Ewing during the 20th-century beginning. The Wohler's test data was used to define the typical shape of the S-N curve by O.H. Baskin in 1910 also brought forward the log-log relationship. Bairstow analyzed the metal-softening and cyclic hardening under cyclic loads. In brittle glass, the cracks were analyzed by Griffith and the fracture mechanics concept was initiated in 1920. It was through the fracture mechanics concepts that fatigue could be understood as they are involved in the characteristics of fatigue cracks. Even after such developments, the designers are not implementing or practicing the fracture or fatigue analysis on a regular basis.

The experimental fatigue data makes use of Wohler's S-N curves which were initially used for the metallic structures life predictions. To attain the S-N curve, a rotating bending test machine is used.

During alternating cycles (R=-1), to record the failure of the specimen, the number of cycles, N_f, with maximum stress, σ_{max}, or stress amplitude, σ_a need to be recorded. The N_f indicates fatigue life under σ_{max}. If any reduction in σ_{max} , the N_f is enhanced and vice versa. The nonferrous metals do not exhibit fatigue or endurance limit by some steels do have this ability. Since the past century, the use of S-N curves has been observed and the conventional designers are still using them. However, these curves do not have the ability to provide enough confidence regarding the component’s failure free performance. Additionally, the fatigue damage concepts must be analyzed along with the theories and fatigue damage rules as part of the fatigue curve characteristics.

A. Linear damage rules (LDR): A stress-based law was brought forward by Basquin (1910), $\sigma_a = {}^{\Delta\sigma}/_{2} = \sigma_f'(2N_f)^b$, and in this case σ_f' is the coefficient for fatigue strength ,$2N_f$ is the failure reversal number or N_f full cycles and b is the exponent for fatigue strength. The high cycle regime is usually present when the stress based approach is applied. The plastic strain range is $\frac{\Delta\varepsilon^p}{2} = \varepsilon_f'(2N_f)^c$ as part of the LDR for the low cycle regime has been brought forward by Coffin and Manson (Coffin Jr 1953; Manson 1954). In this range, the plastic strain amplitude is denoted by $\frac{\Delta\varepsilon^p}{2}$, the fatigue ductility coefficient by $\varepsilon_f'$and the fatigue ductility exponent by c.

In 1945, Miner brought forward the cumulative damage under varying magnitudes for the stress cycles (Miner 1945) as shown in Figure 2.12. The damage function which is defined in the same sense damage produce in a specimen when subjected to (n) cycles at stress amplitude (σ). This function is often written as F(n/N) where N is the lifetime for constant amplitude (σ) cycling. Practical attention has been given to the simplest case of two-stage loading. For multi-stage loadings the damage function is written: (Hashin and Rotem 1978).

$$F(\frac{n_1}{N_1}, \frac{n_2}{N_2}, \ldots., \frac{n_k}{N_k}) \tag{2.25}$$

It is stipulated that ($0 \leq F \leq 1$) then the failure being defined by F=1. The mathematical form of Palmgren (1924) concept was stated which is

$$F = \sum r_i = \sum \frac{n_i}{N_i} = 1 \tag{2.26}$$

Where, F indicates the damage quantum, the cycle ratio is (r_i) and the n_i and N_i are the applied cycles for the provided stress levels and total cycles which are required for failure respectively under the loading cycle i[th] constant amplitude. The cycle ratio attaining the assumption for constant work absorption per cycle is the measure of damage. A diagonal straight line is present for the Miner's damage vs cycle ratio plot and it is independent of the loading levels. The LDR has deficiencies some of which are independence of load level, load sequence and lack of accountability for load interaction. There is no satisfaction present in the life prediction based on the linear rule.

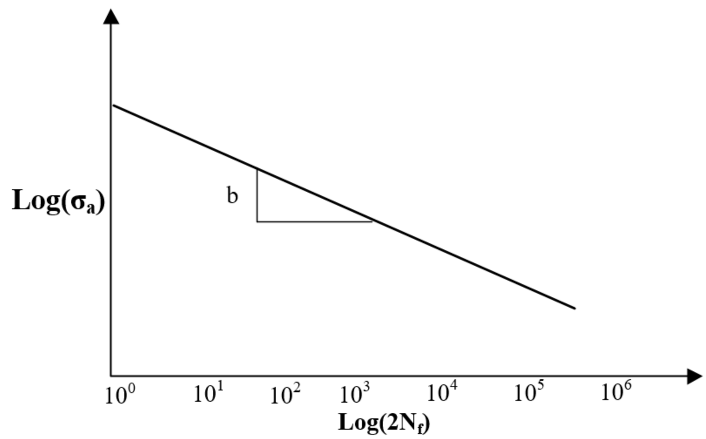

Figure 2.12 Stress and strain amplitudes vs number of cycle reversals to failure

B. *Marco-Starkey theory:* The D-r curves concept was brought forward by Richart and Newmark (1948)) and they are different at different stress levels. The first non-linear load dependent damage theory as the power relationship was brought forward by Marco and Starkey (1954) which is , $D = \sum {r_i}^{x_i}$. Here, the variable quantity that is ith loading related is x_i. For high to low load sequence (H-K) the law indicates $\sum r_i < 1$ and for low to high load sequence (L-H) it is $\sum r_i > 1$.

C. *Endurance limit reduction theory:* The cumulative fatigue damage was largely affected by the change concept within the endurance limit caused by the pre-stress. A two-level step loading method is used to analyze the fatigue pre-stressing effect on endurance properties (Kommers 1945; Bennett 1946). The experimental results clearly indicate that the reduction of endurance strength can be used as the damage measure. These models are nonlinear and must account for the load sequence effect. However, the model is unable to include the effects due to load interaction.

D. *Load interaction effect theory:* These theories have been used for the Corten and Dolan (1956) and Freudenthal and Heller (1959). They are modifications of the S-N diagram and the results show the original S-N curve being clockwise rotated around the reference point upon the curve. For the previous model, selection of the highest load point is made as reference with a corresponding point but in the next model there is a stress level used for reference which corresponds to the fatigue life of 10^3-10^4 cycles. A schematic fatigue life for the L-H and H-L stressing two levels with the Corten-Dolon model is shown in Figure 2.15. The N_f actual values can be observed.

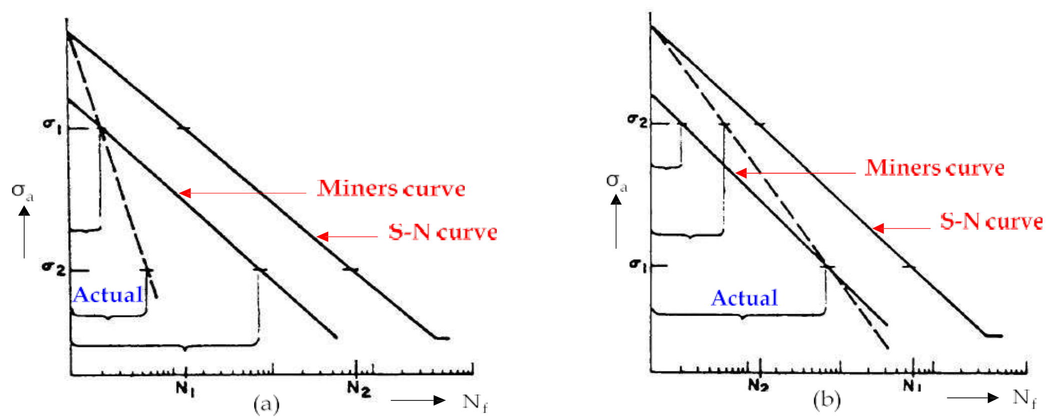

Figure 2.13 Fatigue behavior by rotation method for (a) L-H and (b) H-L load sequences (After Bhat and Patibandla 2011**)**

E. *Two-stage or double linear damage rule (DLDR*): Cycle ratios were considered by Langers concept (1937) and Grover (1960) for the fatigue damage process two separate stages. In Stage I, the damage is caused by crack initiation, $N_I = \alpha N_f$, and crack propagation has caused the damage in stage II, , $N_{II} = (1 - \alpha)N_f$,. For the initiation stage, the α is life fraction factor. Manson (1966) presented another model which had $N_I = N_f - PN_f^{0.6}$and $N_{II} = PN_f^{0.6}$ and the P was used as the coefficient for the fatigue life stage II.

F. *Crack growth based theory:* The essential theories are usually clarified when large and small crack sections are present.

2.4.4.2 Variable amplitude and complex loads

When the variable amplitude load cycles are operating, the safe life of a part can be assessed through the following steps.

1. Techniques like rainbow analysis must be used to reduce the simple or complex cyclic load loading.
2. A cyclic stress histogram must be formed from the rain flow analysis to bring forward the fatigue damage spectrum.
3. The S-N curve cumulative damage degree for each level of stress must be calculated.
4. An algorithm like Miner's rule to be used to integrate the individual contributions.

CHAPTER 3 OPTIMIZED DESIGN OF LAYERED BRIDGE TRANSDUCER FOR PIEZOELECTRIC ENERGY HARVESTING FROM ROADWAY

3.1 INTRODUCTION

Energy harvesting is a promising technique that can help solve global energy challenge without depleting natural resources. New knowledge and innovations in the areas of material science, mechanics, and sensor systems offer revolutionary solutions for preserving transportation infrastructure condition and developing green energy technologies. Energy harvesting technologies capture unused and wasted energy and convert it into a more usable form. Solar, wind, hydro, thermo, and kinetic energy are the common energy sources that can be used for energy harvesting. In recent years, researchers have begun to harvest energy from the ambient environment for different applications, such as structure health monitoring (Dutoit *et al.* 2005) and snow melting on road surface (Xu and Tan 2015).

Piezoelectric materials, which have been widely used in sensor technologies due to their cost-effectiveness, are capable of producing electrical energy from mechanical energy. Therefore, piezoelectric transducers can be designed to harvest the wasted mechanical energy generated under wheel loading that can be stored in an electronic capacitor or integrated with sensors for in-situ road condition monitoring. The collected energy can be also used for traffic signals, electrical signs, lighting, and roadside safety features.

Roadway pavement is designed to carry millions of vehicles passes during its service life, wherein it is subject to considerable stress, strain, deformation and vibration from moving vehicles. These energies are dissipated in the pavement as wasted energy, leading to increased risks of pavement damage. Two types of PZT transducers can be used to harvest energy from the ambient environment: vibration-based and stress-based. Bimorph, Unimorph, and Macro-Fiber Composite (MFC) based cantilevers were used to harvest vibration energy to support wireless network nodes (Anton and Sodano 2007). On the other hand, stress-based Bridge and Cymbal transducers were recommended for energy harvesting for low frequency and non-resonant resources (Kim *et al.* 2004). The Cymbal and Bridge transducers are preferred configurations for energy harvesting in roadway considering the vehicular load pattern and the stiffness consistency between transducer and pavement materials.

A number of studies have been conducted on evaluating the energy-transfer efficiency of Cymbal and Bridge transducer designs using prototype testing and finite element analysis (FEA). The cymbal transducer was developed by Dogan *et al.* (1997) to carry large displacement and generative forces with cost-effective manufacturing. Kim *et al.* (2004) investigated energy harvesting performance of cymbal transducer for several different PZT materials. It was found that multiplication of piezoelectric charge constant and piezoelectric voltage constant was the most important parameter in the material selection for energy harvesting application. Kim *et al.* (2006) further conducted experimental and analytical studies and found that cymbal transducer was the most promising structure for harvesting the electric energy and metal cap improves the endurance of ceramic strip to sustain high stresses.

Yuan *et al.* (2009) presented a new slotted-cymbal structure that was expected to control the circumferential stress and increase the energy transmission coefficient. They concluded that the radial cone slot could produce 60% higher output power than the fringe radial slot. This is because the radial slots of metal end caps can release circumferential stresses and reduce the mechanical energy loss. Zhao *et al.* (2012) examined the performance of the cymbal piezoelectric transducer using FEA and found that increasing the diameter of cymbal transducer and its cavity base increases the potential electric energy.

Leinonen *et al.* (2014) examined the combined electrical and electromechanical properties of the Cymbal transducer for harvesting energy generated by people walking. They found that the unique convex-shaped Cymbal transducer was able to generate 104 milliwatts (mW) more of output power than the traditional sensor design under the same force magnitude and frequency. Daniels *et al.* (2013) investigated several physical parameters of Cymbal transducers and validated the design using FEA for non-resonant energy harvesting applications. They found that widening the angle of metal end cap decreased the output power generation by Cymbal transducer.

Chua *et al.* (2014) examined PZT energy harvesting capabilities in both mechanical and electrical environments using FEA. They concluded that metal end caps made from different materials with different electrical resistive loads had significantly different effects on the power generation. They also found that increasing the thickness of steel end caps and PZT thickness caused higher power outputs. Zhao *et al.* (2015) showed that the trapezoidal bridge transducer was better to resist the applied pressure than the arc, and arch structures, but the arch bridge transducer had the higher energy conversion efficiency. They concluded that the electric potential generated by the arch Bridge transducer decreased when the strip thickness and the modulus of metal cap increased.

New technologies have been developed for thermo- and piezo-electric power generation modules. Zhao and Chew (2012) developed a convection-driven Rijke-Zhao thermoacoustic engine coupled with a piezoelectric generator to demonstrate harvesting thermal energy by converting it into electricity. The Rijke-Zhao engine produces two different temperature thermoacoustic oscillations. One is “hot” and the other is close to ambient temperature, which enable the application of piezoelectric generator to convert heat into electricity via sound. It is can be seen that the maximum output power of this system was about 2.1mW (Zhao 2013). This system produced 60% more power as compared with 1.28mW from the conduction-driven thermo-acoustic-piezo system proposed by Smoker *et al.* 2012). Later, Zhao *et al.* 2014 implemented both thermo- and piezo-electric power generation modules which produces dual-temperature thermoacoustic oscillations. This new system produced 5.71mW total electric power which is higher than the first design system of 2.1 mW.

On the other hand, Ilyas and Swingler (2015) developed an innovative piezoelectric energy harvesting from raindrop impacts. Although the power output and efficiency of single unit is very low, the system can be improved. Xie *et al.* (2015) proposed to use two piezoelectric generators connected by a shared shaft to harvest energy from high-rise buildings. Sensitivity analysis was conducted to evaluate the effects of mass ratio between proof mass and main structure and flexural rigidity of cantilever to the main structure. Xie and Wang (2015) developed a dual-mass piezoelectric bar harvester for energy harvesting from vehicle suspension system. The effects of piezoelectric bar width, vehicle speed, and the level of road roughness on the generated electric power were investigated. Wang *et al.* (2017) studied nonlinear piezoelectric energy harvesting from realistic human motion excitations using numerical and experimental analysis. The optimum resistance to achieve the maximum power output considering complex dynamic characteristics.

3.2 THEORETICAL BACKGROUND OF PIEZOELECTRIC EFFECT

The piezoelectric material can generate an electric field under the application of stress or produce strain under the application of an electric field. The piezoelectric equations for these direct and inverse effects are described in Equation 3.1 and 3.2, respectively.

$$S_i = s_{ij}^E T_j + d_{mi} E_m \tag{3.1}$$

$$D_m = d_{mi} T_i + \varepsilon_{mk}^T E_k \tag{3.2}$$

Where, i, j = 1, 2, 3,…, 6; m, k = 1, 2, 3; S is the strain tensor; T is the stress tensor;s^E is the compliance tensor at the constant E condition; E is the external electric field; D is the electric displacement tensor; d is the piezoelectric charge constant tensor; and ε^T (permittivity) is the dielectric constant tensor at the constant T condition.

The general expression of Equation 3.1 and 3.2 can be written in Equation 3.3 and 3.4.

$$\begin{bmatrix} S_{xx} \\ S_{yy} \\ S_{zz} \\ S_{yz} \\ S_{yz} \\ S_{xy} \end{bmatrix} = \begin{bmatrix} S_{11}^{E} & S_{12}^{E} & S_{13}^{E} & 0 & 0 & 0 \\ S_{21}^{E} & S_{22}^{E} & S_{23}^{E} & 0 & 0 & 0 \\ S_{31}^{E} & S_{32}^{E} & S_{33}^{E} & 0 & 0 & 0 \\ 0 & 0 & 0 & S_{44}^{E} & 0 & 0 \\ 0 & 0 & 0 & 0 & S_{55}^{E} & 0 \\ 0 & 0 & 0 & 0 & 0 & S_{66}^{E} \end{bmatrix} \begin{bmatrix} T_{xx} \\ T_{yy} \\ T_{zz} \\ T_{yz} \\ T_{yz} \\ T_{xy} \end{bmatrix} + \begin{bmatrix} 0 & 0 & d_{31} \\ 0 & 0 & d_{32} \\ 0 & 0 & d_{33} \\ 0 & d_{24} & 0 \\ d_{15} & 0 & 0 \\ 0 & 0 & 0 \end{bmatrix} \begin{bmatrix} E_{x} \\ E_{y} \\ E_{z} \end{bmatrix} \tag{3.3}$$

$$\begin{bmatrix} D_{x} \\ D_{y} \\ D_{z} \end{bmatrix} = \begin{bmatrix} 0 & 0 & 0 & 0 & d_{15} & 0 \\ 0 & 0 & 0 & d_{24} & 0 & 0 \\ d_{31} & d_{32} & d_{33} & 0 & 0 & 0 \end{bmatrix} \begin{bmatrix} T_{xx} \\ T_{yy} \\ T_{zz} \\ T_{yz} \\ T_{yz} \\ T_{xy} \end{bmatrix} + \begin{bmatrix} \varepsilon_{11} & 0 & 0 \\ 0 & \varepsilon_{22} & 0 \\ 0 & 0 & \varepsilon_{33} \end{bmatrix} \begin{bmatrix} E_{x} \\ E_{y} \\ E_{z} \end{bmatrix} \tag{3.4}$$

Where, $C_{ij}^{E} = (S_{ij}^{E})^{-1}$ is the stiffness matrix; and ε_{m}^{s} is the relative dielectric constant at constant strain.

When the piezoelectric transducer is used for energy harvesting application, only the direct piezoelectric effect is considered where the external electric field (E) is zero. If the PZT is embedded in the road pavement subject to traffic loading, the polarization at the axial direction (P_3) appears on the vertical surface of PZT. Thus, Equation 3.2 can be rewritten as Equation 3.5.

$$P_3 = \sum_{i=1}^{6} d_{3i} T_i \tag{3.5}$$

Where, P_3 is the piezoelectric polarization at the 3rd axial direction; d_{3i} is the piezoelectric charge constant of PZT; and T_i is the stress tensor.

The polarization generates an internal electric field in PZT, as shown in Equation 3.6 and 3.7.

$$E_3 = \frac{P_3}{\varepsilon_{33}^T} \tag{3.6}$$

$$E_3 = \sum_{i=1}^{6} g_{3i} T_i \tag{3.7}$$

Where, E_3 is the internal electric field in the PZT; g_{3i} is the piezoelectric voltage constant of PZT; and ε_{33}^{T} is the dielectric constant in the 3rd axial direction.

The relationship between the piezoelectric voltage coefficient (g_{3i}) and the piezoelectric charge constant (d_{3i}) is given in Equation 3.8.

$$g_{3i} = \frac{d_{3i}}{\varepsilon_{33}^T} = \frac{d_{3i}}{\varepsilon_0 \varepsilon_{33r}^T} \tag{3.8}$$

Where, ε_o is the dielectric constant of vacuum; and ε_{33r}^T is the relative dielectric constant of PZT.

The stress tensor on the PZT is caused by vehicle wheel loading at the 3rd axial direction. Thus, it generates an open circuit voltage (V) on the PZT, as shown in Equation 3.9.

$$V_3 = \int E_3 dt_p = \sum_{i=1}^{6} \int g_{3i} T_i dt_p \tag{3.9}$$

Where, V_3 is the electric potential (voltage) at the 3rd axial direction; and t_p is the thickness of PZT;

Therefore, the output electric energy of PZT from energy harvesting can be calculated using Equation 3.10.

$$U_E = \frac{1}{2} P_3 E_3 A\, t_p = \frac{1}{2} V^2 \frac{\varepsilon_{33r}^T \varepsilon_0 A}{t_p} = \frac{1}{2} V^2 C \tag{3.10}$$

Where, U_E is the stored electric energy; A is the surface area of PZT; and C is the capacitance.

The efficiency of mechanical to electrical energy conversion is an essential factor to compare energy harvesters of different transducers. The electromechanical coupling factor (k) and the energy transmission coefficient (λ_{max}) are used to evaluate the efficiency of transducers. High k and λ_{max} values are important to design an efficient energy harvesting transducer. Those two coefficients are defined as shown in Equations 3.11 and 3.12 (Uchino 2009).

$$k^2 = \frac{\text{Stored electrical energy}}{\text{Input mechanical energy}} \tag{3.11}$$

$$\lambda_{max} = \left(\frac{\text{Output electrical energy}}{\text{Input mechanical energy}}\right)_{max} \tag{3.12}$$

Due to cyclic loading effect of traffic on the pavement, the coefficient k can be calculated by the work at different conditions, as shown in Equation 3.13 through 3.15 (Standards Committee of the IEEE Ultrasonics 1987).

$$k^2 = \frac{W_1 - W_2}{W_1} = \frac{U_E}{W_1} \tag{3.13}$$

$$W_1 = \frac{1}{2} s^E T_3^2 At \tag{3.14}$$

$$W_2 = \frac{1}{2} s^D T_3^2 At \tag{3.15}$$

Where, W_1 is the work done by the external force in short circuit condition; and W_2 is the recovered work during the unload period in open circuit condition. Here Equation 3.10 was used to calculate the stored electric energy at low frequency pavement loading.

The output electric energy is related to the load of electric circuit, assuming linear transducers relationships between charge and voltage (Zhang et al. 2007; Roundy 2005). Then, the energy transmission coefficient λ_{max} can be calculated by Equation 3.16.

$$\lambda_{max} = \left(\frac{U_{out}}{U_{in}}\right)_{max} = \frac{Q_s V_o}{4W_1} \tag{3.16}$$

Where, U_{out} is the output electric energy; U_{in} the total input energy; V_o is the electric potential in open circuit condition; and Q_s is an electric charge in short circuit condition.

3.3 NEW TRANSDUCER DESIGN WITH LAYERED POLING

Piezoelectric effects are related to the poling structure of PZT material. Materials like lead zirconate titanate (PZT) are subjected to *poling* process to impart the piezoelectric behavior. PZT structure contains several dipoles that naturally oriented randomly. When mechanical stress is applied to PZT material, the dipoles rotate from its original orientation to direction that causes minimum stored electric and mechanical energy in the dipole (Kamel 2007).

The poling process is used to increase the value of piezoelectric coefficient and the relative dielectric permittivity. The level of anisotropy in piezoelectric coefficient varies depending on the poling direction. In general, mechanical energy is converted to electrical energy more efficiently when the force is parallel to the direction of poling (d_{33}) rather than perpendicular to the direction of poling (d_{31}). This is because that for most PZT materials, the parallel piezoelectric coefficient is more than twice the perpendicular piezoelectric coefficient (Li *et al.* 2014).

Traditional Cymbal or Bridge transducers utilize the lateral piezoelectric coefficient when the stress is applied perpendicular to the direction of polarization, as shown in Figure 3.1(a). The poling direction is vertical and the electrodes are located at the top and bottom of the transducer. This is because it is not feasible to apply poling horizontally due to the relatively long length of PZT strip as compared to the thickness. In this study, a novel poling pattern and electrode configuration was designed to change the direction of polarization in order to utilize the parallel piezoelectric coefficient when the stress is applied in the direction of polarization ().

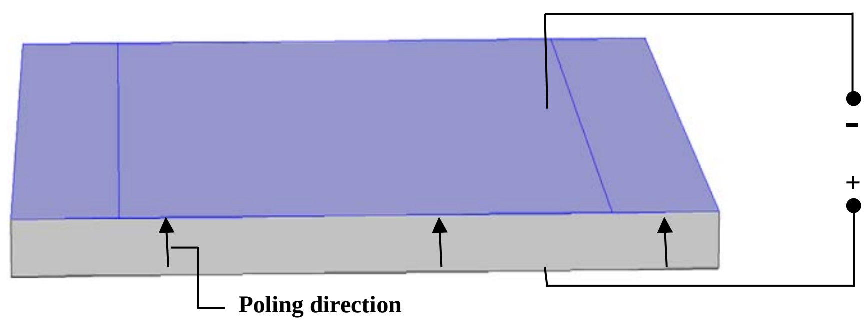

(a)

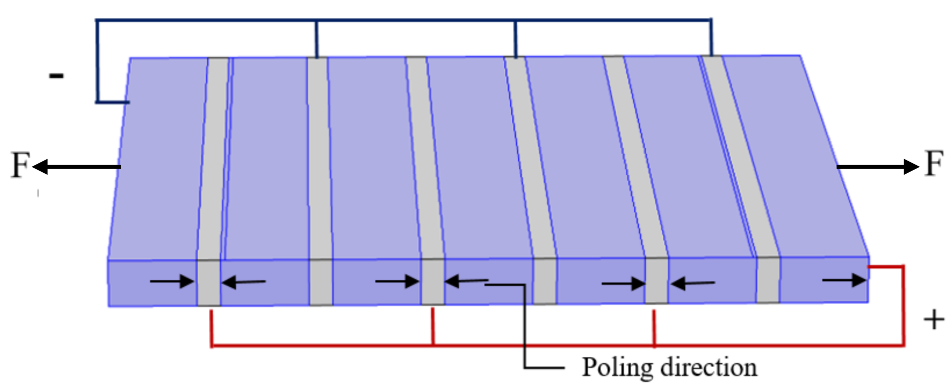

(b)

Figure 3.1 PZT Design with (a) Traditional Vertical Poling; and (b) Layered Poling with Electrode Pattern

The novel design separated the single ceramic into seven sections of capacitive/ piezoelectric cells and each cell was connected in parallel, as shown in Figure 3.1(b). This design was expected to produce the greater energy conversion from the same mechanical energy input as compared to the traditional poling along the thickness of PZT strip. In addition, to increase the effective piezoelectric coefficient, high capacitance is necessary to efficiently utilize the charge stored in the energy-harvesting piezoelectric transducer. The layered electrode pattern would maintain the high capacitance due to the multi-layer electrode configuration. Figure 3.2 shows the poling configuration of the PZT sensor. A very high electric field is applied to the material during poling process that orients all the dipoles in the direction of the field.

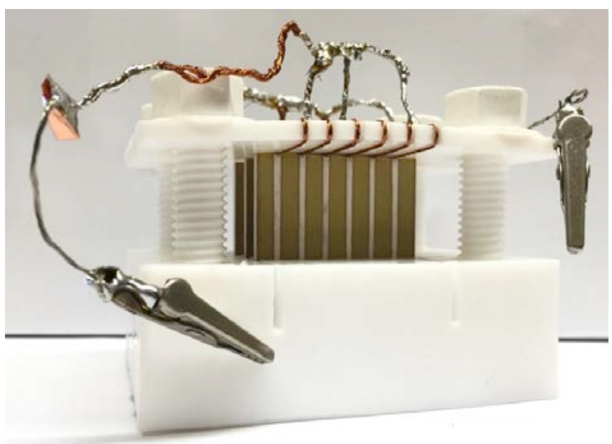

Figure 3.2 Illustration of Poling Configuration for PZT Strip

3.4 FINITE ELEMENT MODEL DEVELOPMENT

This section presents the development details of FE analysis, including model geometry, loading and boundary conditions, mesh sensitivity, and material properties.

The COMSOL software was used for simulation using the multifrontal massively parallel sparse direct solver (MUMPS).

3.4.1 Geometry of Transducer

Multiphysics simulations were conducted to evaluate energy harvesting performance of piezoelectric transducers under external mechanical loading. Figure 3.3 (a) and (b) show the schematic illustrations of Bridge and Cymbal transducers consisting of a PZT disk or strip sandwiched between two metal end caps. The metal end cap can be made of different materials, such as steel, brass, and aluminum. For the purposes of this study, steel was chosen, because its yield strength is higher than that of brass and aluminum and thus can bear the higher loading force. When the vertical loading is applied on the metal end cap and transferred to the PZT material, electric field is generated due to the piezoelectric effect.

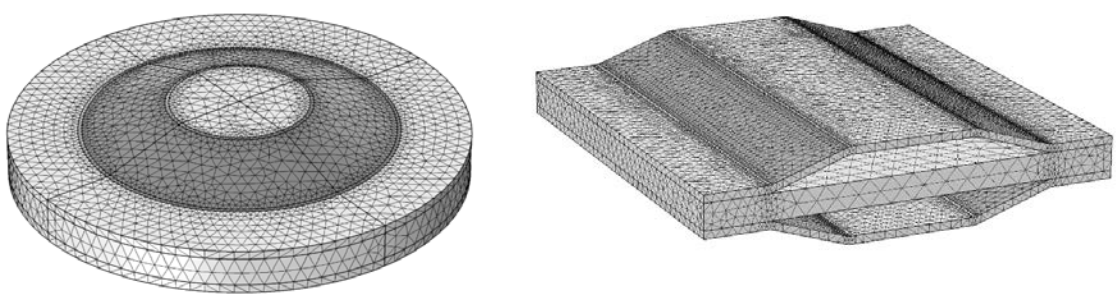

(a) **(b)**

Figure 3.3 Illustrations of (a) Cymbal and (b) Bridge Transducers

Figure 3.4 shows the geometric details of the Bridge transducer with different geometry parameters. The total width and length (L_c) were fixed at 32mm and the thickness of PZT strip (t_p) was kept as 2mm. The length of the cavity base (L_o) was 22mm, the height of the cavity (t_i) was 2mm, the thickness of metal cap (t_c) was 0.6mm, and the inner length of the end cap (L_i) was 10 mm. These parameter values were set as initial dimensions and subject to changes after the geometry optimization. The Cymbal transducer was analyzed with the same cross-section dimensions as the Bridge transducer. The Bridge transducers with the traditional and layered poling configurations were both considered in the analysis.

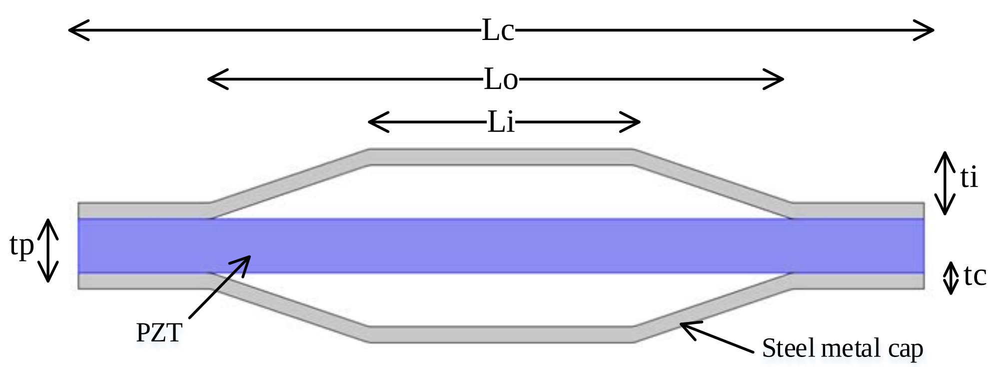

Figure 3.4 Geometry Parameters of Bridge Transducers

The layered poling can increase the effective piezoelectric coefficient and capacitance as compared to the single ceramic poled horizontally. A high capacitance is necessary to efficiently utilize the charge stored in the piezoelectric transducer for energy harvesting. The capacitance and the number of segments (n) between electrodes has the relationship of $C=n^2$. The electrodes were difficult to apply by hand using an extremely small paintbrush. The smaller spacing and width of each segment would have made poling even more difficult. Considering these factors, seven PZT segments (3.71mm each with 1-mm electrode cell) were used in this study, as shown in Figure 3.5. The ceramic strip with six surface electrodes that separates it into seven segments of "capacitive cells" connected in parallel has a capacitance of 49 times the base capacitance obtained with a single segment.

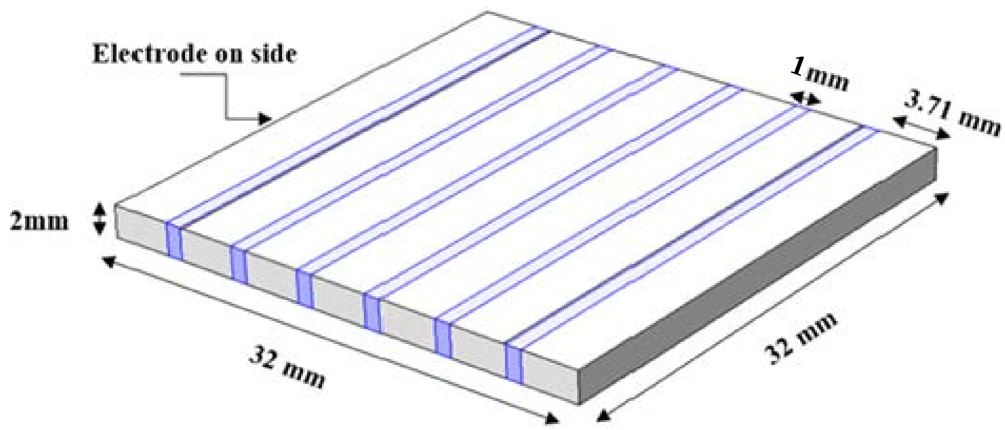

Figure 3.5 Dimensions of Layered Poling in Bridge Transducer

For the mechanical boundary condition, the Cymbal and Bridge transducers were fixed at the bottom end of the cap cavity base, while the distributed load was applied on the top surface of the upper end cap. The electrical boundary condition for the PZT material was configured to ground at the bottom boundary (zero voltage), while the terminal connection was set on top of the PZT material (positive voltage). The voltage and energy generated at the open-circuit condition (as shown in Equation 3.10) were obtained from the simulation.

3.4.2 Mechanical Loading

During the service life of roads, vehicles with different axle loads travel on pavement surfaces. In general, vehicles can be divided into two groups: small (passenger cars) and large vehicles (such as trucks and buses). Truck loading was considered in this study because it generates much greater stress on pavement. The typical truck tire inflation pressure is around 0.7MPa. Previous literature has documented that the contact stresses between the tires and pavement were highly non-uniform distributed, and the peak contact pressure can be 1.5 times tire inflation pressure (Wang and Al-Qadi 2009). Since the piezoelectric transducer is embedded under the pavement surface, the contact stress applied on the transducer may vary depending on the depth at which the transducer is placed. In this study, it was assumed that the top surface of steel cap of the transducer was loaded with 0.7-MPa stress, which is usually achieved at the shallow depth below pavement surface.

3.4.3 Mesh Sensitivity Analysis

An adequate mesh size is important to produce accurate results from finite element analysis. The right mesh size is usually determined considering the balance of accuracy and computational efficiency. Two critical stress outputs were evaluated in the sensitivity analysis; including the maximum tensile stress in the PZT disk, and the shear stress at the inner corner of the contact area between steel cap and PZT disk. The energy output was found not sensitive to the mesh size.

On the other hand, the inner corners of steel cap are very sharp that may cause stress singularity in the calculation. To avoid singularity, adaptive meshes and curved angles were applied at corner edges. The adaptive meshes were used at the inner corner of the contact area between steel cap and PZT disk.

Tetrahedral elements with fine meshes were used in the 3-D FE model. The COMSOL software requires the inputs of minimum and maximum element size and assigns element sizes using geometry dimensions as a guide. For example, the minimum element size is used at small areas or sharp edges; while the maximum element size provides the upper limit as the element sized gradually increases in the model. Figure 3.6 (a) and (b) show the relationships between the minimum mesh size and the maximum tensile and shear stress in the transducer, respectively. The final mesh sizes were selected when the changes of stress outputs were smaller than 5% as the element size decreases. Therefore, the finally selected minimum and maximum element size is 0.322mm and 1.0mm, respectively.

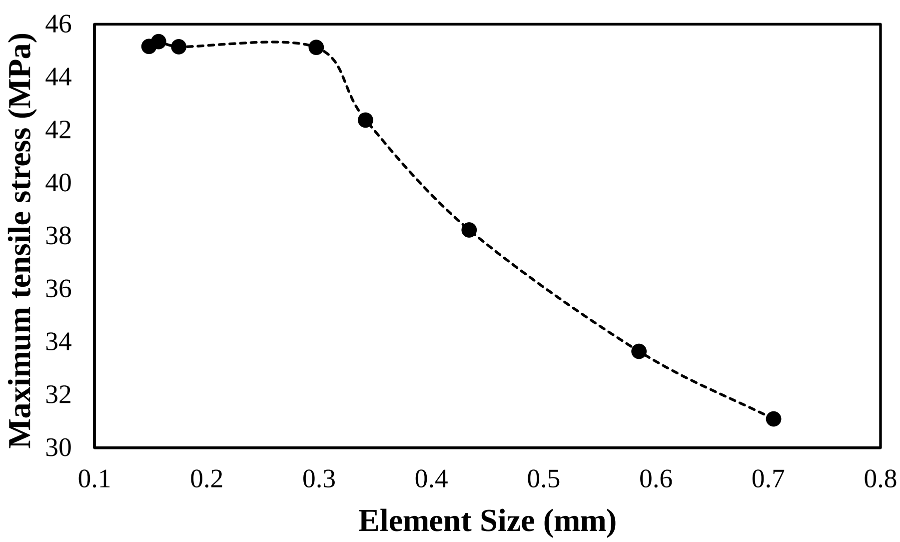

(a)

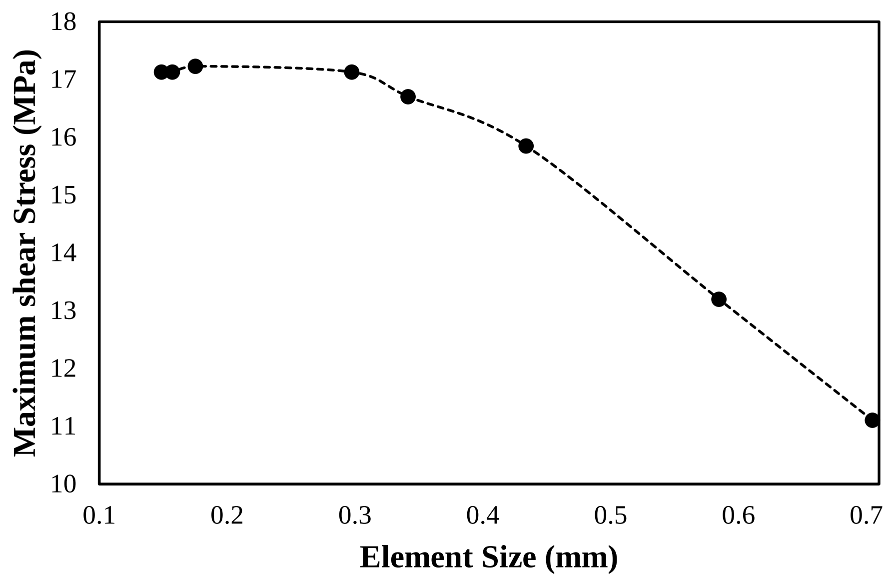

(b)

Figure 3.6 Mesh Sensitivity Analysis Results for (a) Tensile; and (b) Shear Stress

3.4.4 Material Properties

Steel and PZT were the two primary materials used in the transducer. Nine different PZT materials available in the market were considered in the analysis for comparison. The piezoelectric and elastic material properties of PZT materials are summarized in Table 3.1. The goal was to choose the PZT material that produces the highest potential energy. High-strength alloy steel was used for the end cap. The elastic modulus and Poison's ratio are 200GPa and 0.33 for high-strength steel, respectively. Epoxy was used as adhesion material between the PZT strip and steel end cap. The elastic modulus and Poison's ratio of epoxy are 2GPa and 0.33, respectively.

Table 3.1 PZT Material properties for simulation

Material properties	Symbol	PZT Material Type						
		4	**4D**	**5A**	**5H**	**5J**	**8**	**5X**
Piezoelectric Charge Constants (pC/N)	$\mathbf{d_{33}}$	289	320	374	593	530	225	750
	$\mathbf{d_{31}}$	-123	-145	-171	-274	-230	-37	-320
Piezoelectric Voltage Constants ($\times 10^{-3}$Vm/N)	$\mathbf{g_{33}}$	26.1	26.7	24.8	19.7	22.6	25.4	19
	$\mathbf{g_{31}}$	-11.4	-11.8	-11.4	-9.11	-9.8	-10.9	-8.2
Relative Dielectric Constants	$\boldsymbol{\varepsilon^{T}_{33r} = \varepsilon}$	1300	1450	1700	3400	2600	1000	4500
	$\boldsymbol{\varepsilon^{T}_{11r} = \varepsilon^{T}_{11} / \varepsilon_{0}}$	1475	1610	1730	3130	2720	1290	4410
Poison's Ratio	$\mathbf{q^{E}}$	0.33	0.35	0.35	0.34	0.35	0.33	0.35
Elastic Modulus (10^{10} N/m^2)	Y^{E}	8	7.5	7.4	6	6.8	8.6	6.1
Density (Kg/m^3)	$\boldsymbol{\rho}$	7500	7600	7750	7500	7400	7600	7400
Elastic compliance at constant electric field (10^{-12} m^2 /newton)	$\mathbf{S^{E}_{11,22}}$	12.3	13.3	16.4	16.5	16.2	11.5	16.4
	$\mathbf{S^{E}_{12,21}}$	-4.05	-4.76	-5.74	-4.78	-4.54	-3.70	-4.78
	$\mathbf{S^{E}_{32,31,23,13}}$	-5.31	-6.2	-7.22	-8.45	-5.9	-4.80	-8.45
	$\mathbf{S^{E}_{33}}$	15.5	16.8	18.8	20.7	22.7	13.5	23.3
	$\mathbf{S^{E}_{44,55}}$	39	42	47.5	43.5	47	31.9	43.5
	$\mathbf{S^{E}_{66}}$	32.7	36.1	44.3	42.6	41.5	30.4	42.6

3.5 ANALYSIS AND RESULTS

This section presents the analysis of energy output and mechanical stress using different PZT materials, transducer designs, and external loading. Optimization analysis was conducted to find the geometry parameters that achieve the maximum energy output within the limit of mechanical stress. Laboratory testing was conducted to measure energy output of transducer arrays and to validate simulation results.

3.5.1 Comparison between Different Transducers

The electrical potential energy of Cymbal and Bridge transducer using different PZT materials are listed in Table 3.2. As expected, the Bridge transducer can produce much greater electric potential energy than the Cymbal transducer. Depending on the type of material, the novel bridge transducer with the layered poling could result in four to five times energy as compared to the Bridge transducer with the traditional poling. For example, the novel transducer produces 0.839mJ energy using PZT-5X; while the traditional one only produces 0.175mJ energy.

Table 3.2 Electric potential energy output for different PZT materials

PZT material	$d_{33}.g_{33}$	Electric potential energy (0.7 MPa loading) (mJ)		
		Cymbal	Bridge (Traditional)	Bridge (Layered poling)
PZT 4	7543	0.005	0.093	0.400
PZT 4D	8544	0.006	0.099	0.420
PZT 5A	9275	0.007	0.130	0.507
PZT 5H	11682	0.010	0.168	0.652
PZT 5J	11978	0.007	0.143	0.572
PZT 8	5715	0.004	0.075	0.313
PZT 5X	14250	0.010	0.175	0.839

The results show that the transducer with PZT 5X material produced much higher energy than the other PZT materials. It is noted that electric potential energy was related to the multiplication of piezoelectric charge constant and piezoelectric voltage constant (d·g) if the applied stress on the top of the transducer was constant. Thus, the PZT 5X material with the highest (d·g) value was most suited for energy harvesting purpose.

The stored electric energy was analyzed with different magnitudes of stress to examine the relationship between external loading and the potential electrical energy generated. The same geometric parameters and material type were used in the analysis of loading effect. Figure 3.7 shows that the energy output increases significantly as the load level increases, regardless of transducer configuration. A nonlinear relationship was observed between the applied stress and the energy output.

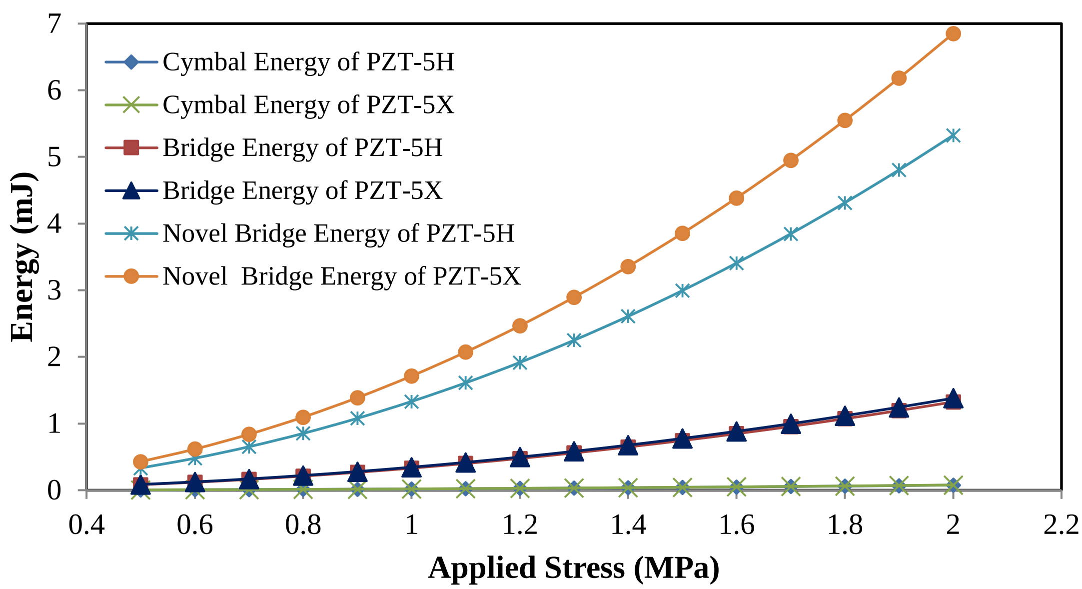

Figure 3.7 Effects of Applied Stress on Energy Output

3.5.2 Comparison between Analytical and Finite Element Solutions

Theoretical analysis has been conducted to predict energy-harvesting performance of Cymbal and Bridge transducers based on the assumption that the in-plane stress is uniformly transferred to the piezoelectric strip from the load applied on the steel cap

(Ugural 1999; Mo *et al.* 2013). Finite element analysis results of energy harvesting performance and mechanical stresses were compared with the analytical solutions, respectively, for Cymbal, traditional and novel Bridge transducers. The energy-related results are compared in Table 3.3. The results are based on applying 0.7MPa stress on the top of a transducer using PZT 5H and high-strength alloy steel end cap. The results show that the differences between the voltage results from analytical solutions and FEA are negligible, although slight differences (up to 5%) were observed. On the other hand, the energy transmission efficiency of new transducer was found being about four times the one of traditional transducer.

Table 3.3 Comparison of FEA & Analytical Solutions and Energy Conversion Efficiency

Transducer	**Symbol**	C (F)	Q (C)	V_o (V)	U_E (mJ)	K^2	λ_{max}
Cymbal	Analytical	1.21E-08	4.46E-07	38.36	0.010	0.02	0.010
	FEA	1.24E-08	4.81E-07	38.68	0.0093		
	Difference	2.855%	3.70%	0.820%	4.55%		
Traditional Bridge	Analytical	1.54E-08	2.28E-06	148.00	0.168	0.04	0.019
	FEA	1.49E-08	2.20E-06	147.76	0.162		
	Difference	-3.56%	-3.59%	-0.03%	-3.61%		
New Bridge	Analytical	3.63E-09	2.16E-06	595.13	0.643	0.16	0.078
	FEA	3.63E-09	2.18E-06	599.16	0.652		
	Difference	0.00%	0.68%	0.68%	1.36%		

Where, C= capacitance; Q=Charge; V_o =Voltage; U_E= Energy; K^2= Electromechanical coupling factor; and λ_{max}= Energy transmission coefficient

Figure 3.8 compares stress distributions along the transducer length calculated from FEA (3-D models) and the analytical solutions (Mo *et al.* 2013), respectively, for tensile and shear stresses. The general assumption of stress distributions in the inner and outer regions of ceramic strip used in the analytical solutions were confirmed by the FEA results. It was found that two primary types of stresses were caused in the PZT strip by external loading: tensile and compression stresses. The tensile stress was mainly induced in the inner region that is the major source of stress producing piezoelectric effect; while the compression stress was primarily distributed in the outer regions of the ceramic strip where the steel cap and ceramic strip were bonded together.

However, the FEA results show that the stress concentration exists at the inner corner of the contact area between the steel cap and the ceramic strip due to the geometry of Bridge transducer. In the outer region, it was found that small magnitudes of compression stresses extended to 1.5mm from the connection line between the PZT strip and the steel end cap. In the inner and outer region of Bridge transducer, the maximum tensile and shear stress reached 45MPa and 17MPa, which would cause the mechanical failure of transducer at these critical locations.

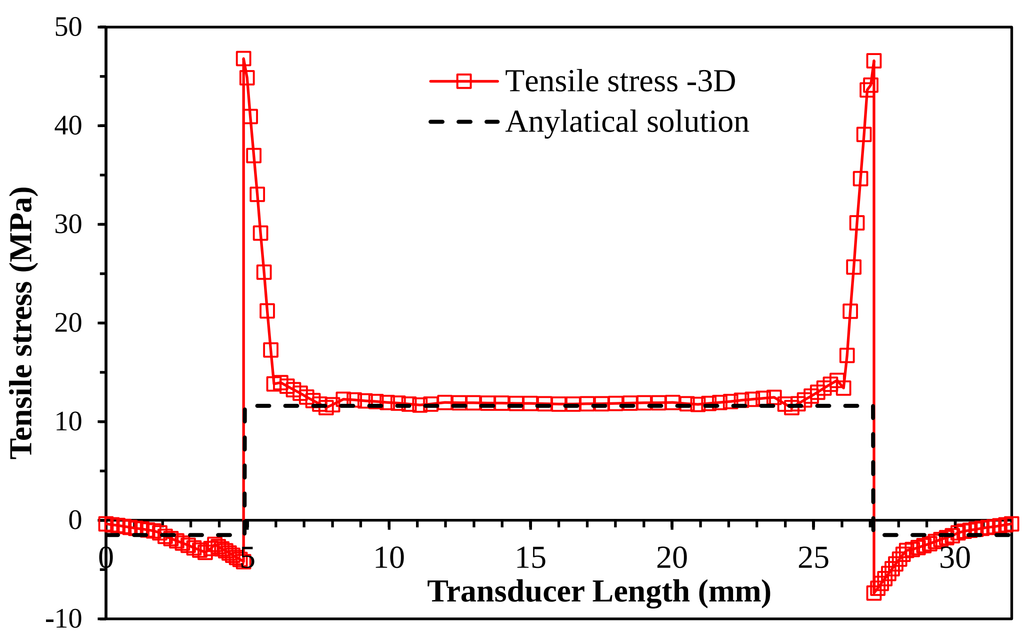

(a)

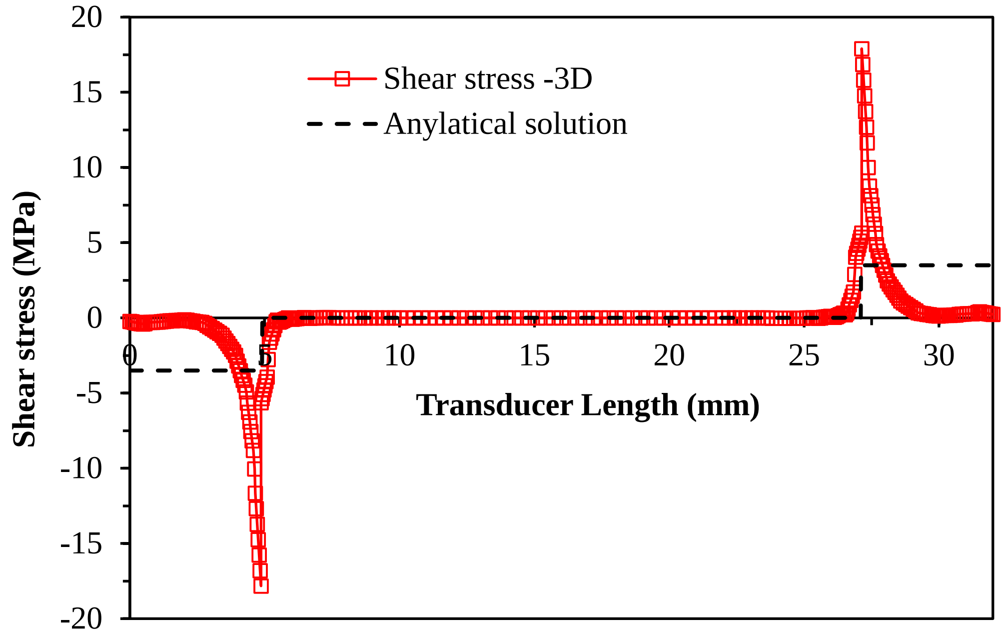

(b)

Figure 3.8 FEA Results and Analytical Solutions of (a) Tensile and (b) Shear Stress Distributions along Transducer Length

3.5.3 Optimization of Transducer Geometry

The electric energy generated by the Bridge transducer is proportional to the tensile stress induced in the inner region of PZT strip, which was affected by the external loading magnitude and the geometry of transducer. However, the maximum stress generated in the Bridge transducer should be limited to prevent material failure. Based on the material strength of PZT and epoxy obtained from material suppliers, the maximum tensile and shear stresses at the inner corner of the contact area between the steel cap and the PZT strip need to be smaller than 40MPa and 17MPa, respectively. Therefore, it is needed to optimize the geometry of Bridge transducer to generate the maximum electrical potential energy within the failure stress criteria.

The geometric parameters considered in the optimization analysis are the PZT strip thickness (t_p), the length of cavity base (L_o), the height of cavity (t_i), the thickness of metal end cap (t_c) and the inner length of metal end cap (L_i) (as shown in Figure 4). The total length of the PZT strip was kept constant (32 mm), and the external loading was 0.7MPa. The ranges of these geometric parameters are listed in Table 3.4. A total of 3,528 combinations of geometrical parameters were considered in the optimization analysis.

Table 3.4 Geometry Parameters of Bridge Transducer Considered in Optimization

Parameters	Baseline value	Range (Min.)	Range (Max.)	Incremental Interval	No. of variables
L_o (mm)	22	18	24	2	4
L_i (mm)	10	5	17	2	7
t_p (mm)	2	1	3	1	3
t_c (mm)	0.6	0.2	0.8	0.1	7
t_i (mm)	2	0.5	3	0.5	6
		Total combinations			3,528

Figures 3.9 and 3.10 present the FEA results for the relationship between geometry parameters and simulation outputs in the Bridge transducer, respectively, for the generated stresses and electric potential energy. Although full factorial analysis with all parameters was conducted, the relationships were plotted to show the effect of individual geometry parameter on the outputs (while the other parameters were kept at constant values) for better illustration. The results show that the interaction between geometry parameters and the stress and energy outputs was complicated. In general, there were no universal patterns that could be observed. Instead, the relationship varied depending on the specific geometry parameter and the output of interest. In general, the

thickness of steel end cap (t_c), the thickness of PZT strip (t_p), and the cavity height (t_i) show relatively more significant effects, as compared to the other parameters. This emphasizes the necessity of optimization analysis that considers the combination of different geometry parameters to achieve the balance between energy harvesting performance and mechanical failure potential.

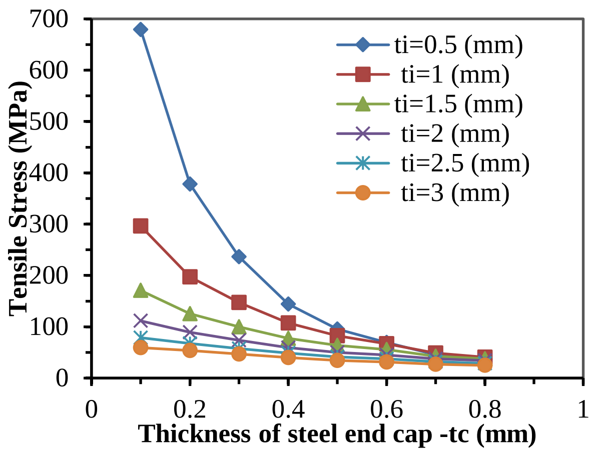

(a)

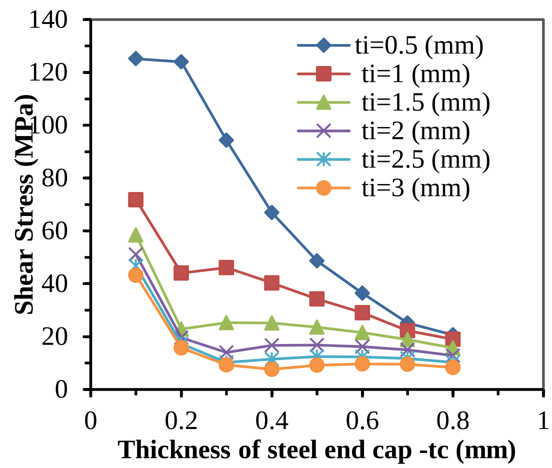

(b)

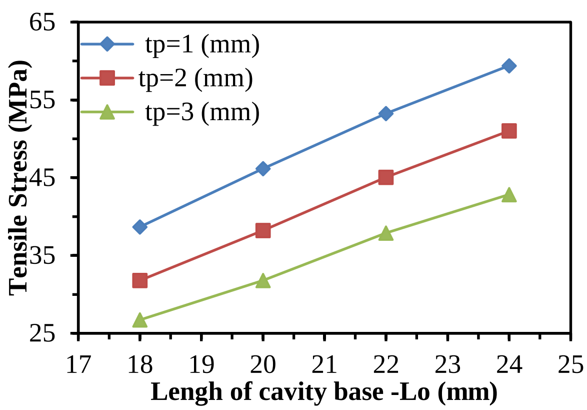

(c)

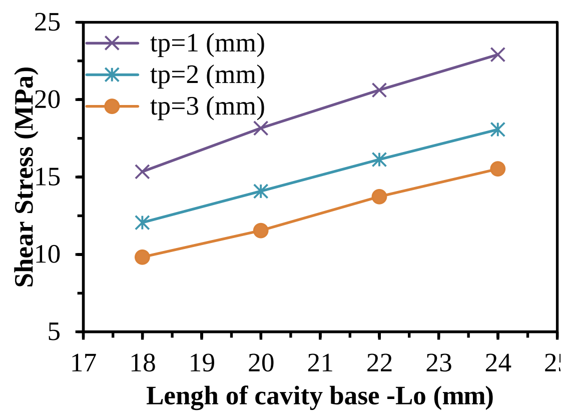

(d)

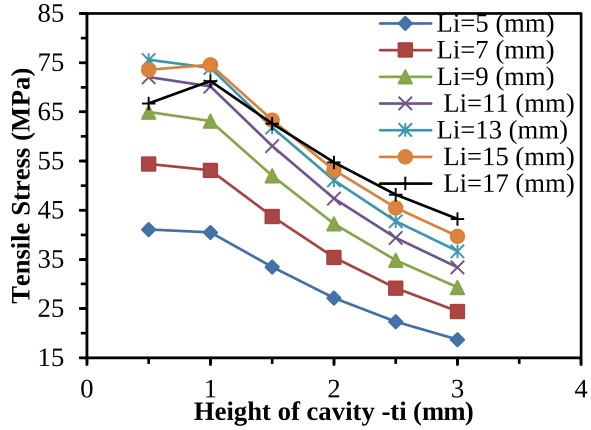

(e)

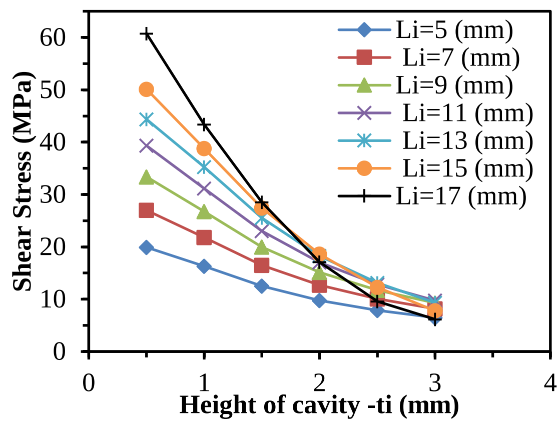

(f)

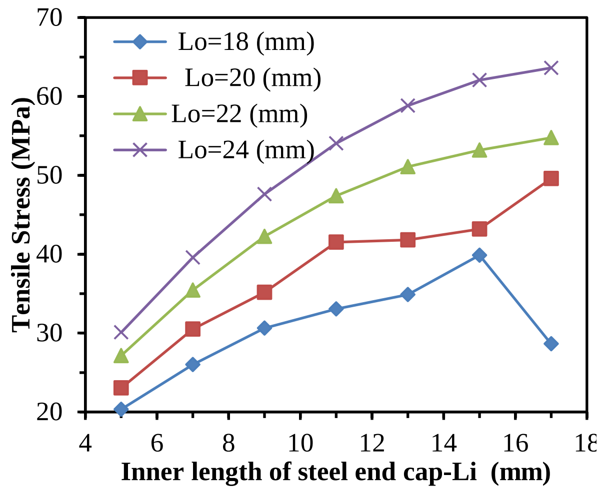

(g)

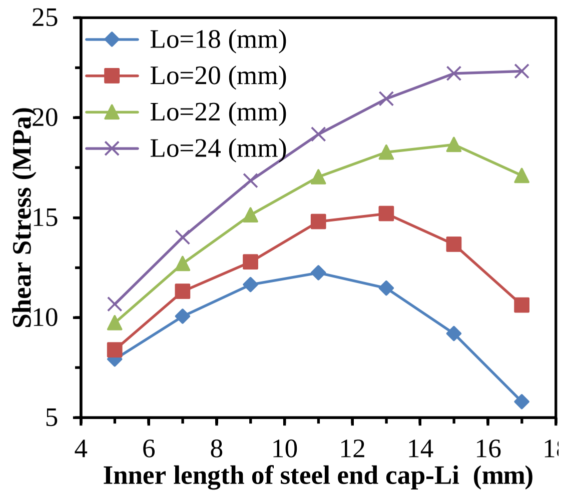

(h)

Figure 3.9 Effect of Geometric Parameters on Generated Stresses for (a) t_c tensile stress;(b) t_c shear stress (c) L_o-tensile stress;(d)) L_o-shear stress (e) t_i-tensile stress; (f) t_i-shear stress; (g) L_i-tensile stress; and (h) L_i-shear stress

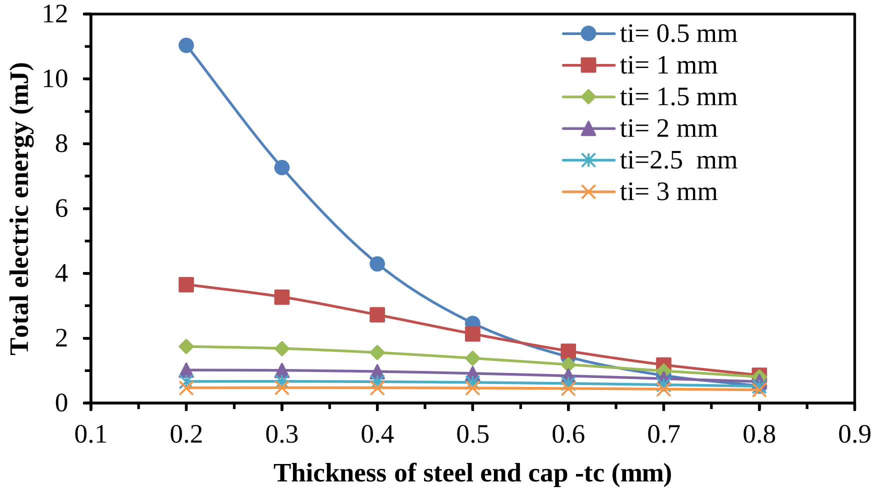

ti= 0.5 mm
ti= 1 mm
ti= 1.5 mm
ti= 2 mm
ti=2.5 mm
ti= 3 mm
Total electric energy (mJ)
Thickness of steel end cap -tc (mm)

(a)

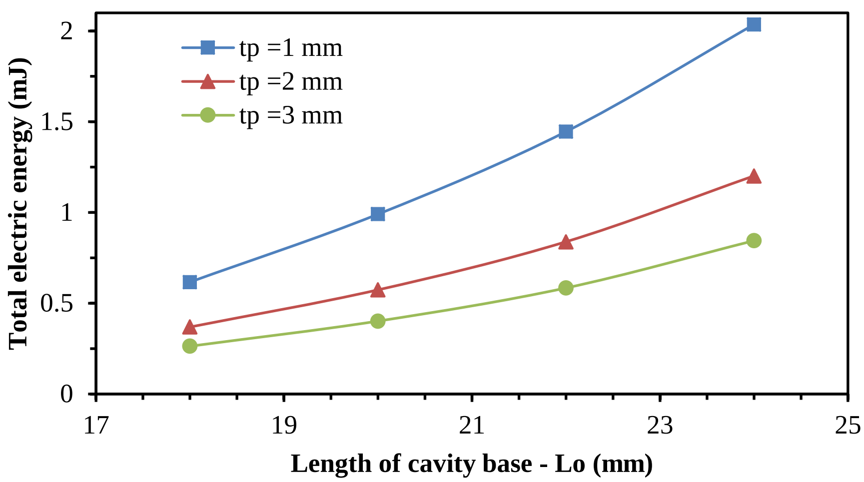

tp =1 mm
tp =2 mm
tp =3 mm
Total electric energy (mJ)
Length of cavity base - Lo (mm)

(b)

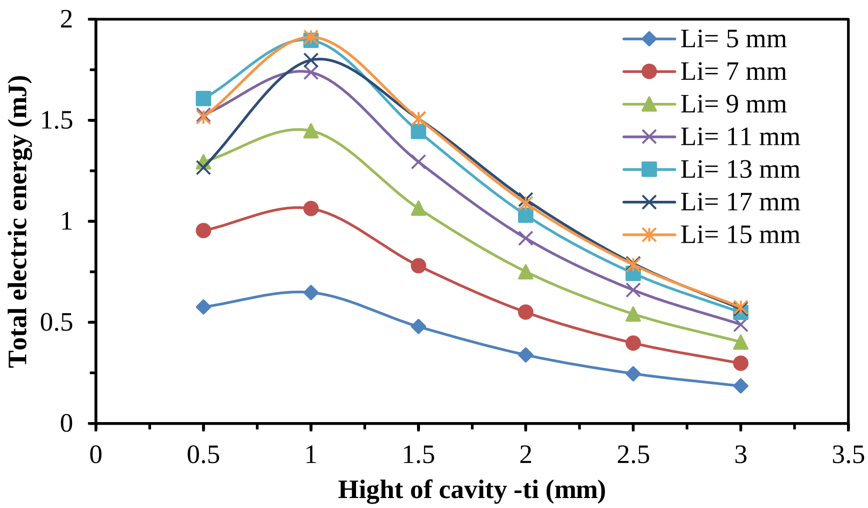

Li= 5 mm
Li= 7 mm
Li= 9 mm
Li= 11 mm
Li= 13 mm
Li= 17 mm
Li= 15 mm
Total electric energy (mJ)
Hight of cavity -ti (mm)

(c)

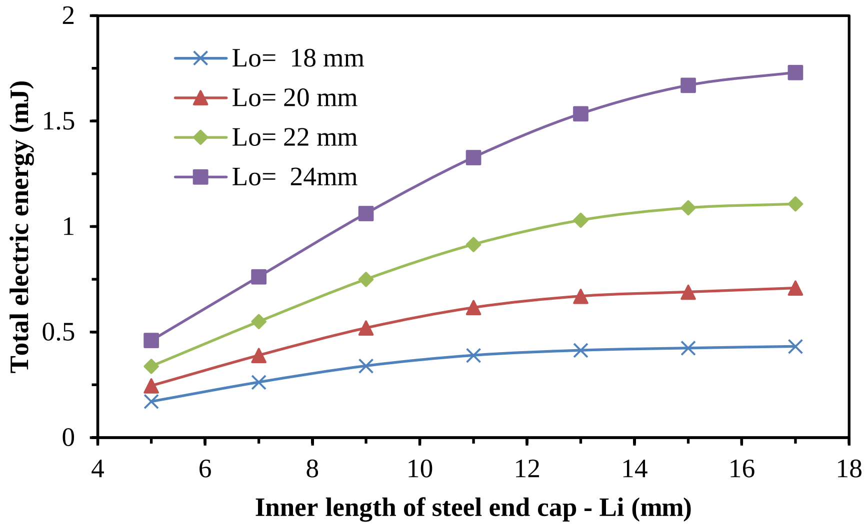

(d)

Figure 3.10 Effect of Geometric Parameters on Generated Energy for (a) tc; (b) Lo; (c) ti; and (d) Li

The induced stresses and total electric energy depends on the thickness of steel endcap. The tensile stress decreases rapidly with the increasing thickness of endcap, which confirms that the transmission ratio of the mechanical energy is higher with thinner endcap. On the other hand, the tensile stresses increase when the cavity height decreases that increases the horizontal component of the applied stress (stretching stress).

It is noted that the total electric energy depends on the thickness of PZT strip under the same boundary condition. The maximum electric energy is obtained with 1-mm PZT strip. Even though the output voltage increases with the thicker PZT strip, the electric energy does not increase. This may be due to the variation of effective elastic compliance depending on the steel endcap thickness and PZT strip thicknesses.

Based on the FEA results, the optimized geometric parameters were found as follows: the height of cavity (t_i) = 2.72mm, the thickness of metal cap (t_c) = 0.4mm, the inner length of metal end cap (L_i) = 9.72mm, the length of cavity base (L_o) = 21.5mm, and the PZT strip thickness (t_p) = 2mm. The generated stresses and electrical potential from FEA of the optimized geometry are presented in Figure 3.11, respectively. The results show that within the failure stress criteria, the optimized design of Bridge transducer produced an electrical potential of 556V, which could result in 0.743mJ of potential energy (open circuit condition) for a single transducer under the external stress of 0.7MPa.

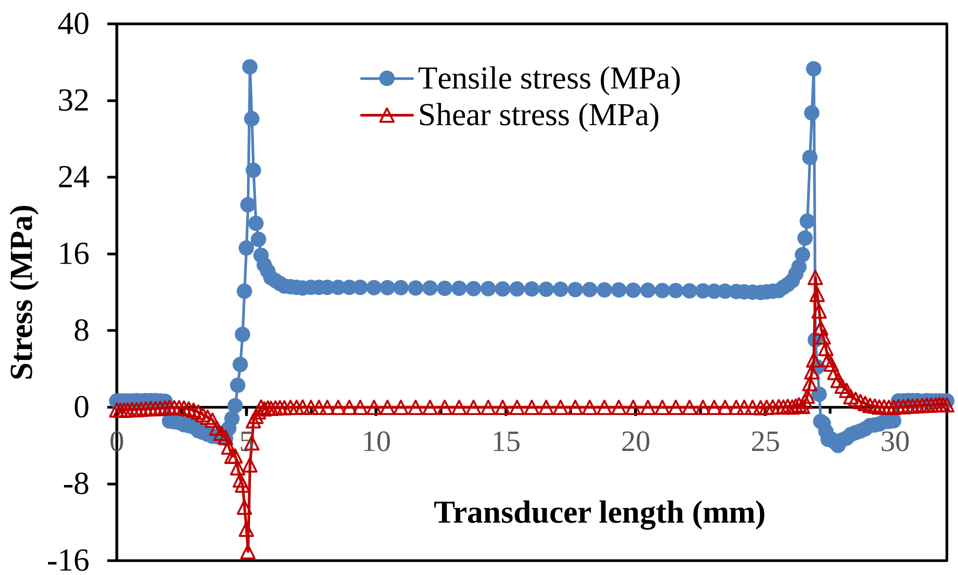

(a)

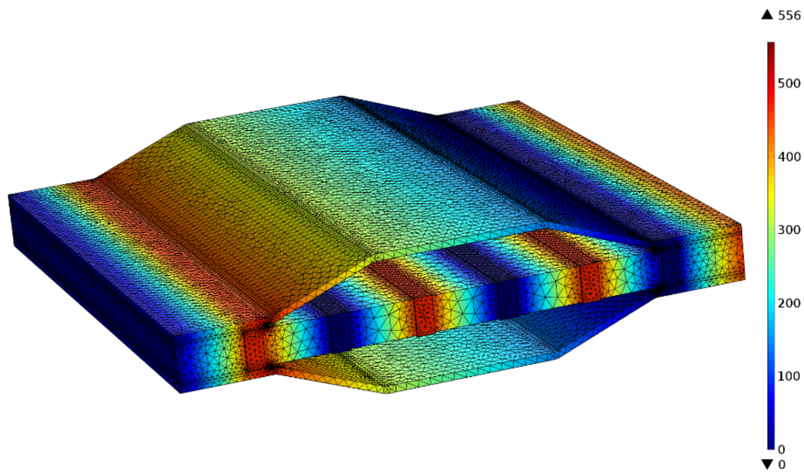

(b)

Figure 3.11 (a) Stress Distributions and (b) Electrical Potential (V) Using Optimized Geometric Parameters of Bridge Transducer with Layered Poling

3.5.4 Laboratory Testing and Validations

The PZT transducer were fabricated and assembled in the modular energy harvester for laboratory testing. The PZT-5X (Sinocera, State College, PA) square plates with side length of 32mm and thickness of 2mm were electroded with DuPont 4095 air fired silver paste. Six electrodes with thickness of 1 mm and an electrode spacing of 3.7mm were applied to the surface and fired. The steel end caps were stamped from 0.6mm thick 4130 alloy steel sheets and then heat-treated to increase hardness. End caps were attached to the ceramics using Henkel Loctite Ablestic 45LV epoxy. The other geometry parameters of transducer were optimized considering the maximum energy output and the failure criteria of mechanical stress.

A total of 64 transducers were assembled in an aluminum casing in four layers, consisting of 16 transducers in a 4x4 configuration within each layer, as shown in Figure

3.12(a). The energy harvester module was fabricated using aluminum with the outer dimension of 177.8mm×177.8mm×76.5mm (7inches × 7inches × 3inches). Nylon strips were used to separate the transducers within each layer vertically. Copper plates were used to separate between layers and act as current collectors. The copper plates were wired together in an alternating configuration to allow for parallel connectivity. The thickness of copper plate is 1.58mm and the thickness of nylon sheet is 1.58mm. A small gap was kept between the top cover and transducer arrays to allow for the applied stresses on the top cover transmitted into transducers. The gap thickness is 5mm (0.2 inch) and the base thickness is 12.7mm (0.5 inches).

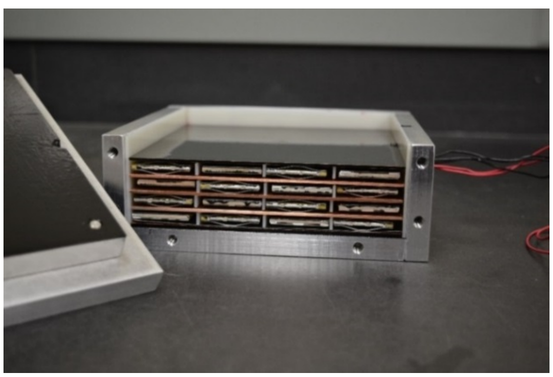

(a)

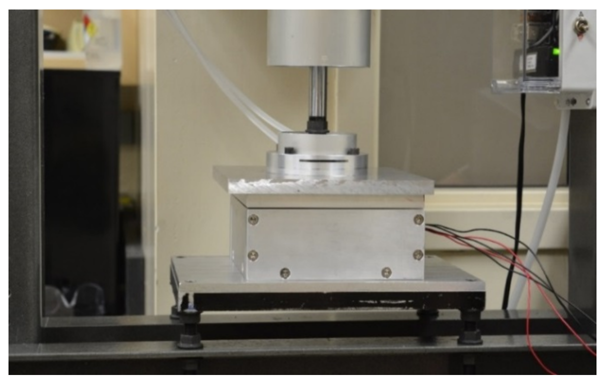

(b)

Figure 3.12 (a) Energy Harvester with 64 Transducers Assembly; and (b) Compression Testing on Energy Harvester

The material and geometry parameters of the optimized Bridge transducer were used in FE simulation of energy module to predict energy output. The elastic modulus of aluminum, nylon, and copper was 70GPa, 2Gpa, and 110Gpa, respectively. The Poison’s ratio of aluminum, nylon, and copper was 0.35, 0.4, and 0.35, respectively. The same mesh sizes (minimum and maximum) of single transducer were used to in the FE model of energy harvesting module that contains 64 transducers.

Vehicular loading was simulated using a pneumatic piston. The loading pressure was 70kPa repeated at 5Hz. Figure 3.12(b) shows the experimental setup of energy harvester module under compression loading. The simulation results were compared to laboratory measurements and showed good agreements, as shown in Figure 3.13. In addition, the energy efficiency of energy-harvesting module with new transducer design was compared to the one with conventional design using finite element simulation. The maximum output power of 2.1mW was found at resistive load of 400kΩ for the system with new design; while the system with conventional design only produced 0.3mW energy. As the resistive load increases, the output power increases first and then decreases. The output power is greater at relatively high resistive loads due to the high impedance of transducers. Therefore, it is necessary to use a step down converter to decrease the impedance to utilize energy output for powering electronic devices.

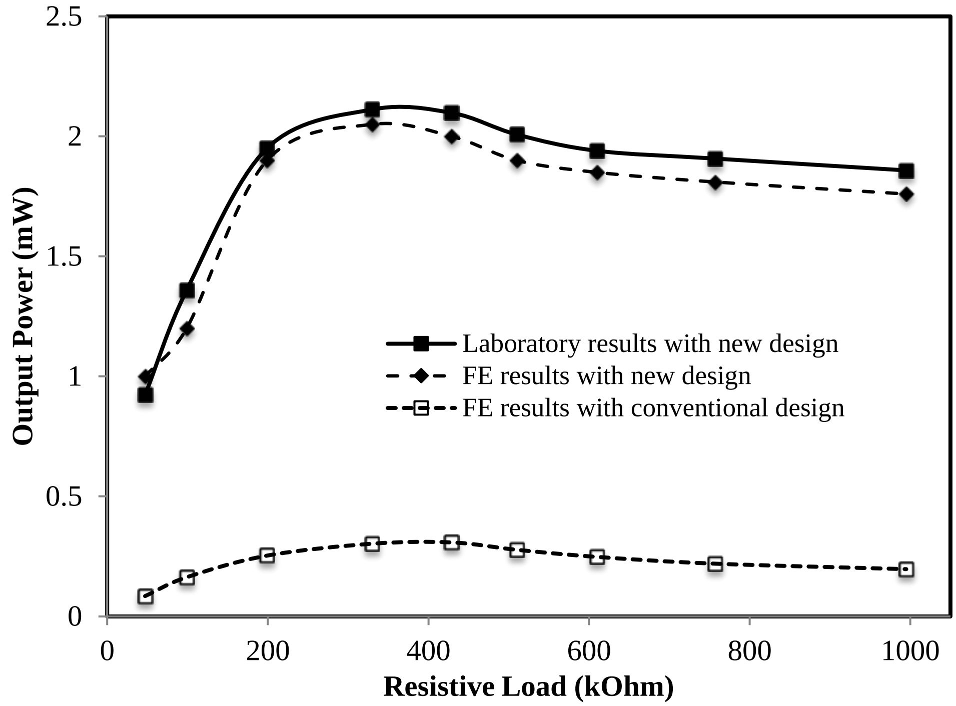

Figure 3.13 Output Power of Energy Harvester (70kPa loading pressure at 5Hz)

3.6 SUMMARY

This chapter aims to develop a novel design of piezoelectric transducer with the optimized geometry that is targeted for energy harvesting in roadway under vehicular loading. The Bridge transducer with layered poling and electrode design is proposed to enhance energy output. Finite element analysis (FEA) was conducted to predict energy output and stress concentration in the transducer. Multi-physics simulations were conducted to evaluate energy outputs using different lead zirconate titanate (PZT) materials, loading magnitudes, transducer types, and geometry parameters. The optimum configuration of transducer geometry was evaluated considering the balance between energy harvesting performance and mechanical failure potential due to stress concentrations. The novel design of Bridge transducer with layered poling and electrodes produces much greater energy than the traditional Bridge and Cymbal transducer. The results show that within the failure stress criteria, the optimized design of Bridge transducer produced an electrical potential of 556V, which could result in 0.743mJ of potential energy (open circuit condition) for a single transducer under the external stress of 0.7MPa. Laboratory testing on energy harvester module showed that simulation results agreed well with the measured power.

It was found that there were no universal relationships that could be observed between geometry parameters and mechanical stresses and energy outputs for the Bridge transducer. The effects of geometry parameters on stress concentration and energy outputs were complicated. The thickness of steel end cap and PZT strip and the cavity height show relatively more significant effects.

CHAPTER 4 LABORATORY TESTING AND NUMERICAL SIMULATION OF PIEZOELECTRIC ENERGY HARVESTER FOR ROADWAY APPLICATIONS

4.1 INTRODUCTION

Roadways are one of major civil infrastructures that plays an important role in connecting communities and moving people. Traditionally, roadways are regarded as structures that carry traffic loading. Recently, researches have been conducted to explore the potential of energy harvesting from roadways, including solar, thermal, and kinetic energy Chiarelli *et al.* 2017; Guldentops *et al.* 2016; Guo and Lu 2017; Pascual-Muñoz *et al.* 2013; Shaopeng *et al.* 2011; Wang *et al.* 2018.

Vehicle movement on roadways induces mechanical deformation in the pavement system, which produces mechanical energy that can be harvested using piezoelectric material. There are two important types of PZT transducers that can be used to harvest energy from the ambient environment: vibration-based and stress-based. The common design of piezoelectric energy-harvesting devices is based on cantilevers, which utilize vibrations as the source of mechanical input Ali *et al.* 2011; Beeby *et al.* 2006. However, this energy harvesting method requires piezoelectric device to be tuned to the source's specific vibration frequency. On the other hand, stress-based piezoelectric transducers were recommended for energy harvesting for low-frequency non-resonant resources Hill *et al.* 2013; Kim *et al.* 2004.

Zhao *et al.* (2012) compared different designs of piezoelectric transducers and concluded that the Cymbal and Bridge transducers were recommended configurations for energy harvesting in roadway considering the vehicular loading pattern and the stiffness consistency between the transducer and pavement materials. Moure *et al.* (2016) fabricated and tested different configurations of Cymbal piezoelectric sensor to optimize the conversion of mechanical to electric energy. The Cymbal sensors were placed directly in asphalt mixture to evaluate their performance as vibration energy harvesters in roads. The power output of each single sensor was recovered up to 16 μW for one pass of heavy vehicle wheel.

Xiong and Wang (2016) investigated the effect of coupling configuration and material selection on energy efficiency of piezoelectric energy harvester. The harvester was built with PZT rods covered by aluminum alloy to distribute the load. They reported that for roadways applications 15% of applied mechanical energy was transferred to transducers under real traffic condition. Roshani *et al.* (2016); Roshani *et al.* 2017 developed highway sensing and energy conversion (HiSEC) modules using various configurations of boxes containing different numbers of PZT rod elements sandwiched between two copper plates. Through laboratory testing, they concluded that the number and size of piezoelectric disks and the loading magnitude and frequency can significantly the output voltage. Yang *et al.* (2017) designed a piezoelectric energy harvester with multilayer stacked array. The energy harvesters consisted of nine piezoelectric disks (PZT-5H) stacked in parallel inside a 30×30×6.8 cm (length× width ×height) box. After repeated loadings, it was found that the average output of the energy harvester was 174 V (open circuit) and there was no significant reduction in power generation.

Song *et al.* (2016) designed and optimized an energy harvester for roadway applications using piezoelectric cantilever beams. The designed energy harvester had a volume of 30×30×10 cm^3 containing 48 piezoelectric beams. The developed energy harvester generated output power of 184 mW. Jung *et al.* (2017) demonstrated a piezoelectric energy harvester module based on polyvinylidene fluoride (PVDF) polymer for roadway applications. The module of 15×15×9 cm (length× width ×height) exhibits 0.2W output with 8W/m^2 power density. In addition, the stable performance and durability was noticed after over million cycles of loading.

Chen et al. Chen *et al.* 2016 developed mechanical harvesting energy (MEH) device made of two square-shaped thickness-polarized PZT bimorph of parallel type. The MEH device was embedded in the asphalt mixture specimen at a depth of 10 mm and found that the output power depended on the loading period, location, and size of the piezoelectric device. In addition, the researchers concluded that selecting appropriate material and geometry parameters for practical traffic conditions are very important for energy harvesting system.

Guo and Lu (2017) introduced the energy harvesting pavement system (EHPS) that consisted of one piezoelectric material layer in the middle of two conductive asphalt layers. The prototype was tested in the laboratory and compared to the results from three-degree-of-freedom electromechanical model. It was found that more piezoelectric elements with higher piezoelectric stress constant and more flexibility of conductive asphalt mixtures can improve the energy harvesting performance of EHPS.

Most previous researches have investigated different piezoelectric energy harvester designs for stress-based energy harvesting from roadway, including disk or rod shape, cantilever beam, bimorph, Cymbal, and Bridge. Among different designs, disk- or rod-shape PZT transducers were most commonly used due to its easy fabrication, although its energy harvesting performance may not be as significant as other transducer designs. On the other hand, the generated energy output is usually small for single piezoelectric transducer. Thus, multiple arrays of piezoelectric transducers are usually stacked and packaged to generate the energy under repeated traffic loading. However, the effects of packaging material and fatigue loading on the durability of piezoelectric materials have not been studied. Therefore, further investigation is needed to evaluate energy output and long-term performance of energy harvester with different transducer types and packaging designs.

4.2 BRIDGE TRANSDUCER WITH LAYERED POLING

4.2.1 Theoretical Background

Piezoelectric materials like lead zirconate titanate (PZT) contain dipoles that naturally randomly orient. When mechanical stress is applied to PZT material, the dipoles rotate from original orientation, causing electric and mechanical energy to store in the dipole Kamel 2007. The constitutive equations for linear piezoelectric material under low stress levels can be written as shown in Equation (4.1), (4.2), and (4.3).

$$x = s^D X + gD \tag{4.1}$$

$$E = -gX + \beta^X D \tag{4.2}$$

$$g = \frac{d}{\varepsilon_o \varepsilon_r^X} \tag{4.3}$$

Where, X is the stress; x is the strain; D is the electric displacement; E is the electric field; s is the elastic compliance; β is the dielectric susceptibility which is equal to the inverse dielectric permittivity tensor component; g is the piezoelectric voltage coefficient; d is the piezoelectric charge constant; ε_r^X is the relative dielectric constant of PZT in the 3rd axial direction; and ε_o is the dielectric constant of vacuum (8.85 x 10^{-12} Farad / m).

Under an applied force, the open circuit output voltage of the piezoelectric ceramic can be calculated from Equation (4.4).

$$V = E \cdot t = -g \cdot X \cdot t = -\frac{g.F.t}{A} \tag{4.4}$$

Where, V is the voltage; t is the thickness of piezoelectric ceramic; F is the applied force; A is the area of piezoelectric ceramic element; and X is the stress.

The charge (Q) and capacitance (C) generated on the piezoelectric ceramic can be determined from Equation (4.5) and (4.6).

$$D = \frac{Q}{A} = \frac{E}{\beta^X} = \frac{V.\varepsilon_o.\varepsilon_r^X}{t} \tag{4.5}$$

$$\frac{Q}{V} = \frac{\varepsilon_o.\varepsilon_r^X.A}{t} = C \tag{4.6}$$

Where, Q is the charge of piezoelectric ceramic; and C is the capacitance of piezoelectric ceramic.

The above relationship shows that at low-frequency loading, the piezoelectric ceramic can be assumed to behave like a parallel plate capacitor. Hence, the electric power available under the cyclic excitation is given by Equation (4.7).

$$P = {}^1\!/_2\, CV^2.f \tag{4.7}$$

Where, P is the electric power; and f is the frequency of cyclic loading.

The electrical power is dependent upon the capacitance of piezoelectric material. The increase of capacitance will generate high power when the piezoelectric ceramic is directly employed for energy harvesting. The relationship between piezoelectric capacitance and the number of segments between electrodes is shown in Equation 4.8 and 4.9.

$$\mathrm{C} = n^2 \times \frac{\varepsilon_r^X \, \varepsilon_0 \, \mathrm{A}}{t} \tag{4.8}$$

$$\mathrm{t_p} = t/n \tag{4.9}$$

By substituting Equation 4.9 in 4.8, Equation 4.10 can be obtained as follows.

$$\mathrm{C} = n^2 \times \frac{\varepsilon_r^X \, \varepsilon_0 \, \mathrm{A}}{t} \tag{4.10}$$

Where, n is the number of PZT segments; and t is the thickness of each segment along the poling direction.

4.2.2 Fabrication of Bridge Transducer

In general, mechanical energy is more efficiently converted to electrical energy when the force is parallel to the poling direction rather than the case when the force is perpendicular to the poling direction. For most PZT materials, the parallel piezoelectric coefficient is more than twice the perpendicular piezoelectric coefficient Li *et al.* 2014.

The Bridge transducer consists of a PZT disk sandwiched between two metal end caps. The PZT disk usually has the square shape for Bridge transducer. Traditionally, vertical poling is used to produce electrodes positioned on the upper and lower surfaces of PZT strip and the perpendicular piezoelectric coefficient is utilized. It is not feasible to apply horizontal poling due to the electric field required for poling along the length/width of PZT strip. In this chapter, a new design of Bridge transducer with layered poling and electrode configuration was developed based on available laboratory material (Jasim *et al.* 2017). The new design employs the parallel piezoelectric coefficient under the applied stress, which results in the greater energy output than the conventional design with poling along the thickness of PZT strip (Yesner *et al.* 2016).

The available laboratory material had the following dimensions: PZT (L_c) = 32×32 mm (square shape), PZT thickness (t_P) = 2 mm, and steel end cap (t_c) = 0.6 mm. The inner length of the steel end cap attached to the ceramic plates was modified to satisfy the tensile and share requirement of 40 and 17 MPa, respectively. An inner length value (L_i) range between 4-12 mm was selected using finite element analysis to maximize the output energy and satisfy stresses limitations. The results shows that the inner length (L_i) of 5 mm satisfied both tensile and shear stresses.

The Bridge transducers were fabricated using the following procedure. A square-plate ceramic PZT-5X with the side length of 32 mm and the thickness of 2 mm were electroded using silver paste. Figure 1(a) shows that the single ceramic strip with seven sections of horizontally-poled cells connected parallel to each other. The electrodes divide the ceramic into seven segments with an inter-electrode spacing of 3.71 mm and an electrode width of about 1 mm, as shown in Figure 4.1(b). The electrode ceramics were poled at 80ºC in silicon oil while held in a Teflon fixture. Wires were pressed against the surface electrodes to connect them in parallel and 8kV was applied. After poling, epoxy was applied on the side of ceramics to form insulating layers between electrodes. Then conductive epoxy is applied on top of the insulating layer to connect the electrodes in parallel. Finally, the steel end caps were stamped from annealed 0.6-mm thick 4130 alloy steel sheets and then heat-treated to increase hardness. Steel end caps were attached to the ceramics using Henkel Loctite Ablestic 45LV epoxy with constant pressure during curing. Figure 4.1(c) and (d) show the fabricated Bridge Transducer and the detailed geometry parameters, respectively.

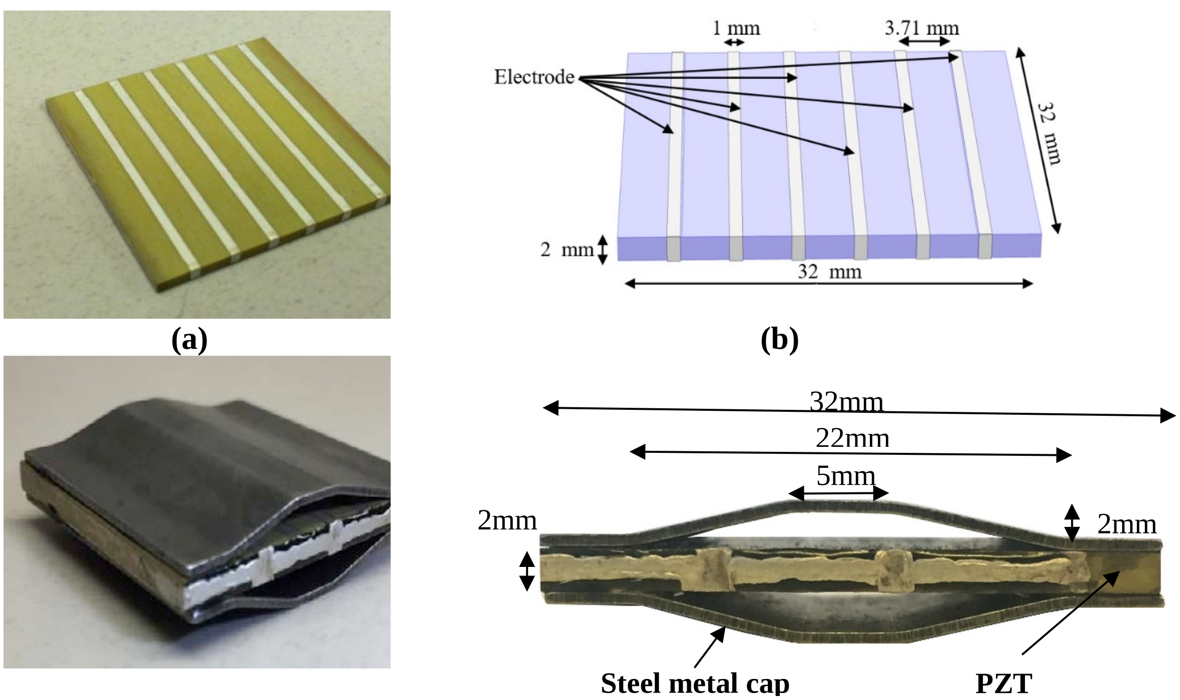

(c) (d)

Figure 4.1(a) PZT strip with layered poling and electrodes; (b) dimensions of PZT strip; (c) fabricated Bridge transducer; and (d) geometry parameters

The multi-layer electrode arrangement in the Bridge transducer produces large capacitance, which enhances the effective piezoelectric coefficient and can effectively employ the charge stored in the transducer. Base on Equation (10), the current design of Bridge transducer with seven segments of capacitive cells has the capacitance that is 49 times that obtained with single segment (traditional transducer).

4.3 EXPERIMENTAL TESTING AND NUMERICAL MODELING OF ENERGY HARVESTER

4.3.1 Laboratory Testing

A total of 64 transducers were assembled in the energy harvester in four layers, consisting of 16 transducers in 4×4 configurations in each layer, as shown in Figure 4.2. The assembled transducers were arranged inside an aluminum case. The case interior was coated with insulating epoxy, and the sides were lined with nylon. Nylon strips were used to separate the transducers within each column. Copper plates were used to separate each layer and act as current collectors, as shown in Figure 4.2(a). The copper plates were wired together in an alternating configuration to allow for parallel connectivity. The outer dimension of energy harvester module was 17.8×17.8×7.6 cm, as shown in Figure 2(b).

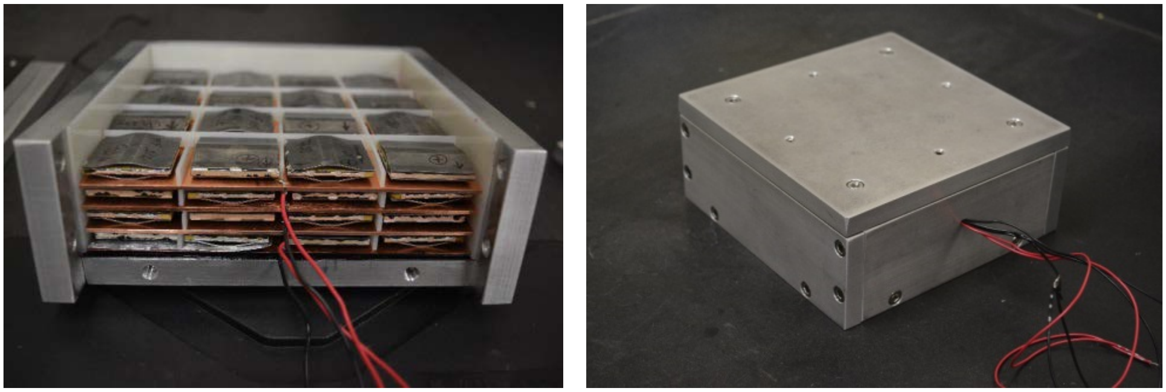

(a) (b)

Figure 4.2 Energy harvester with transducer arrays: (a) inside; (b) outside configurations

Laboratory testing of the fabricated energy harvester was conducted to simulate repeated traffic loading on roadway. The pneumatic loading system can repeatedly apply the maximum load of 3.56 kN (800 Ib) at a frequency up to 5 Hz. Figure 4.3 shows the experimental setup of energy harvester with compressive loading. Single loading pulses were applied with different loading magnitudes; while cyclic loading pulses were applied at different frequencies.

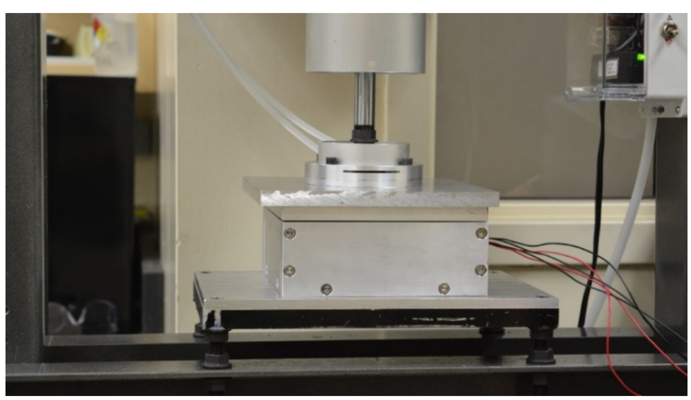

Figure 4.3 Experimental setup of energy harvester under compressive loading

To measure the energy generated from a single loading, the voltage was measured across the capacitor in an open circuit. The value of the resistor R in the circuit is 10 MOhm, which came from the high impedance probe of the oscilloscope. A low-loss 90 nF capacitor was used. The power generated from cyclic loading depends on the resistance, or impedance of the electric load. Power was calculated using the product of the voltage across the resistive load and the current that flows through it. If the resistive load was small, current could easily pass through but the voltage will be low. If the load was very large, voltage would be high but little current would flow through the resistor. The maximum power occurred at an intermediate resistive load and it was determined experimentally. A larger capacitor with a value of 10 μF was used to smooth the ripples in voltage caused by cyclical loading. A load of 500 lb at different frequencies of 0.5, 1, 2, and 5Hz were used. The voltage on the capacitor increased until a constant voltage was obtained. This was repeated using different resistive loads from 50 kOhm to 1 MOhm. Figure 4.4 illustrates the electric circuit for measuring the generated power using capacitance, resister and rectifier.

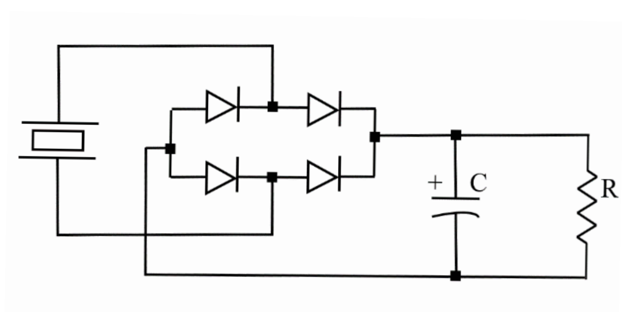

Figure 4.4 Electrical circuit for measuring generated power

4.3.2 Finite Element Simulation

Multiphysics finite element (FE) simulations with commercial software, COMSOL, were conducted to evaluate energy harvesting performance of piezoelectric transducers under external mechanical loading. For the mechanical boundary condition, the module was fixed at the bottom, while the distributed load was applied on the top surface of module. The movements of the vertical boundaries were restrained only in the horizontal directions (x and y-direction). The electrical boundary condition of PZT transducer was set on copper layers (ground and terminals). Two copper sheets were set as ground boundary (zero voltage), while the terminal connection was set on the remaining three copper sheets (positive voltage). Figure 4.5(a) shows the schematic illustration of energy harvester module with boundary conditions.

An adequate mesh size is important to produce accurate results from finite element analysis. Tetrahedral (3-D) elements with different mesh sizes were used in the FE model. The COMSOL software requires the inputs of minimum and maximum element size and assigns element sizes using geometry dimensions as a guide. The right mesh size was determined considering the balance of accuracy and computational efficiency. The final mesh sizes were selected through sensitivity analysis when the changes of stress outputs were smaller than 5% as the element size decreases. The selected minimum and maximum element size is 0.322 mm and 1.0 mm, respectively. Figure 4.5(b) shows the element meshes of energy module and single Bridge transducer in FE model.

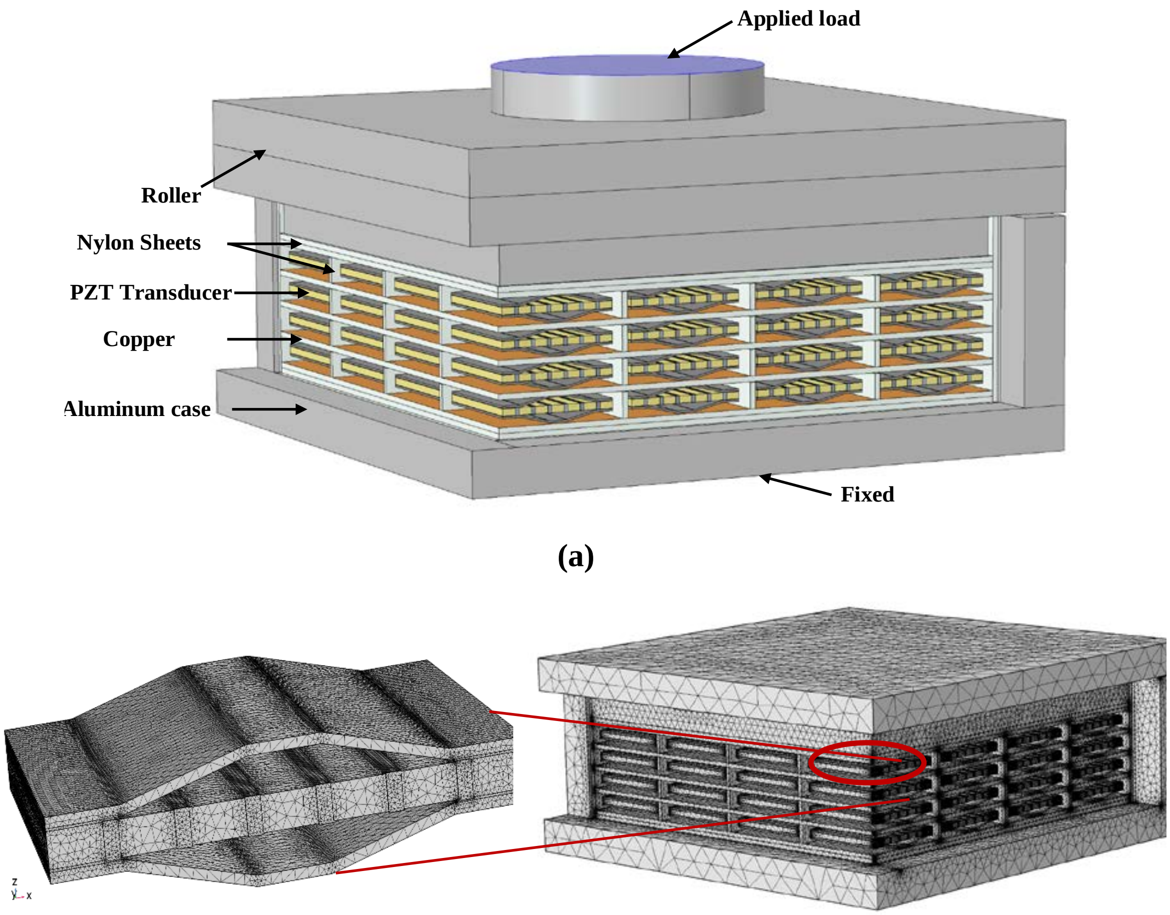

(a)

(b)

Figure 4.5 Schematic illustrations of (a) energy harvester module; and (b) finite element model meshes

The mechanical properties of each material used in the Bridge transducer and energy module were summarized in Table 4.1. The piezoelectric properties of PZT 5X was summarized in Table 4.2.

Table 4.1 Mechanical material Properties for Simulation

Material	**Elastic modulus (GPa)**	**Poison's ratio**	**Density (Kg/m^3)**
PZT strip	61	0.35	7400
High-strength alloy steel	200	0.33	7850
Epoxy	2	0.33	1430
Copper	110	0.35	8700
Aluminum	70	0.33	2700
Nylon	2	0.4	1150

Table 4.2 PZT 5X Piezoelectric Properties for Simulation

Material properties	**Symbol**	**Value**
Piezoelectric Charge Constants (pC/N)	$\mathbf{d_{33}}$	750
	$\mathbf{d_{31}}$	-320
Piezoelectric Voltage Constants (10^{-3}Vm/N)	$\mathbf{g_{33}}$	19
	$\mathbf{g_{31}}$	-8.2
Relative Dielectric Constants	$\boldsymbol{\varepsilon^X_r = \varepsilon^X_{33}/\varepsilon_0}$	4500
	$\boldsymbol{\varepsilon^X_r = \varepsilon^X_{11}/\varepsilon_0}$	4410
Elastic compliance at constant electric field (10^{-12} m^2 /newton)	$\mathbf{S^E_{11,22}}$	16.4
	$\mathbf{S^E_{12,21}}$	-4.78
	$\mathbf{S^E_{32,31,23,13}}$	-8.45
	$\mathbf{S^E_{33}}$	23.3
	$\mathbf{S^E_{44,55}}$	43.5
	$\mathbf{S^E_{66}}$	42.6

Figure 4.6 compared the voltages and energy outputs under single pulse loading at different load levels, respectively, obtained from laboratory measurements and FE simulation. Only the loading stage of the transducers was counted for this measurement because loading and unloading would generate energy twice from the rectified output of transducers. A positive relationship between loading force and energy generated was

found. This indicates that the field performance of energy harvester depends on vehicle weights and axle configurations, in addition to the traffic volume.

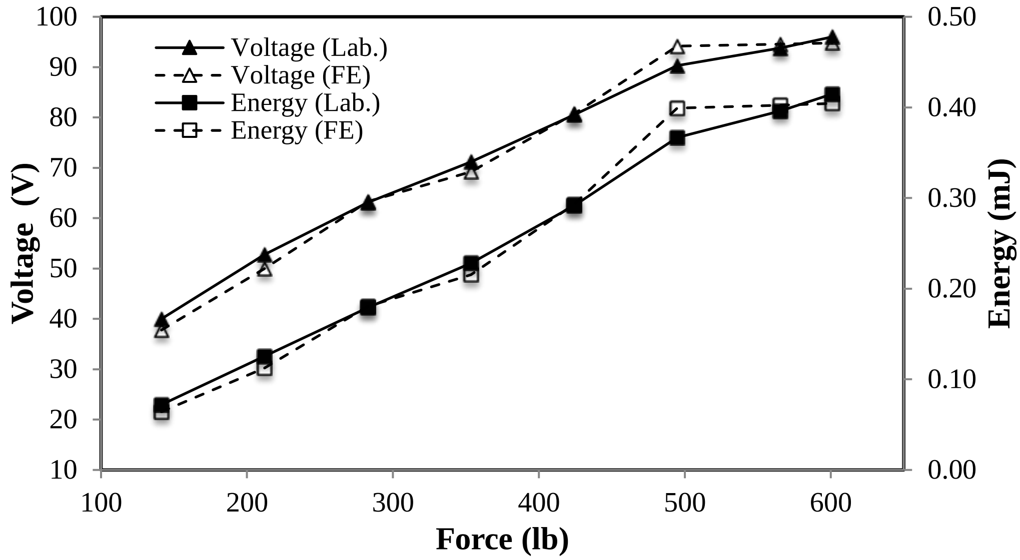

Figure 4.6 Output voltage and energy of energy harvester module under single pulse loading

Figure 4.7 shows the calculated and measured power output values at different loading frequencies and resistive loads. For the purpose of comparison with experimental results, the same load of 2.224 kN (500 lb) were applied on the top of harvesting module. Four different frequencies were selected to examine the effect of loading frequency on energy output of energy harvester module. The output of the transducers was rectified so the charge generated from loading and unloading within each loading cycle is additive for energy generation. The results show that the energy output increases as the loading frequency increases. This indicates that the energy output will be significantly affected by vehicle speeds when the energy module is embedded in the roadway. On the other hand, the maximum output power of 2.1 mW was found at a resistive load of 400 kΩ at the loading frequency of 5 Hz. The output power is greater at high resistive load due to the high impedance of transducers. Both Figure 4.6 and Figure 4.7 indicate that the predicted voltages and power outputs obtained from FE simulation match well with experimental measurements. This validates the developed simulation model that is used for further analysis.

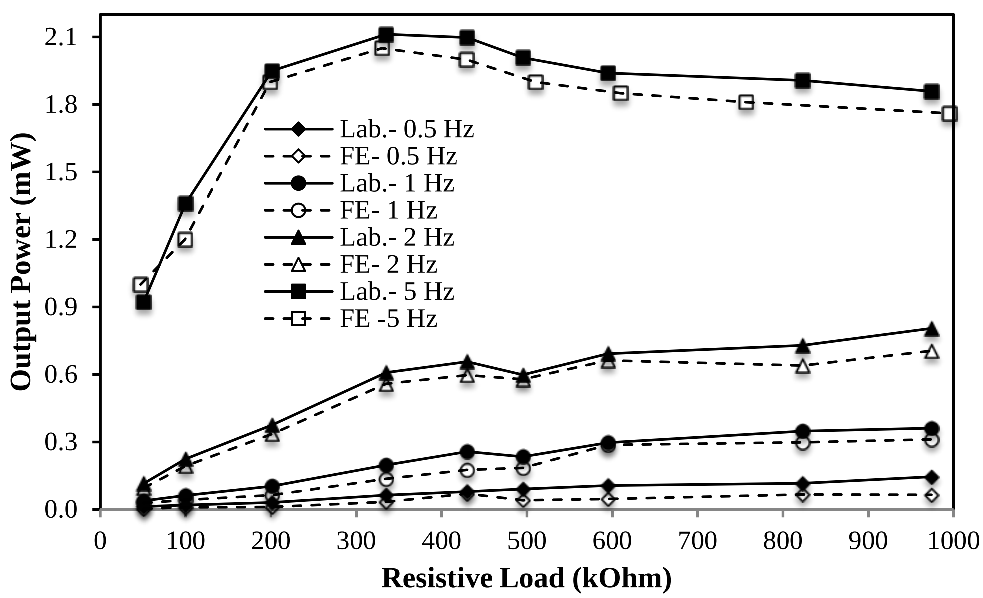

Figure 4.7 Output power of energy harvester module at different frequencies

4.3.3 Fatigue Failure of Transducer

Cyclic loading was applied to evaluate the fatigue behavior and durability of piezoelectric transducers. After 36,000 loading cycles of 2.224 kN (500 Ib) at 5 Hz and 21,600 loading cycles of 3.114 kN (700 Ib) at 1 Hz, the output energy and power of piezoelectric generator decreased. The transducer module was then disassembled for forensic study, which revealed that 12 transducers were not functioning (Yesner *et al.*

2017). The failure patterns are debonding of PZT strip from steel cap and cracks in the PZT strip. None of the failed transducers caused short-circuiting, which would have completely eliminated the electrical output of piezoelectric generator.

The broken transducers were removed for closer observation. It was found that the epoxy bond between steel cap and PZT strip was separated at one side and the PZT strip was fractured at the other side as shown in Figure 4.8(a) and (b). The thickness of the epoxy layer was measured by microscopy. The typical thickness of epoxy bonding layer between steel cap and PZT strip was found in the range of 90-150 microns; while the thickness of epoxy layer of the transducers with debonding and cracks was about 30 microns as shown in Figure 4.8(c) and (d). This indicates that the reduction of epoxy thickness would increase of stress in the transducer and cause the early failure, which will be further investigated using FE simulations.

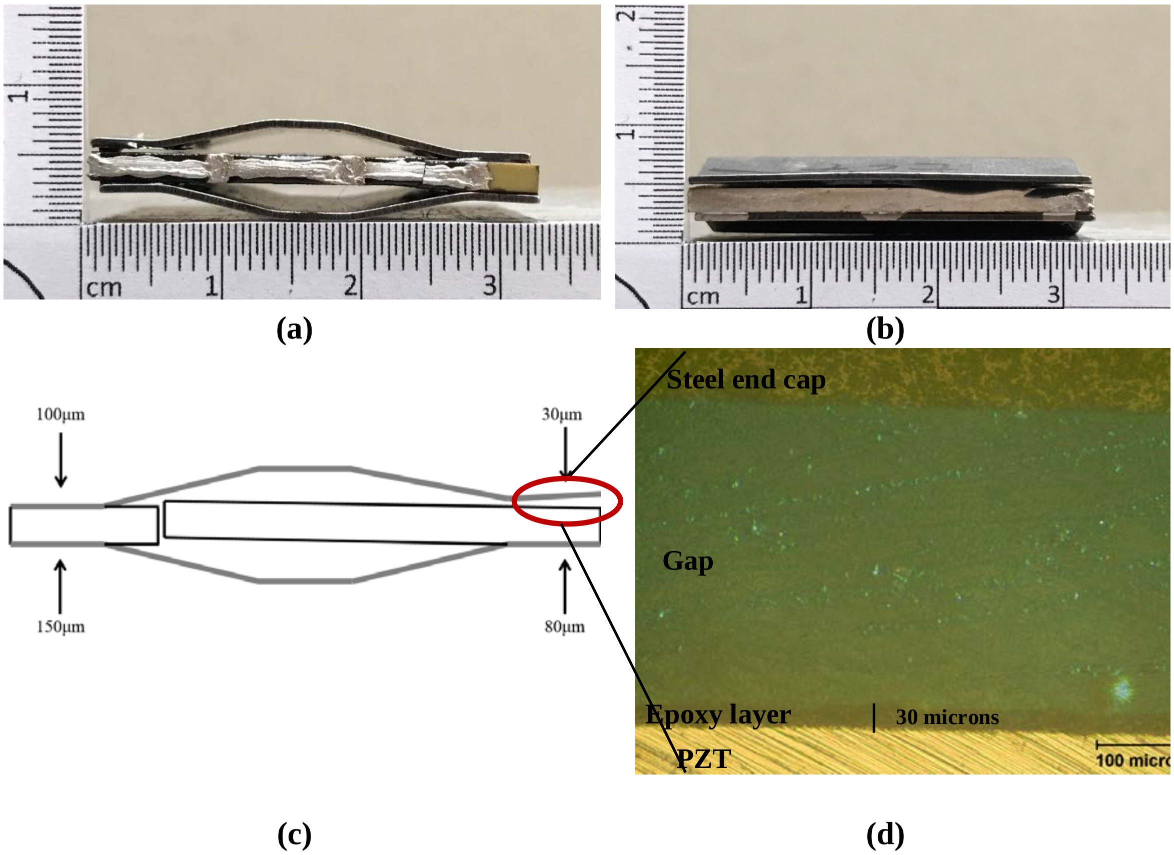

Figure 4.8 Failed Bridge transducers after cyclic loading: (a) front view; (b) side view; (c) thicknesses of epoxy layers; and (d) magnified picture of debonded epoxy

4.4 FACTORS AFFECTING ENERGY HARVESTER PERFORMANCE

4.4.1 Effect of Epoxy Thickness on Transducer Failure

The cyclic testing results in the laboratory show that the thickness of epoxy layer is critical for fatigue failure of Bridge transducer. Therefore, the effect of epoxy layer thickness on mechanical stresses and failure potential of PZT transducer was analyzed using the results obtained from FE models.

The mechanical stress in the Bridge transducer under the external loading was investigated. The applied stress was assumed as 0.7MP at 5Hz on the top surface of Bridge transducer as the representative external loading considered in this study. Although the real stresses in the pavement vary depending on traffic loading (vehicle axle weights and speed) and the embedded location of energy module in the pavement structure, the typical stress condition at the near-surface of asphalt pavement was used Wang and Al-Qadi 2009. Figure 4.9 shows the distribution of axial stresses along the PZT strip and shear stresses at the interface between steel cap and PZT strip, respectively. It was found that the stress concentrations exist at the inner corner of contact area between steel cap and PZT strip. The critical stresses indicate that two different material failure models need be considered in relation to mechanical failure of Bridge transducer, namely tensile and shear failure.

The strength and fatigue characteristics of PZT ceramic material have been studied in previous researches. Anton *et al.* (2012) found that most of soft PZT ceramic materials exhibited similar brittle behavior during three-point bending tests. Chuang *et al.* (1996) measured the fatigue life of PZT-8 specimen using four-point bending configuration. The stress limit of failure was found being 101 MPa with a standard deviation of 7 MPa. The fatigue life of was expresses as a function of maximum tensile stress applied and the results indicated that the macroscopic cracks initiate at load point and inner span which link together to cause failure. Okayasu *et al.* (2009); Okayasu *et al.* 2010 studied the damage characteristics of PZT ceramic during cyclic loading using different electrode materials and poling directions. They found that different mechanical strengths were attributed to the characteristics of electroplating on the PZT ceramic.

To establish the relationship between stress and the number of cycles to failure of epoxy composite, Loos *et al.* (2012) studied the fatigue life of neat epoxy and carbon nanotube reinforced epoxy composite under five different peak loading levels. West System (2005) showed that the stress level to achieve 10^7 cycles in shear was about 11 MPa. The test results did not indicate an endurance limit and an extrapolation of the trend line suggested 9 MPa for 10^8 cycles shear capability. Gonçalves *et al.* (2017) tested batches of specimens under definite levels of stress ratio as a function of loading cycles to obtain the S-N curve of epoxy. The researchers found the limit of 120,000 cycles for the epoxy that exhibited shear strength of 18 MPa with stress ratio of 0.5 or 10 MPa with stress ratio of 0.1.

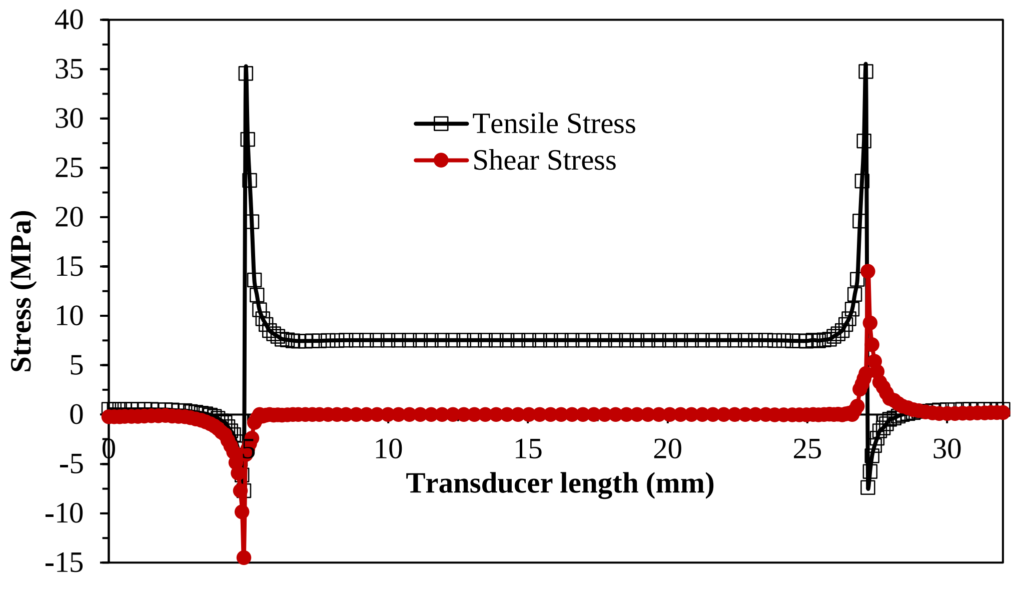

Figure 4.9 Tensile stress and shear stress of single PZT transducer (epoxy thickness is 150µm) at 0.7 MPa

In this study, the fatigue models of PZT ceramic material and epoxy were selected from the existing models presented in the previous work, respectively, as shown in Equation 4.10 and 4.11 Chuang *et al.* 1996; System 2005. In both fatigue models, the relationship between the cyclic stress amplitude (σ) and the number of cycles to fatigue failure (N) is practically linear in semi-logarithmic representation.

$$\text{Log (N)} = 13 - 0.2\,\sigma \tag{4.10}$$

$$\text{Log (N)} = 11.65 - 0.422\,\tau \tag{4.11}$$

Where, σ is the cyclic stress amplitude in tension (for PZT strip); τ is the cyclic stress amplitude in shear (for epoxy); and N is the number of cycles to fatigue failure.

In order to evaluate the effect of epoxy thickness on fatigue failure, the thickness of epoxy layer between steel cap and PZT strip was changed from 50 μm to 150 μm at one location, but kept at 150 μm at the other three locations. Figure 4.10 shows the calculated stress and fatigue life with different thicknesses of epoxy layer in the Bridge transducer, respectively, for tensile and shear failure. The results show that the fatigue life of Bridge transducer decreases significantly as the thickness of epoxy layer decreases, especially for tensile failure. This indicates that cracks may appear first in the PZT strip, which can further increase shear stress and cause the debonding between steel cap and the PZT strip. This finding was consistent with the fatigue failure pattern of transducers observed in the laboratory testing of energy harvester, although the applied stress magnitude was different. It suggests the importance of maintaining the uniform epoxy thickness at the four contact faces between steel cap and PZT strip in the fabrication of Bridge transducer.

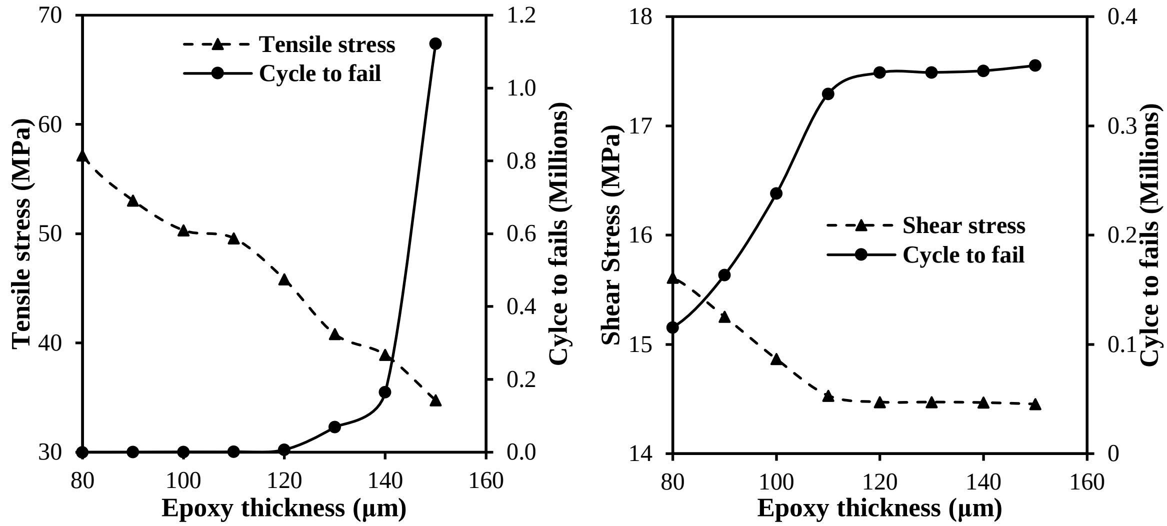

(a) **(b)**

Figure 4.10 Effect of epoxy layer thickness on (a) tensile stress and fatigue life; and (b) shear stress and fatigue life of single transducer under 0.7-MPa compressive stress

4.4.2 Effect of Gap Design on Energy Harvester Performance

After the simulation model of energy harvester is validated with laboratory experiments, it is used to investigate the factors affecting energy harvester performance, including the gap design, the cover and base material, and the transducer type. A gap was originally designed between the top cover and base support part in the energy harvester module, as shown in Figure 4.11. The existence of gap can transfer all the stresses applied on the top cover to the first row of transducers, thus increase the generated energy output. However, in practice, the gap may be clogged by very fine particles when the module is embedded in pavement layers. Therefore, the effect of gap design on energy output is investigated.

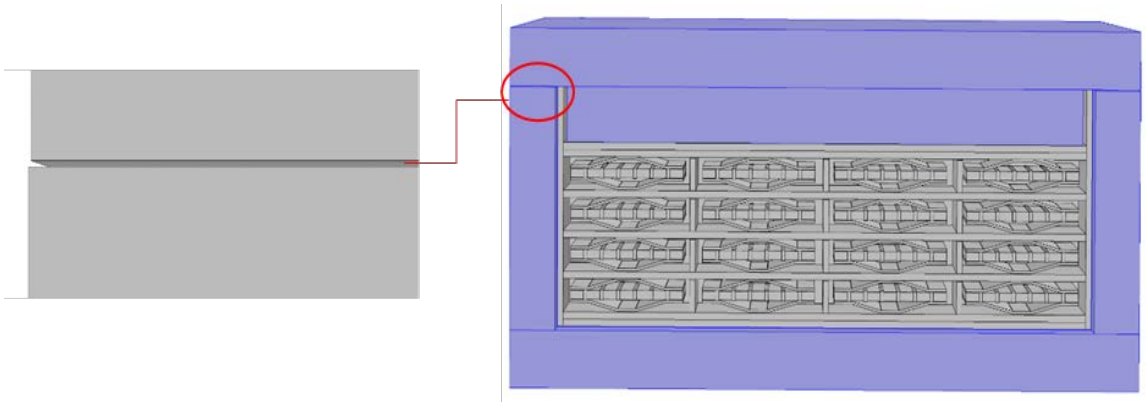

Figure 4.11 Gap design between top cover and base of energy harvester module

Figure 4.12 (a) and (b) show the effect of cover gap on tensile and shear stresses of PZT transducers at the top layer under 0.7-MPa loading stress on the top surface of energy harvester. The stresses distributed uniformly on each transducer in the case with gap; while the stress becomes smaller and slightly concentrated at the transducers in the central region in the case without gap. Therefore, the gap design has a significant effect on the amount of produced power and fatigue failure of PZT transducer.

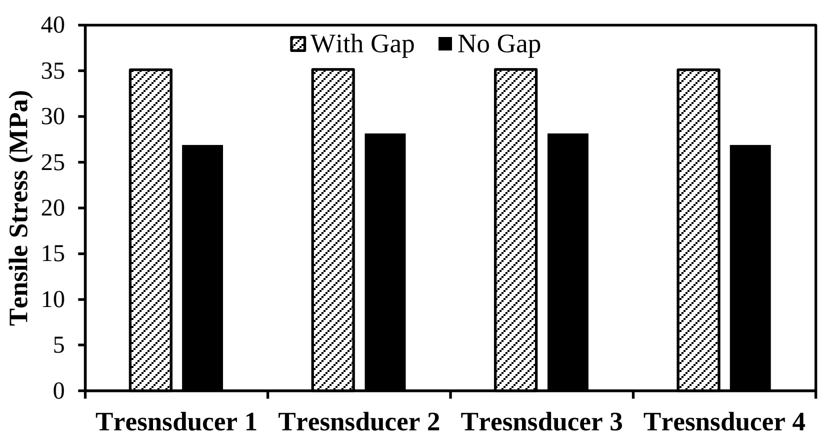

(a)

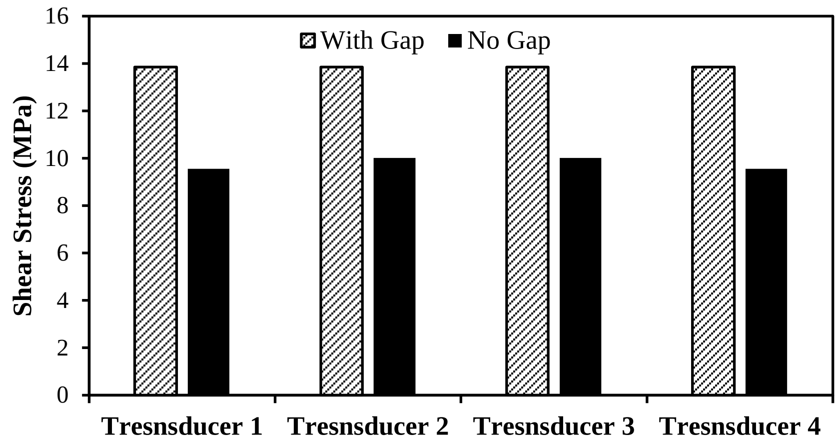

(b)

Figure 4.12 Effect of cover gap on (a) tensile stress and (b) shear stress of PZT transducers at the top layer

Using the resulted tensile stress in the PZT material under external loading, the energy produced from the case without gap was found about 50% of that generated by the gap configuration. At 0.7-MPa loading stress with loading frequency of 5 Hz, the energy module with gap can produces 28.7 mW while the energy module without gap produces 15.1 mW at resistive load of 400 kΩ. On the other hand, the fatigue life of the energy module with the gap is 2.06×10^6 cycles while the fatigue life increases to 10.4×10^6 cycles with closing the gap of energy harvester. The fatigue life here was defined as the number of loading cycles that caused 50% of total transducers in the energy module nonfunctional due to mechanical failure. The results indicate that although the energy output under single loading event is reduced when the gap is closed, the fatigue of PZT transducer increases due to the reduction of mechanical responses.

4.4.3 Effect of Cover/Base Material on Energy Harvester Performance

The energy harvester contains two main parts: the top part (cover) and the bottom part (base). It is expected that for the energy harvester module without gap between the cover and base, the mechanical properties of material used for cover part will affect the deformation of cover and accordingly the stress induced on the PZT transducers. In the analysis, four types of materials, including high-strength alloy steel, copper, aluminum, and concrete were used for the cover and base part of energy harvester, respectively. The properties of different materials used are listed in Table 4.3. Totally 20 different combinations of cover/base material were considered.

Table 4.3 Materials Properties of Box Cover and Base for Simulation

Material	Elastic Modulus (GPa)	Poisson's ratio	Density (kg/m^3)
Steel	200	0.33	7850
Copper	110	0.35	8960
Aluminum	70	0.33	2700
Concrete	25	0.33	2300

The displacement on the top of energy harvester module and the generated stresses on each layer of PZT transducers were obtained from FE analysis. Figure 4.13 show the displacements on the top cover of energy harvester under 0.7-MPa loading stress when aluminum is used as base material of energy module with different cover materials. The analysis was conducted for the energy module with gap. As expected, the material with the higher modulus has the lower deflection. The analysis results show that the concrete cover has higher surface displacement as compared to all other materials. The displacements are general small and thus the energy module will not affect the structural capacity of pavement if it is directly embedded in the pavement.

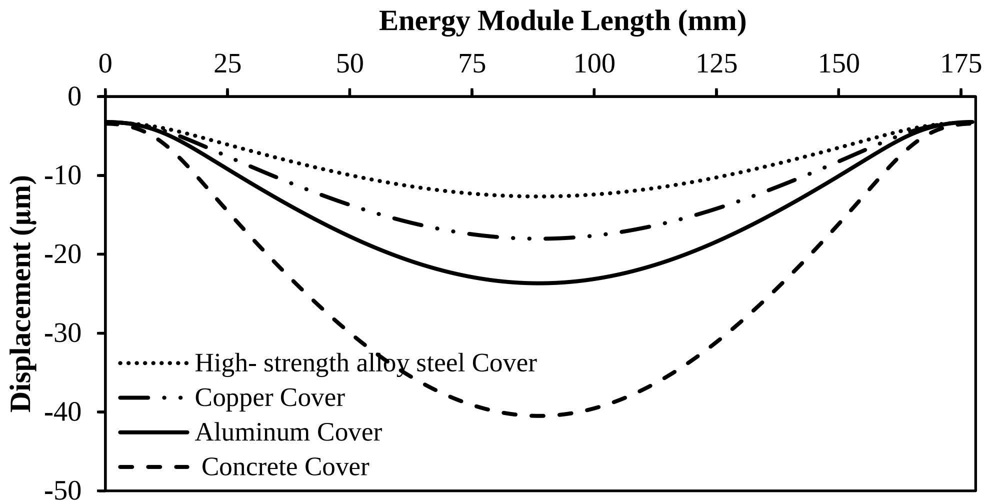

Figure 4.13 Displacement of top cover with different materials used as top cover

Figure 4.14 shows the tensile and shear stresses of transducers at the top row in the energy harvester module when different top and cover materials are used. The loading stress was 0.7-MPa on the top surface of energy harvester. The transducers at the top row were selected since the resulted stresses in the Bridge transducer were higher at the top row compared to the ones at the lower rows. It was found that the top cover material played relatively more important role as compared to the base material because the vertical stresses was transferred from the top cover to the transducer arrays. As the elastic modulus of cover or base material decreases (from steel to concrete), the resulted tensile and shear stresses increase slightly.

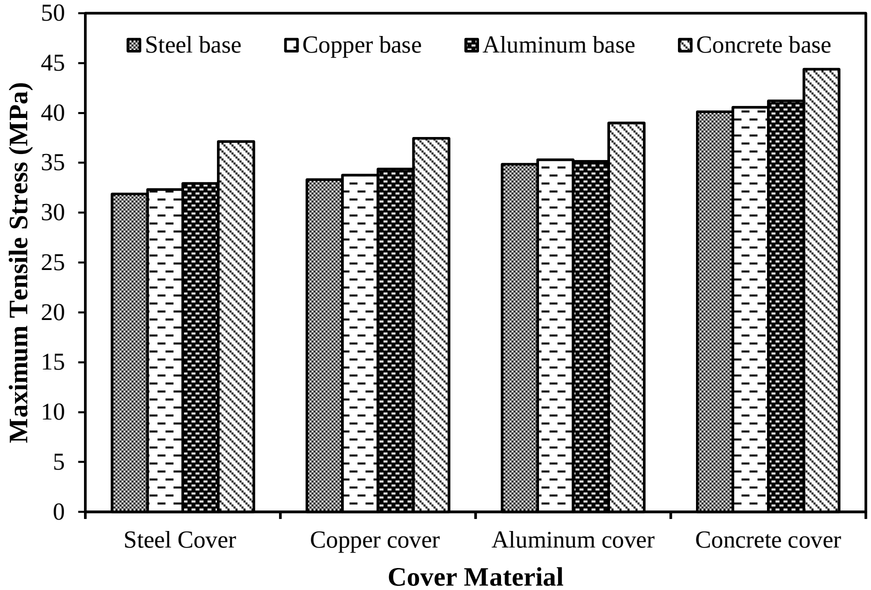

(a)

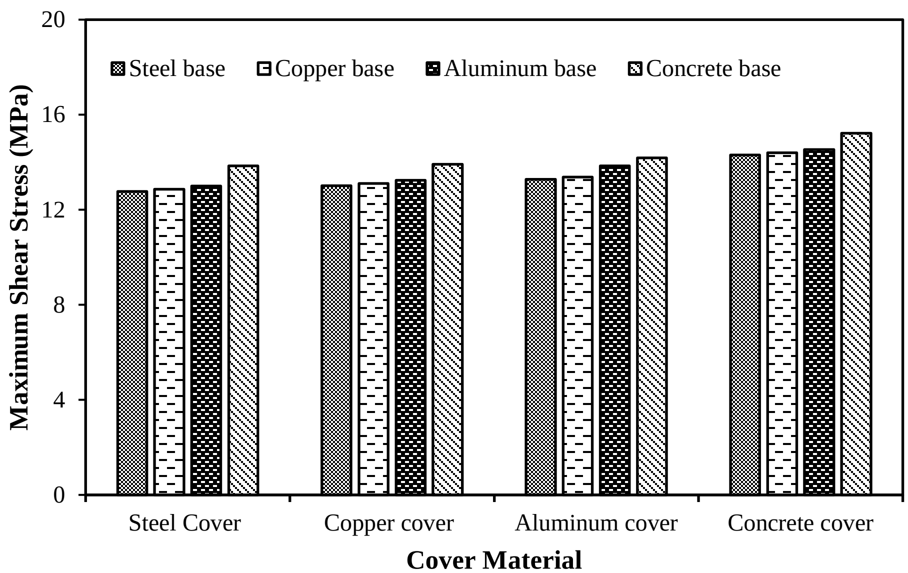

(b)

Figure 4.14 Effect of base and cover material on (a) tensile (b) shear stresses of PZT transducers at the top layer (with gap)

The amount of energy harvested under traffic loading is related to the applied stresses on PZT transducers. When different cover and base materials were used in the module at resistive load of 400 kΩ, the power outputs of energy harvester module varied among 26.6-30.1 mW under 0.7-MPa loading stress at 5 Hz. On the other hand, the fatigue life of PZT transducer varied from 0.97×10^6 to 3.54×10^6 cycles depending on the critical tensile or shear stress. Therefore, the selection of package material for energy harvester module should consider the total energy output within the service life of PTZ transducers.

4.5 SUMMARY

The main objective of this chapter is to evaluate energy output and mechanical failure of piezoelectric energy harvester for roadway applications. An energy harvester module that contains multiple stacked transducers was fabricated and tested under single pulse and cyclic loading events. Forensic analysis was conducted to investigate fatigue failure of piezoelectric transducers after repeated loading. Finite element simulation was used to evaluate output power and mechanical stress of energy harvesters with different layer thicknesses of epoxy adhesive, material types of packing material, and gap design. The predicted voltages and power outputs obtained from numerical simulation match well with experimental measurements. On the other hand, the resistive load can be optimized to increase the energy output. The analysis results showed that two different material failure models need be considered in relation to mechanical failure of Bridge transducer, namely tensile and shear failure. It emphasizes that the optimum design of energy module should consider the balance of energy output and fatigue life that are affected by fabrication of single Bridge transducer and the packaging design of energy module.

CHAPTER 5 PERFORMANCE ANALYSIS OF PIEZOELECTRIC ENERGY HARVESTER IN ASPHALT PAVEMENT

5.1 INTRODUCTION

Harvesting energy from roads and bridges is a new area of research that includes technologies that can capture the wasted energy and store it for later use. In recent years, several studies have attempted to convert the available mechanical energy potential in the pavement into electrical energy using piezoelectric materials (Xiang *et al.* 2013).

Previous researchers have investigated different energy harvester designs for vibration-based or stress-based piezoelectric energy harvesting from roadways or bridges (Wang *et al.* 2018). For vibration-based applications, Wischke *et al.* (2011) studied the application of piezoelectric modules in road pavements in tunnels. The researchers concluded that the vibrations caused by vehicles were small due to vehicle suspension. Song *et al.* (2016) used piezoelectric cantilevers in the design of their roadway energy harvester, with 48 beams placed within a 30x30x10cm box. The researchers considered important environmental conditions and design constraints to maximize its output power by conducting impedance matching to optimize the piezoelectric circuits. The optimized harvester was found to have an output power of 184mW, with a full scale module predicted to be capable of generating 736mW.

Jasim *et al.* (2017) optimized bridge piezoelectric sensor to increase the output power within failure criteria. The researchers concluded that the optimized design of Bridge transducer produced 0.743 mJ of potential energy (open circuit condition) for single transducer under the external stress of 0.7 MPa. Later, Jasim *et al.* (2018)

developed an energy harvesting module consisted of a 7x7x3in (length x width x height) Aluminum box containing 64 novel bridge transducers stacked in four layers. The researchers mentioned that the at 0.7-MPa loading stress with loading frequency of 5 Hz, the energy harvesting module can produces 28.7 mW at resistive load of 400 kΩ. The energy harvesting module can last for 2.06×10^6 cycles under vehicular loading.

Edel-Ajulay (2010) developed piezoelectric generator with mechanical-electrical association and embedded it under the road surface along the path of both wheels. The researcher found that one lane kilometer of road could produce about 200 KWh using 600 heavy vehicles per hour traveling at speed of 72 Km/h on average. Xiong and Wang (2016) analyzed the energy collection efficiency of a piezoelectric energy harvester with an assembly of PZT rods. They found that, under real traffic conditions, an applied loading of around 15% was transmitted to the piezoelectric materials based on calculation from instant and average output voltages and currents.

An experimental field study using a prototype energy harvester formed from disk-shaped piezoelectric transducers, with an aluminum coating intended to distribute the load across the disks, was conducted by Xiong (2014). Test results indicated that the harvester was capable of generating up to 3.1mW from each vehicle driven over it, the primary conclusion of the study being that this power output was strongly correlated with the vehicle's total axle weight.

Papagiannakis *et al.* (2016) also recently developed highway sensing and energy conversion (HiSEC) modules using various configurations and different numbers of PZT rod elements. Different configurations of boxes containing selected numbers of PZT elements of various shapes were considered in developing the prototypes. The analysis also involved the modeling of the stress distribution inside the boxes and laboratory testing of the power output and durability as well as economic feasibility analysis. The feasibility of the harvester design was tested in the laboratory to measure the electrical energy. The results of this study showed that HiSEC modules have promise in powering LED traffic lights and wireless sensors embedded in pavement structures.

Roshani *et al.* (2016) conducted and an experimental program sensors to evaluate the potential of harvesting energy from roadways using piezoelectric materials. The researchers run a sensitivity of the power to loading frequency, vertical load, test temperature, and loading time. The primary recommendation of their study is that the piezoelectric devices could be perfect candidates for harvesting energy in asphalt pavement roadways. Also, the researchers concluded that increasing the frequency minimizes the loading time on the piezoelectric disks while increasing the load cycles per second which results in increasing generated power. In addition, the researchers concluded that there was a low sensitivity low sensitivity of the prototype to temperature.

Another piezoelectric energy harvester was designed by Yang *et al.* (2017), in this case the module consisted of a 30x30x6.8cm box (length x width x height) containing nine disk-shaped piezoelectric transducers stacked in parallel. After 100,000 accelerated loadings the average power output of the harvester was found to be 174V (open circuit), with no significant reduction in the power generation of the transducers. A further result was that the open circuit voltage and power output of the module was found to increase with the load vehicle speed.

A study conducted by Jung *et al.* (2017) used polyvinylidene (PVDF) polymer in the construction of a roadway energy harvester. Their 15x15x9cm module was put through over a million test cycles, proving to be durable and demonstrating stable performance, with an output power of 200mW, and a power density of 8W/m^2.

A new technique for harvesting electrical power from the deformation of highways under vehicle load was suggested by Chen *et al.* (2016); their approach involved the construction of a mechanical energy harvesting (MEH) device from two squares of polarized PZT bimorph, which was then embedded in the specimen asphalt mixture at a depth of 10mm. Results indicated that the output power of the MEH device varied both according to its location and size, and with the loading period. A further conclusion was that when designing an energy harvesting system, it was important to consider the traffic conditions when selecting the appropriate material and configuration.

Previous researchers have investigated different energy harvester designs made of piezoelectric material, but it is still unknown what effects traffic volume, energy harvesting embedded depth, speed, and material fatigue have on piezoelectric materials. Thus, the efficacy of these trials was limited, due to a lack of comprehensive laboratory evaluations and the associated lack of understanding of how traffic loading and pavement conditions affect power generation from piezoelectric materials. Therefore, the current concept of piezoelectric energy harvesting systems must be expanded, and an energy harvester module must be created that can produce greater energy in the life cycle of the piezoelectric transducer.

Another consideration is that the energy harvester module is embedded in the pavement, which may cause concentration stress due to the rigidity of the module. For simplicity, previous studies usually assumed the generated stress on the piezoelectric transducer and neglected the impact of the energy harvester on pavement deterioration. Therefore, investigation is needed to take into account the integrity of energy harvester and pavement material considering the interaction between the pavement structure, traffic loading, and the transducer design. The results can help researchers understand the effects of the embedded depth on piezoelectric output power and to recognize the key factors in improving design and efficiency of these devices.

5.2 OBJECTIVE AND SCOPE

This study focused on maximizing the energy output of piezoelectric transducer by changing the embedded depth of energy harvester under vehicle loading. To take into account the nature of energy harvester-pavement interaction and to achieve better computation efficiency, the effect of this interaction on pavement responses was studied using a decoupled approach. First, a 3D pavement model was built, and then the pavement responses under the tire contact stresses were calculated. The effects of energy harvester-pavement interaction at different locations, horizontally and vertically, were also analyzed. At the same time, the amount of energy for each heavy vehicle pass was determined until the service life of the energy harvesting module is reached. In addition, a cost-benefit analysis of the energy harvester module was conducted to quantify the required cost per unit of energy generation. Figure 5.1 shows the flowchart of the analysis plan. The following are the main objectives of this study;

1) Develop and calibrate finite element models to calculate the energy output of the energy harvester under different loading conditions.
2) Develop finite element models of pavement to calculate compressive stress pulses with and without the embedded energy harvester module. The model incorporates tire loading conditions and appropriate material characterizations for each pavement layer and harvester module.
3) Analyze energy outputs of energy harvester module under vehicular loading at different locations, temperature, and vehicular speeds.
4) Analyze the effect of energy harvester module on pavement responses especially surface displacement and shear strain.
5) Develop an accurate placement strategy of the energy harvester based on maximum power output and service life.

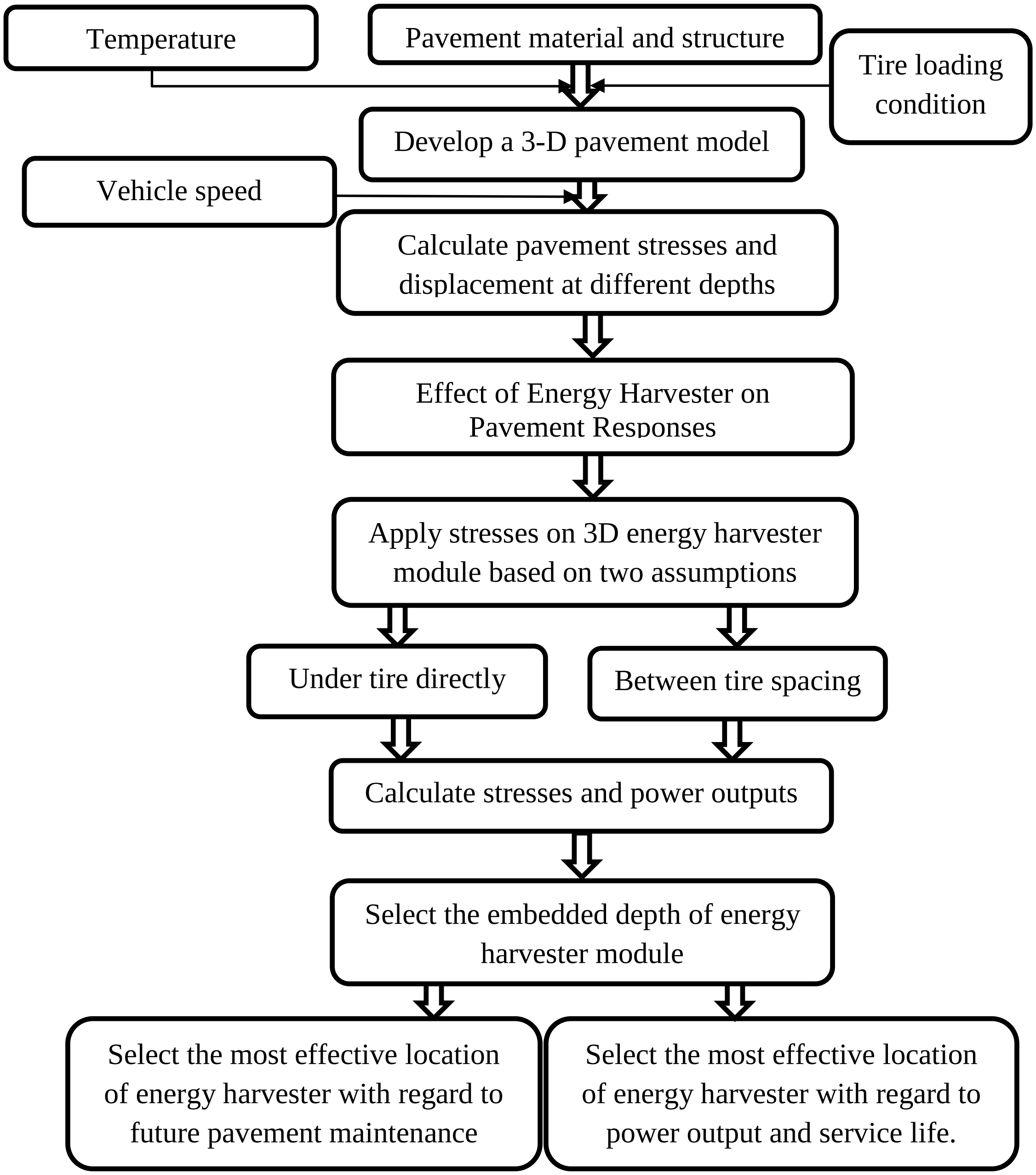

Figure 5.1 Flowchart of analysis approach

5.3 ENERGY HARVESTING MODULE

5.3.1 Laboratory Testing

Energy harvesting module is used to convert mechanical stresses from pavement surface to electrical energy. In the authors' earlier work, Jasim *et al.* (2017) developed a novel design of piezoelectric transducer for energy harvesting from roadway with optimized geometry design considering the balance of energy harvesting and mechanical stress concentration. The innovative bridge transducer was designed to have layered poling pattern and electrode configuration that modified the polarization direction to have the parallel piezoelectric coefficient for the stress applied in the direction of polarization. The researchers concluded that the generated energy output is usually small for a single piezoelectric transducer. In order to generate the energy that is applicable for energy storage or direct use, multiple sensor arrays under repeated traffic loading are needed.

A total of 64 transducers were arranged in four layers, each consisting of 16 transducers in a 4×4 configuration in each layer, as shown in Figure 5.2. The energy harvester module was fabricated using aluminum with the outer dimension of 177.8mm×177.8mm×76.5mm (7inches × 7inches × 3inches). The interior part of the aluminum case was coated with an insulating epoxy (Jasim et al. 2018). Nylon strips were used to separate the transducers within each column. Copper plates were used to separate each layer and acted as current collectors. The copper plates were wired together in an alternating configuration to allow for parallel connectivity.

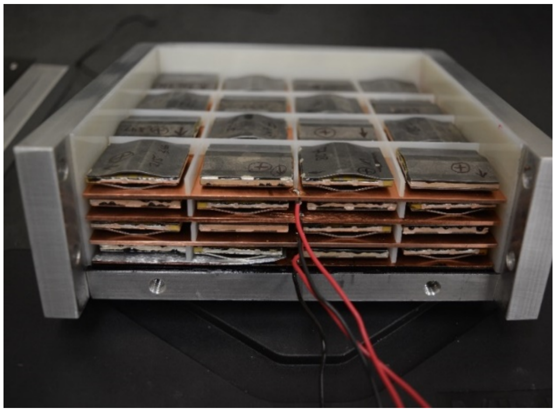

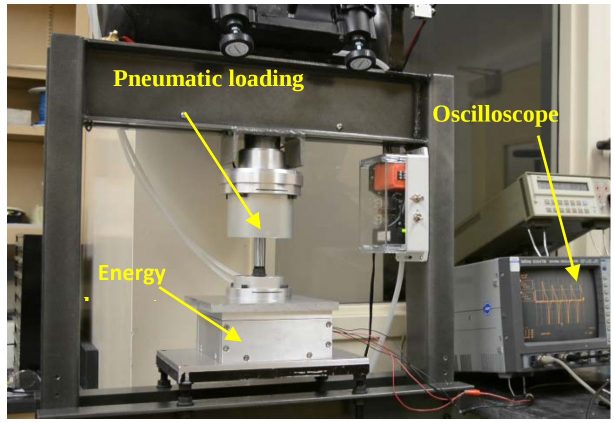

(a) **(b)**

Figure 5.2 2 Energy harvester module: (a) array of Bridge transducer; and (b) test setup

Testing of the energy-harvesting module was conducted, using a pneumatic loading system, which can repeatedly apply a load of up to 800lb at a frequency up to 5Hz. The output voltage of the transducer module was measured across an 88 nF capacitor to calculate the energy produced.

5.3.2 Finite Element Model of Energy Harvester

3-D FE analysis was used to evaluate the entire module using free tetrahedral elements fine mesh. The minimum element size is used at small areas or sharp edges; while the maximum element size provides the upper limit as the element sized gradually increases in the model.

The mechanical and electrical boundary conditions were selected carefully in order to simulate the actual behavior of the energy harvesting module. For the mechanical boundary condition, the energy harvesting module was fixed at the bottom (z-direction) of the Aluminum base, while the distributed load was applied on the top surface. Also, movements of the vertical boundaries were restrained only in the horizontal directions (in x and y-direction). The electrical boundary condition was configured using copper sheets (five sheets). Two copper sheets were set as ground boundary (zero voltage), while the terminal connection was set on the remaining copper sheets (positive voltage). Figure 5.3 illustrate the voltage output of the energy harvesting module and mechanical stresses generated under 0.7MPa compressive loading.

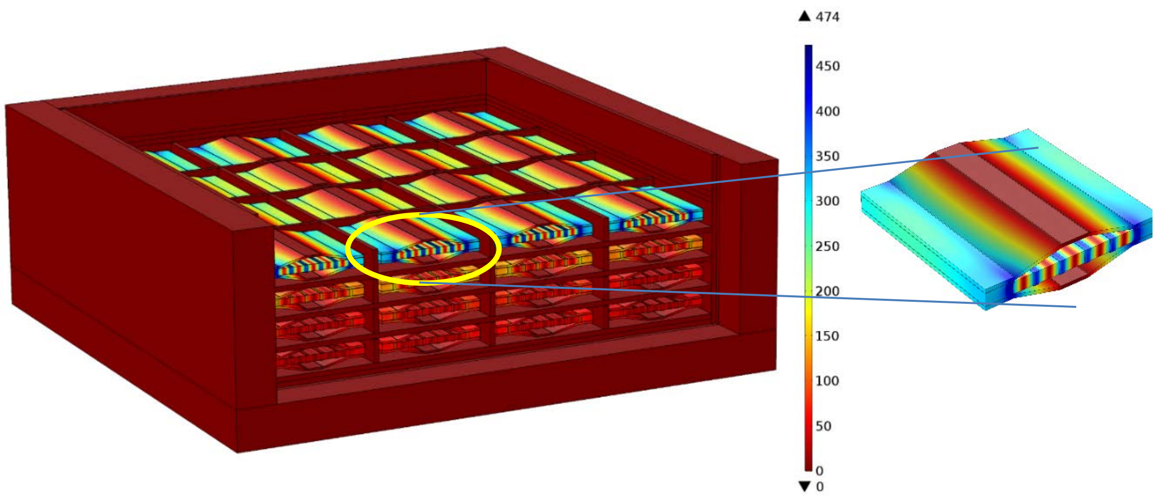

(a)

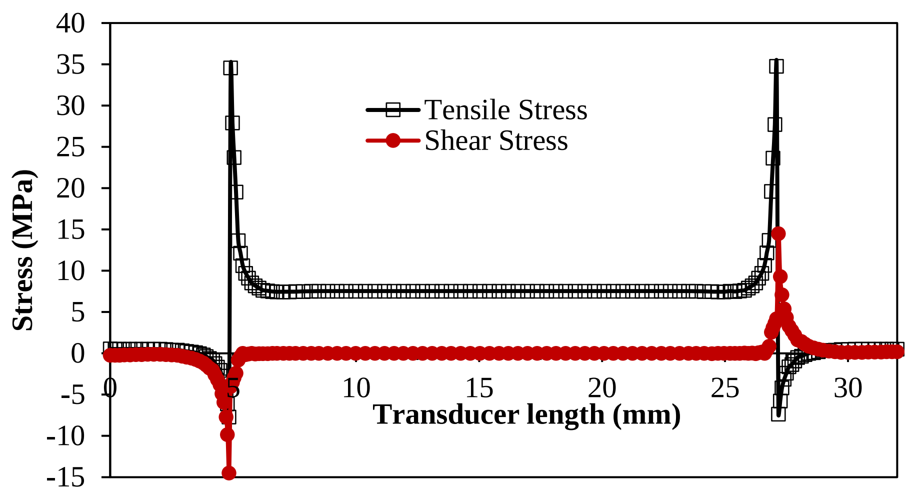

(b)

Figure 5.3 Illustration of (a) energy output and (b) mechanical stress of Bridge transducer under compressive loading of 0.7MPa

During cyclical loading, the power generated depends on the resistance of the electrical load, the formula being $P=V^2/R$ where V is the voltage and R the resistance. For a low value of resistance, a high current will flow but the voltage will be low, whereas for a large resistive load there will be a high voltage but low current, there will therefore be some intermediate value of R for which maximum power occurs, this value is determined experimentally. Cyclical loading was performed at frequencies of 0.5, 1, 2 and 5Hz, with a load of 500lb, and with a variety of resistive loads ranging from 50kOhm to 1MOhm. A larger 10μF capacitor was used to smooth out the oscillations in voltage caused by the dynamic loading. During loading, the voltage on the capacitor was seen to increase until a constant voltage was reached, at which point the voltage was measured and output power calculated using the formula $P=V^2/R$.

The comparison of output power from lab testing and numerical model is shown in Figure 5.4. The results show that the maximum output power of 2.1mW was measured at 500 lb loading and 5 Hz, at a resistive load of 400 kΩ. The output power is greater at high resistive load due to the high impedance of the transducers. Based on Maximum power transfer theorem, a plot of load power versus load resistance reveals that matching load and source impedances will achieve maximum power (Phillips 2009). It was found that the increase of loading frequency caused a significant increase of power output.

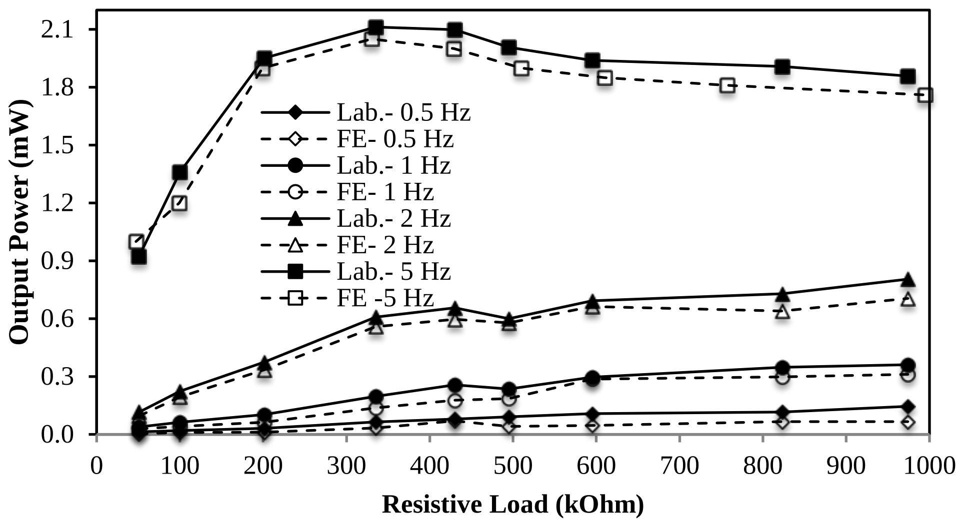

Figure 5.4 Output power versus resistive load for energy harvesting module loaded at 500lb

5.4 DEVELOPMENT OF PAVEMENT FINITE ELEMENT MODELS

5.4.1 Pavement Structure and Material Properties

The pavement structure considered in the analysis includes a 254-mm a 300-mm lime-modified soil and natural subgrade, which duplicates the full-depth pavement structure used in the accelerated pavement testing (Wang and Al-Qadi 2009). Constitutive models of each pavement layer are critical for mechanistic analysis of pavement responses. A linear viscoelastic constitutive model was applied to simulate the asphalt surface layer. Relaxation moduli of the asphalt mixture are required as input parameters in the FE model. The relaxation modulus of asphalt mixture was modeled as a generalized Maxwell solid model in terms of Prony series, as shown in Equations 5.1 and 5.2.

$$G(t) = G_0\left[1 - \sum_{t=1}^{N} G_i(1 - e^{-t/\tau_i})\right] \tag{5.1}$$

$$K(t) = K_0\left[1 - \sum_{t=1}^{N} K_i(1 - e^{-t/\tau_i})\right] \tag{5.2}$$

Where, G is shear modulus; K is bulk modulus; t is reduced relaxation time; G_0 and K_0 are instantaneous shear and volumetric elastic moduli; G_i, K_i, and τ_i are Prony series parameters; N = number of terms in the equation; and e = base of natural logarithm.

It was essential to consider temperature distribution in the asphalt layer because of the temperature dependence of viscoelastic material. The temperature dependency of the asphalt layer modulus was characterized by the time-temperature superposition using Williams-Landell-Ferry (WLF) function (equation 5.3). Table 5.1 summarizes the fitted Prony series and WLF parameters for the asphalt layer. In this paper, one temperature profile, 25ºC, was used as a uniform distribution. The Poisson's ratio of asphalt layer was assumed to be 0.3.

$$\log(a_T) = -\frac{C_1(T-T_0)}{C_2+(T-T_0)} \tag{5.3}$$

where T_0 is reference temperature; T is actual temperature corresponding to the shift factor; and C_1, C_2 are regression parameters.

Table 5.1 Viscoelastic Parameters of asphalt concrete at 25°C

i	***G_i or K_i***	***τ_i***	**WLF parameters**	
1	4.52E-01	0.000113		
2	2.78E-01	0.003144	C_1	20.7
3	1.48E-01	0.013001		
4	1.08E-01	0.183525	C_2	173.6
5	7.46E-03	2.289579		

The lime stabilized soil, and natural subgrade soil was assumed as linear elastic material. The elastic modulus of stabilized soil and natural subgrade was estimated to be 450MPa and 150 MPa, respectively, based on the back-calculation from falling weight deflectometer (FWD) test. The Poisson's ratio of soil was assumed to be 0.35.

5.4.2 Three-Dimensional Finite Element Model

A 3-D FE model of flexible pavement was simulated with the general purpose FE software ABAQUS. In the model, eight-node, linear brick elements with reduced integration were used in the finite domains, whereas infinite elements were applied at boundaries to reduce a large number of far-field elements without significant loss of accuracy and to create a silent boundary for the dynamic analysis.

Figure 5.5 illustrates the 3-D FE model that discretizes the pavement structure. The FE mesh was refined around the loading area along the wheel path, and a relatively coarse mesh was used far away from the loading area. The horizontal element dimensions along the vehicle loading area were dictated by the tire rib and groove geometries. Hence, the length of the elements in the loading area selected was 15 to 18 mm in the transverse direction and 20 mm in the longitudinal (traffic) direction to have proper aspect ratios. Based on a mesh convergence study, the element thicknesses selected were 9.5 mm for the asphalt surface layer and 20 to 30 mm for the granular base layers to have a smooth stress transition between elements.

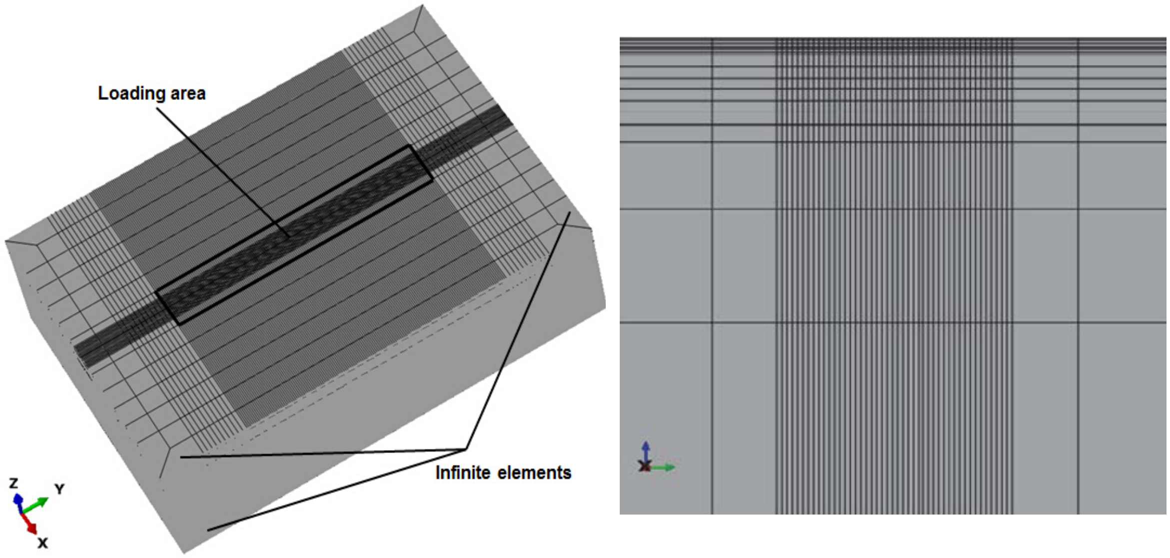

(a) (b)

Figure 5.5 FE model layout: (a) 3-D domain with infinite boundary and (b) cross-section

Infinite elements were used in the transverse and at the bottom of subgrade to reduce the degrees of freedom at far field and to absorb stress waves for dynamic analysis. The infinite element has a unique shape function for the geometry at the infinite boundary and has zero displacements as the coordinate approaches infinity (Wang and Li 2016). Sensitivity analysis was conducted to define the location of infinite boundaries so that the strains in the asphalt layer show less than 5% changes as the domain sizes increase. After yielding the resulting transverse and longitudinal tensile strains in the asphalt layer, the finite dimension of the model was selected to be 9.0 m (length) × 6.0 m (width) × 3.0 m (depth) with an in-plane loading area of 6.0 m × 1.0 m to balance the computation cost and accuracy. A frictional interface was considered.

A set of dual tires with a load of 39.5 kN (8.9 kips) and a tire inflation pressure of 0.724 MPa (105 psi) was considered. The realistic tire-pavement contact stresses are critical in the evaluation of tire pressure effect on pavement responses. For each tire loading, non-uniform contact stress distributions were assumed in the tire imprint area with five ribs (Wang *et al.* 2015).

A 0.5 inches thickness Aluminum box was used to represent the energy harvesting module. The elastic modulus, Poison's ratio and density are 70GPa, 0.33 and 2700 Kg/m^3 for Aluminum, respectively. The effects of energy harvester-pavement interaction at different locations, horizontally and vertically, were also analyzed. Also, the stresses and loading time on the top of the box were reordered at different embedded depth. Based on the simulation results, the amount of energy for each heavy vehicle pass was determined until the service life of the energy harvesting module is reached.

5.5 RESULTS AND DISCUSSION

5.5.1 Effect of Energy Module on Pavement Responses (vertical stress and strains)

It is important that energy-harvesting module is located horizontally, across the width of road lane, to maximize the number of passing tires. In order to select the required horizontal distance from the pavement edge, a number of simple assumptions and calculations were carried out. It is already known that the average highway lane is 3.65 m and the average width of an 18-wheel truck is around 2.6 m; this gives a clearance width of around 0.525 m between the tire and the lane edge assuming no wandering. However, it has been noted that not all vehicles pass in the same wheel path (Gillespie 1993); as such, according to the identified truck tire footprint, it is suggested two different horizontal locations. The first location is that the energy harvesting modules are located directly under one tire. The second case is that the module is located directly under the center of dual tires. Figure 5.6 illustrates the location of energy harvesting module across the lane width.

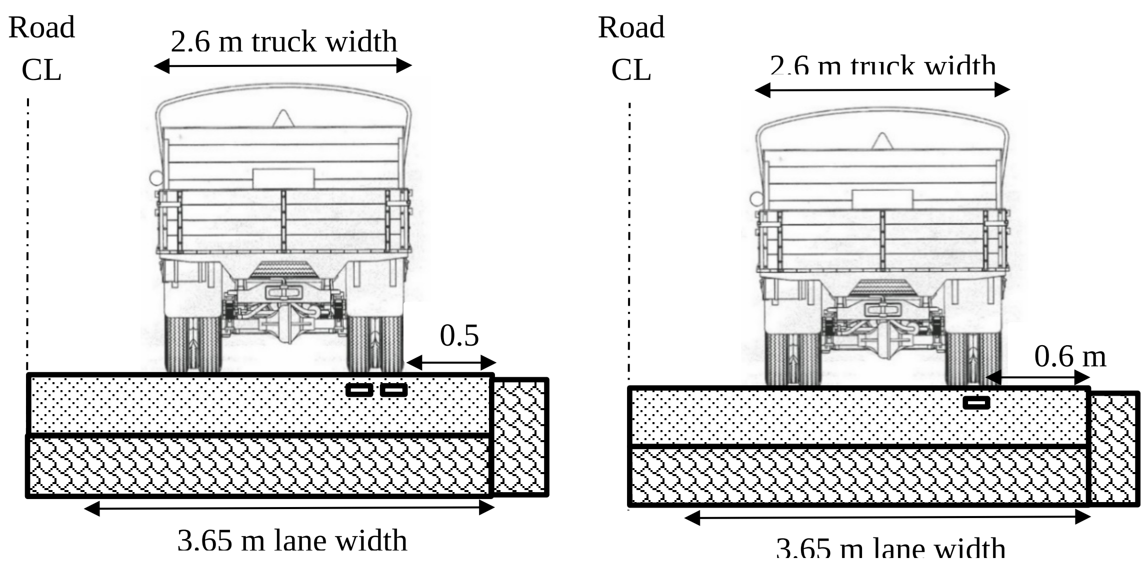

(a) **(b)**

Figure 5.6 Location of energy harvesting module across the lane width with (a) located directly under one tire; and (b) located directly under the center of dual tires

Figure 5.7 shows the vertical stress distribution along pavement depth with and without energy harvesting module. The amount of stresses generated due to inserting the energy harvesting module under the tire directly is higher than placing the same module between tires due to intensive stresses. Also, Figure 5.7 shows that the amount of stresses with embedded energy harvester module is higher as compared with original pavement stresses. For accuracy purpose, it is important to use the stresses due to embedded energy harvesting module for both horizontal locations.

Figure 5.7 (a) and (b) indicate that increasing depth results in a larger pressure distribution area but there is a corresponding reduction in the total average vertical stress. As such, the traffic-induced vertical stress magnitudes and distributions change with pavement depth. Indeed, reductions in vertical stress value throughout the depth and increases in vertical stress distribution areas were found using the finite element modeling.

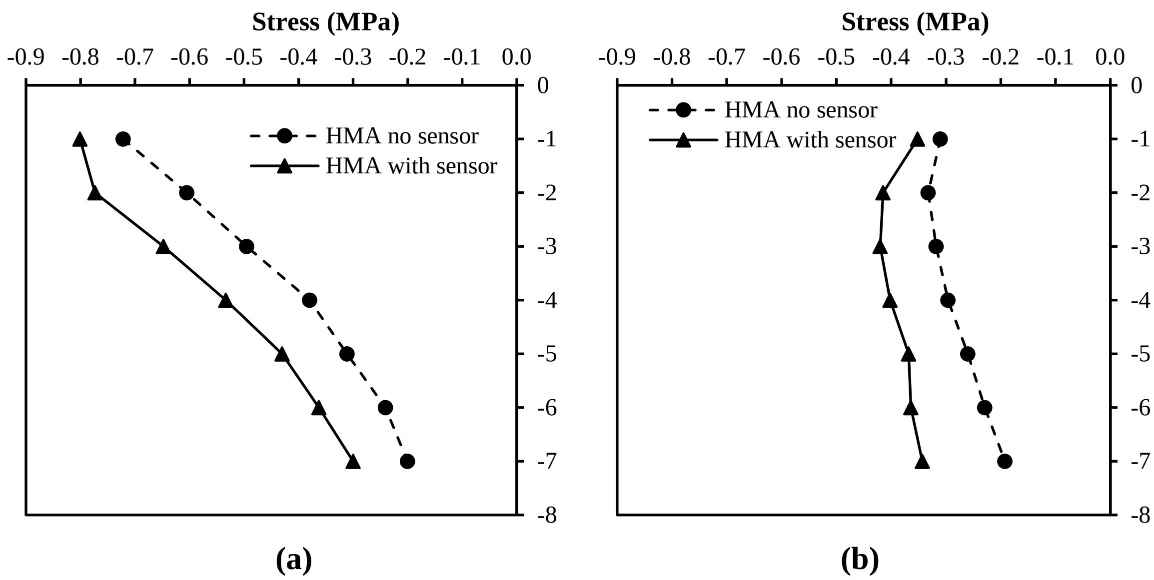

Figure 5.7 Stress distributions within pavement layers for energy harvester (a) under one tire directly; and (b) under middle of two tires at speed 50mph

Since the stiffness of modulus box material will be similar or greater than asphalt concrete, it is expected that the inclusion of module box in the pavement will cause similar or smaller displacement on road surface. In this case, the energy harvester may not cause an adverse effect on road surface displacement. In addition, the energy-harvesting module should not cause stress concentration in the pavement and cause performance deterioration of the pavement. It requires the energy harvester modulus has good coupling effect with pavement, which means that the module should not cause high-stress concentration in the surrounding pavement material.

5.5.2 Effect of Embedment Location on Energy Output

Using the developed FE model, the stress distribution along pavement depth under different magnitudes of wheel loads will be considered. The predicted value of vertical stress is dissipating along the depth, however, the stress distribution is affecting a larger area. As vehicles move along the pavement surface, a large number of rapidly varying stress pulses are applied to each element of the material within the pavement (Yin *et al.* 2007). The loading time at a specific depth is not only related to the vehicle speed but also to the depth magnitude. In general, at deeper layers in the pavement, the time period of stress pulse acting on a certain region will increase, indicating that the duration of moving load will also increase. Figure 5.8 shows loading time and load magnitude at the top of energy harvester module at different pavement depths. For all above reasons, the load magnitude and loading time at various embedded depths were used at the energy harvester module to determine the power output.

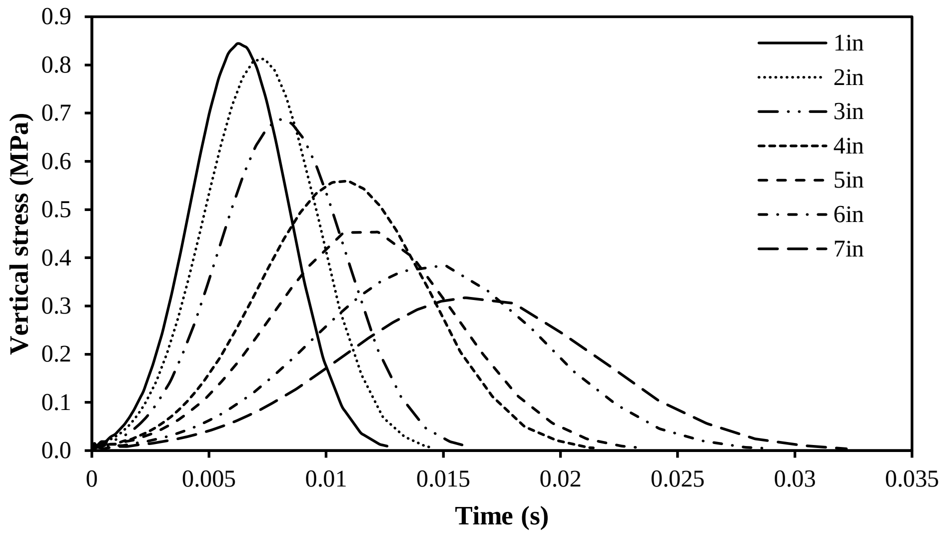

Figure 5.8 Loading pulses of compressive stresses on energy harvester at 50 mph

A successful energy harvester should have the ability to convert as more as possible mechanical energy and maintain its deformation within limits. Figure 5.9 represents the voltage and power output of the energy harvester module at vehicle speed 50mph at different depths. As expected, the generated power related to applied stress on energy harvesting module. Deeper embedded depth of the energy harvester module will produce less power.

There is also a need to protect the module from the excessive tire impact, as being exposed to millions of traffic load cycles during its lifespan is likely to take its toll; as such, it is discerned that the two inches depth would be enough to protect the module whilst also maximising exposure due to the extended stress distribution. For this reason, the depth of two inches depth will ensure that the majority of the passing tire generated stresses are harvested.

The finite energy modeling result combined with the future fieldwork on pavement maintenance operations has identified that the module should be positioned at a depth of two inches. This depth has been deduced from a number of factors. Firstly, by positioning the module under the asphalt layer during scheduled repaving, will have no effect on the surface smoothness of the road and will, therefore, not have any noticeable effect on the passing traffic regarding emissions or fuel efficiency.

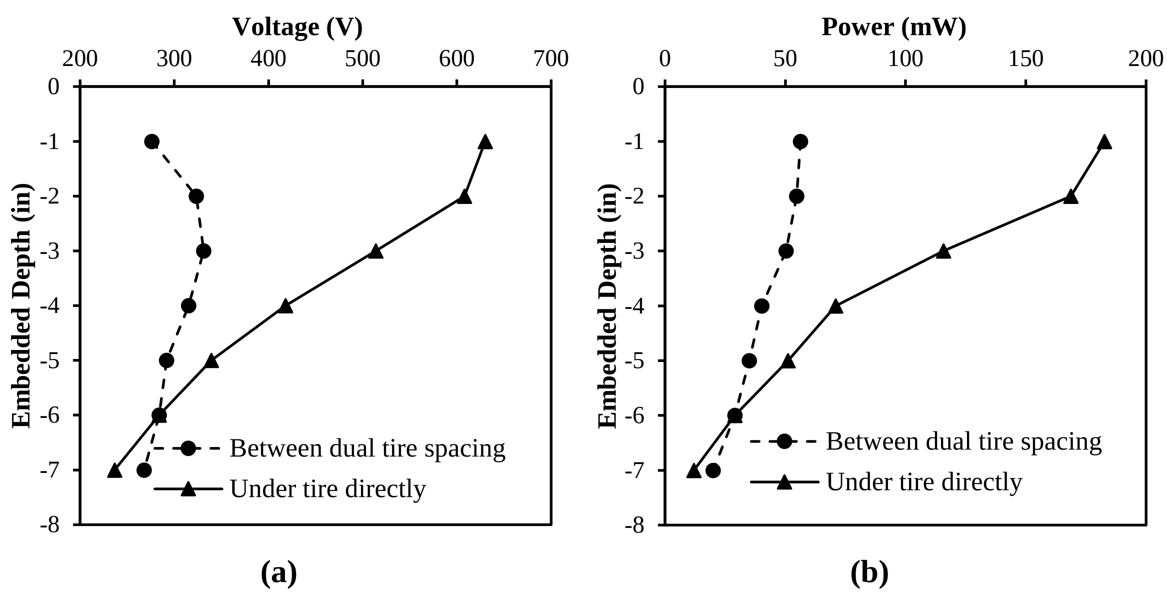

Figure 5.9 Voltage output (open circuit) at different embedded depth for (a) one box between dual tire spacing; and (b) two boxes under each tire directly at 50mph

5.5.3 Effect of Speed and Temperature on Energy Output

Traffic moving over a pavement structure results in a large number of rapidly applied stress pluses being applied to the material comprising each layer. Typically, these stress pulses last for only a short period of time. The type, magnitude, and duration of the pulse vary with the type of vehicle and its speed, the type and the pavement structure, and the position of the element of the material under consideration.

The effect of vehicle speed on pavement performance was simulated using the correlation between vehicle speed and the resilient modulus of the asphalt concrete layer. In this section, the energy harvester box embedded in the pavement under tire imprint directly. Five different speeds were selected in this paper which is 10, 25, 40, 50 and 65 mph that represent too low, low, intermediate, normal and high speeds respectively. As expected, increasing the frequency results in decreasing of loading time that is related to increasing speed.

At a depth of 1 inches, the results show that there is a little change of stress magnitude based on vehicle speed effect as shown in Figure 5.10. The vertical stress change is related to viscoelastic properties of the HMA layer. Although the vertical stress change is not significant at different speeds, the loading time still has the primary effect on the energy harvesting module.

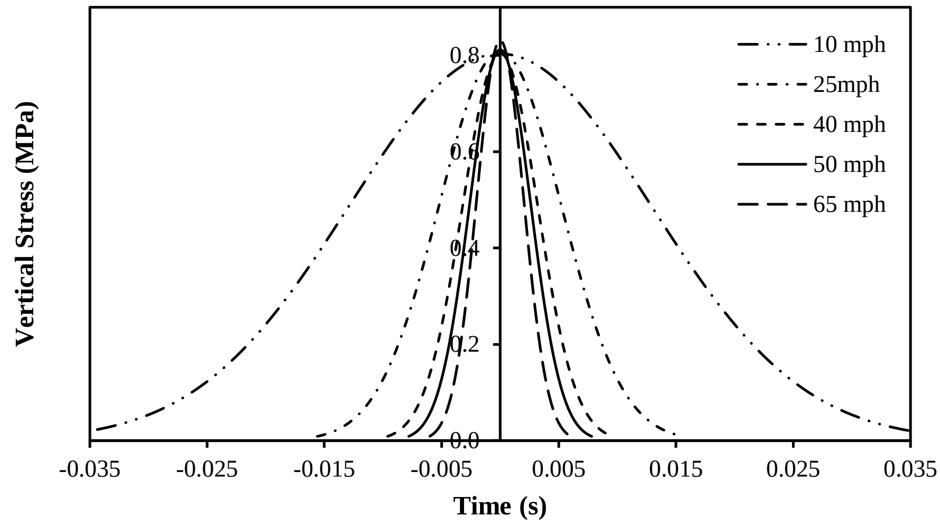

Figure 5.10 Stress magnitude and loading time below 1 inches above energy harvester at different speeds under tire directly

Figure 5.11a shows that increase vehicle speed caused a significant increase of power output at different depth especially at shallow depth due to increase of frequency. Figure 11b indicates that higher speed produces more power since the loading frequency is increased. According to the fitting equation, it can be concluded that the relationship between speed and output power at different embedded depth is linear since the R-squared is very close to 0.9. Assuming that the vehicles' speed in the field is 70 mph and the embedded depth energy harvester module is 2 inches below the pavement surface, the predicted output power is around 207.4 mW that obtained by extrapolating the fitting curve. Also, Figure 5.11b shows that the power output increases when the speed is increased and this increase is more significant at shallower depth compared to deeper depth.

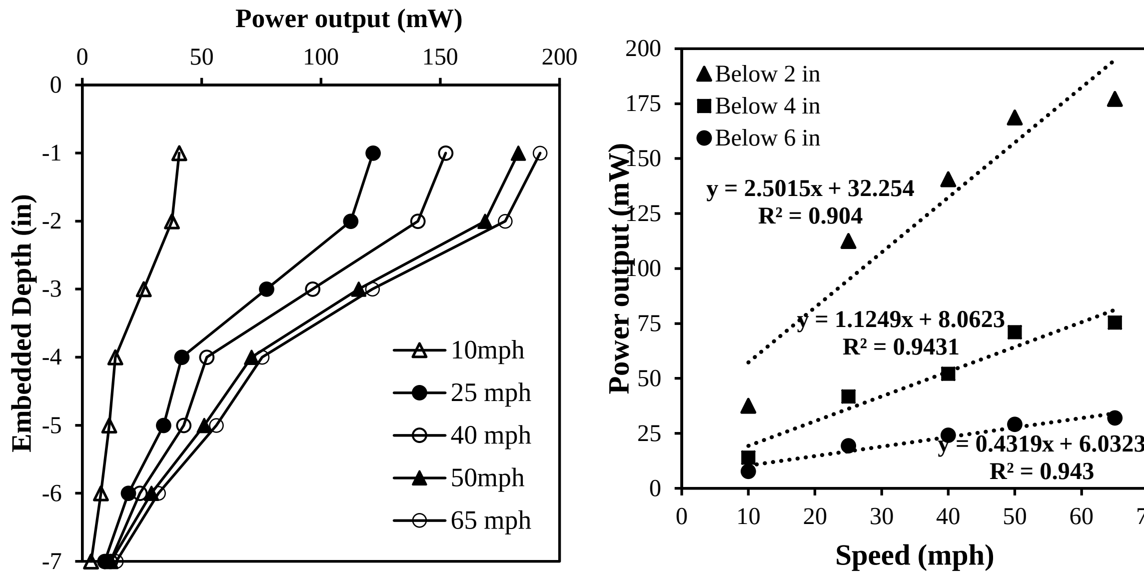

(a) (b)

Figure 5.11 Energy harvester output results (a) power along pavement depth and (b) power output with different vehicle speeds at different embedded depth

The pavement temperature is an important parameter that needs to be studied to evaluate the prototype performance. The temperature of asphalt pavement increases throughout the day due to its absorption of solar radiation, which affects the stiffness of the pavement materials, piezoelectric materials and hence the stress intensity on the piezoelectric module. Therefore, temperature is a governing variable that influences the output power. In this study, simulation was performed at 10, 25 and 40 °C representing the standard testing protocol for performance testing of asphalt mixes.

Figure 5.12 shows that there were slightly change in vertical stresses due to changing pavement temperature. In this study, increasing the temperature resulted in sight decrease in output power. This could be because of viscoelastic behavior of asphalt mixture that affects the stress transformed to the piezoelectric module.

For Piezoelectric materials, many papers stated that this material can work in a wide range of temperature. Although the functionality of piezoelectric materials depends on the temperature, but the temperature influence is negligible around room temperature. The effect of temperature is tangible in a very low or high temperature. Miclea *et al.* 2007 stated that increasing the temperature slightly increases the piezoelectric charge constants d_{33} and d_{31}, however, the effect of temperature is negligible under the temperature of 150 °C.

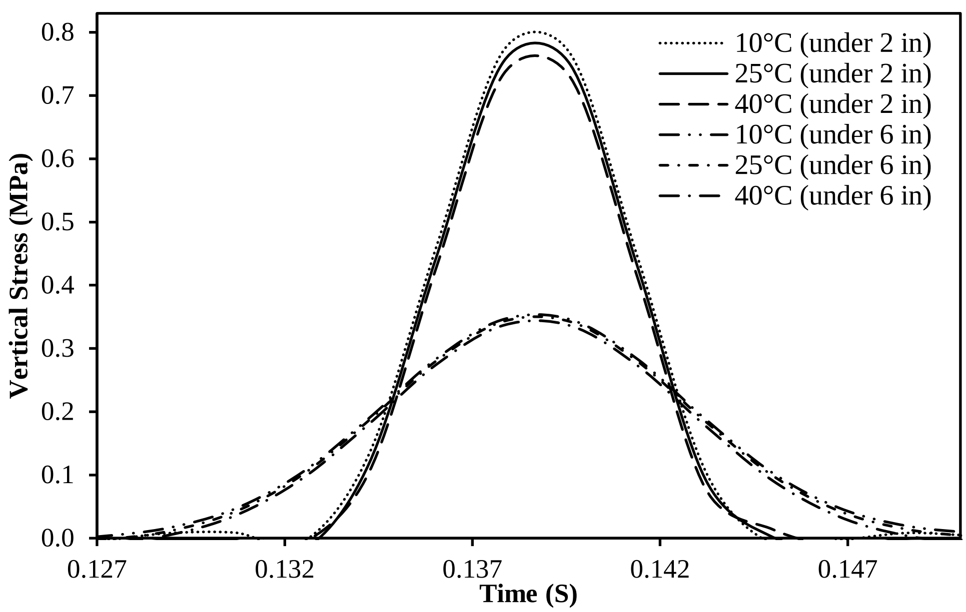

Figure 5.12 Effect of temperature on vertical stresses under 2 and 6 inches at 50 mph speed

5.5.4 Total Energy Output during Service Life

In order to maximize the energy output of the energy harvesting module in roadways, many studies suggested that the depth of 1-2 inches could be reasonable to locate the energy module considering maintenance operation in filed only. All available studies not considered the fatigue life and the cost-benefit of optimum embedded depth. It emphasizes that the optimum embedded depth of energy module should consider the balance of energy output and fatigue life that are affected by fabrication of transducers and the packaging design of energy module.

The maximum stress generated in the Bridge transducer should be limited to prevent material failure. Based on the material strength of PZT and epoxy obtained from material suppliers, the maximum tensile and shear stresses at the inner corner of the contact area between the steel cap and the PZT strip need to be smaller than 40MPa and 17MPa, respectively. Therefore, it is needed to consider both tensile and shear stresses to generate the maximum power within the failure stress criteria.

In this study, the fatigue models of PZT ceramic material and epoxy were selected from the existing models presented in the previous work, respectively, as shown in Equation 5.4 and 5.5 (Chuang *et al.* 1996; System 2005). In both fatigue models, the relationship between the cyclic stress amplitude (σ) and the number of cycles to fatigue failure (N) is practically linear in semi-logarithmic representation.

$$\text{Log}(N) = 13 - 0.2\,\sigma \tag{5.4}$$

$$\text{Log}(N) = 11.65 - 0.422\,\tau \tag{5.5}$$

Where, σ is the cyclic stress amplitude in tension (for PZT strip); τ is the cyclic stress amplitude in shear (for epoxy); and N is the number of cycles to fatigue failure.

Figure 5.13 shows the fatigue life of the energy harvesting module at different embedded depths. The results show that the energy harvester module has longer life at deeper depth as compare to shallower depth because of vertical stress reduction. Furthermore, the same trend is noticed for all speeds at different depths.

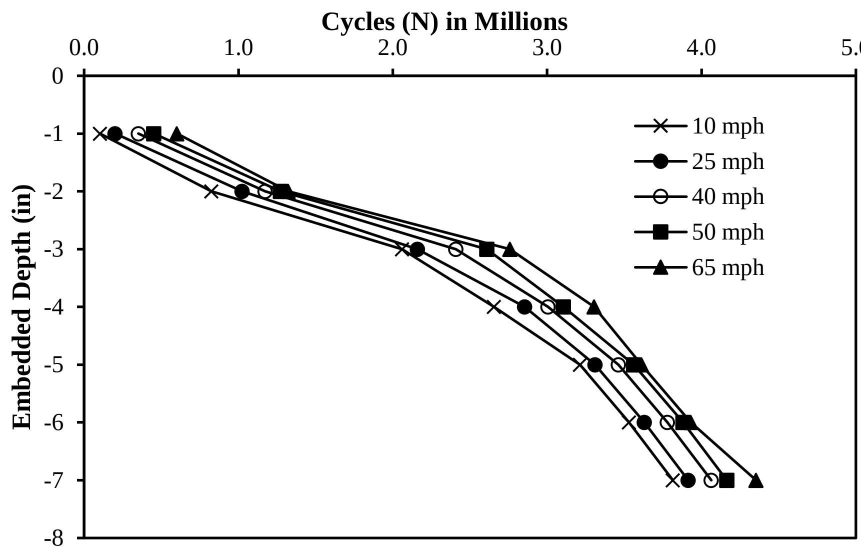

Figure 5.13 Energy harvesting module service life at different embedded depth and speed

To calculate the service life of the current energy harvester module in years, the total number of axles should be counted. Therefore, the total number of axles based on different truck type, volume and axle/truck ratio can be calculated using Equation 5.6.

$$\text{Total axle loading } = \sum_{i=1}^{10} (\text{Ni} \times \sum_{j=1}^{4} (k_j \times X_j)) \quad (5.6)$$

Where, N_i is the number of truck traffic for class i; k_j is the ratio between number of axles to number of trucks for type j axle load and X_j is the number of axles for type j axle load; I is the number of vehicle class (4 – 13); j is the axle load type (single, tandem, tridem and quad).

To make the results more realistic, a real data was collected in New Jersey from urban expressway with annual average daily truck traffic (AADTT) of 1348 veh./day and design speed of 55mph. Table 5.2 shows that the total number of axles (cycles) is around one million per year. For example, if the energy module embedded below 3 inches, the average service life of energy harvesting module will be 2.5 years.

Table 5.2 Total number of cycles form urban expressway in New Jersey

Vehicle class	**Number of trucks**	**Axle/Truck**				**Number of Axles**
		Single	**Tandem**	**Tridem**	**Quad**	
4	2202	1.37	0.59	0	0	5615
5	72530	2.07	0.04	0	0	155940
6	53408	0.93	0.99	0	0	155417
7	9641	0.95	0	0.88	0	32297
8	13320	1.83	0.87	0	0	47552
9	93518	1.95	1.86	0	0	530688
10	894	0.98	0.99	0.60	0	4398
11	360	3.69	0	0	0	1328
12	10	4.63	1.16	0	0	70
13	123	1.29	1.64	0	0	562
Sum	**246005**					
		Total number of axles (cycles)				**933,868**

To calculate the amount of total output generated by the energy harvester module, the amount of power generated at each depth multiplied by fatigue life at specific embedded depth. For example, the module generates 182.72 mW of power at vehicle speed 50 mph and 1-inch embedded depth. At the same speed and embedded depth, the service life of the energy module is 451323 cycles to failure. The total amount of power output at the mentioned speed and depth is 82.47 KW. Figure 5.14 shows the total energy harvesting module in (KW) during its service life at different vehicle speed and embedded depth along pavement structure.

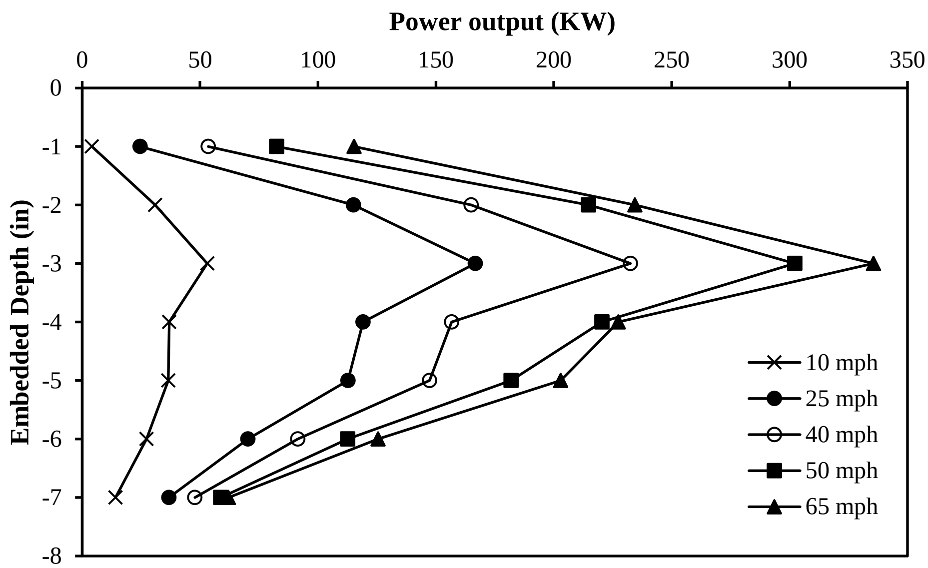

Figure 5.14 Power output of the single energy harvesting module during whole life at different depths and vehicle speeds

Figure 5.14 shows that the embedded depth of three inches is a perfect location for different speed to maximize the output power and service life. At three inches embedded depth, the energy harvester module can produce 53.02, 166.7, 232.51, 302.17, and 335.52KW of power during the service life for a vehicle speed of 10, 25, 40, 50, and 65mph respectively.

5.6 SUMMARY

Understanding the location of the energy harvesting module across pavement in vertical and horizontal direction is important to maximize number of tire passing that results in maximizing the energy. This chapter investigated the mechanical and electrical behavior of a piezoelectric energy harvesting module embedded in asphalt pavement using finite element analysis. In addition, this chapter analyzed the mechanism of energy harvester-pavement interaction and the effect of this interaction on pavement responses (stresses and displacement) using a decoupled modeling approach. The energy harvesting module was composed of PZT sensors with bridge configuration connected in parallel. A total of 64 transducers were arranged in 4 layers, each consisting of 16 transducers in a 4×4 configuration in each layer.

The effect of the tire load and its distribution along the pavement depth was also significant to determine the best location of an energy harvester within the pavement. For this purpose, the sensitivity of the power output to the loading frequency (duration), load magnitude, temperature and vehicle speed was also studied. This study found that the voltage output of the energy harvesting module decreased with the increase of the embedded depth since the stress distribution is decreased. Moreover, the magnitude and the loading time (frequency) also significantly affected the output power. The higher the load frequency (high vehicle speed), the more the output power because it causes a shorter load width. Finally, this paper found that the effect of the pavement temperature on the output power of the energy harvesting module is negligible

CHAPTER 6 COST-EFFECTIVENESS ANALYSIS OF DIFFERENT RENEWABLE ENERGY TECHNOLOGIES

6.1 INTRODUCTION

Finding renewable green energy resources is a major challenge in the contemporary world in terms of sustainable development. The most frequently used energy resources for power generation are currently petroleum, coal, hydraulic, natural gas, and nuclear energy. Energy harvesting serves as a beneficial means of producing clean, renewable energy and enhancing infrastructural sustainability. The way that energy harvesting technologies work is by capturing unused and wasted energy and subsequently converting it to more usable energy forms. Conventional energy sources for harvesting energy nowadays are solar (Kang-Won and Correia 2010), wind (Fthenakis Fthenakis and Kim 2009), hydro (Pacca Pacca and Horvath 2002), thermo (Yildiz and Coogler 2017), and kinetic (Zhang *et al.* 2016). Researchers in recent times have started investigating the harvesting of electrical energy using various methods, including piezoelectric, thermoelectric, photovoltaic and electromagnetic energy harvesting (Cook-Chennault *et al.* 2008).

Roadway is one important type of civil infrastructure and plays a critical role in connecting communities, and transporting people. Roadways are traditionally deemed to be the structure platform for carrying traffic loading. Wang and Li (2016) and Chen *et al.* (2017) explained that roadway surfaces and bridge decks experience vehicle loading and solar radiation diurnally, which causes mechanical vibrations and thermal gradients to occur in pavement layers. Mechanical energy is able to be converted into electricity using a magnetic field for electromagnetic material or strain field for piezoelectric material. Furthermore, solar energy is able to be harvested using a photovoltaic cell, heat flux, or thermoelectric field. Thus, the wasted energy from the roadway could be harvested and made into usable energy that can used in various ways.

The last few years have observed a significant increase in the numbers of publications in energy harvesting area. Most of the work, however, has focused on specific technical details of adding an energy harvesting device into pavement and evaluating its power output potential. There have been fewer discussions on some other aspects such as comparison of various energy harvesting technologies in the network level of pavement (Guo and Lu 2017). A recent literature review is required to focus on some of these less researches and to best characterize present information condition of energy harvesting pavements. Future study trends for energy harvesting pavements may be recognized with understanding of the recent accomplishments and determinations of different energy harvesting technologies.

The main aim of this chapter is to outline various energy-harvesting technologies that are used in manufacturing roadways. This chapter will also discuss the potential electric energy generation thermoelectric and piezoelectric energy. To identify the potentials that each form of technology has in terms of harvesting energy from a pavement network, this chapter will present a case study of the New Jersey roadway network, and this will serve as the key example for analysis. This case study will use literature review findings as inputs in order to evaluate and compare the level electrical energy that can be harvested using the energy-harvesting technologies available to the

New Jersey roadway network. Case study results will subsequently be applied in the analysis of cost-effectiveness.

6.2 CONCEPT OF ENERGY HARVESTING TECHNOLOGIES

6.2.1 Thermoelectric Generator (TEG)

Thermoelectric generator's (TEG) is used to harvest energy made in the thermal change of the surrounding environment. TEG can make effective use of the temperature differences between pavement layers in order to create generate electricity based in accordance with thermoelectrical principles.

Uchida *et al.* 2016 explained that the direct conversion of thermal energy to electrical power means that thermoelectric generation is one of the most critical and promising forms of technologies in harvesting heat energy. The Seebeck effect was revealed by T.J. Seebeck in 1821 and has subsequently been widely applied in a majority of thermoelectric-generation technologies. The Seebeck effect is described as the creation of an electric field in instances where there is a temperature gradient at both ends of a thermoelectric generator device (Goldsmid 2016). It is thus possible to reverse the temperature gradient of the conductor and the electric current generation. The TE module is typically made up of two parallel N-type and P-type semiconductors with heat sources and heat sinking on each side, which can be seen in Figure 6.1 (Datta *et al.* 2017; Hasebe *et al.* 2006; Wu and Yu 2012).

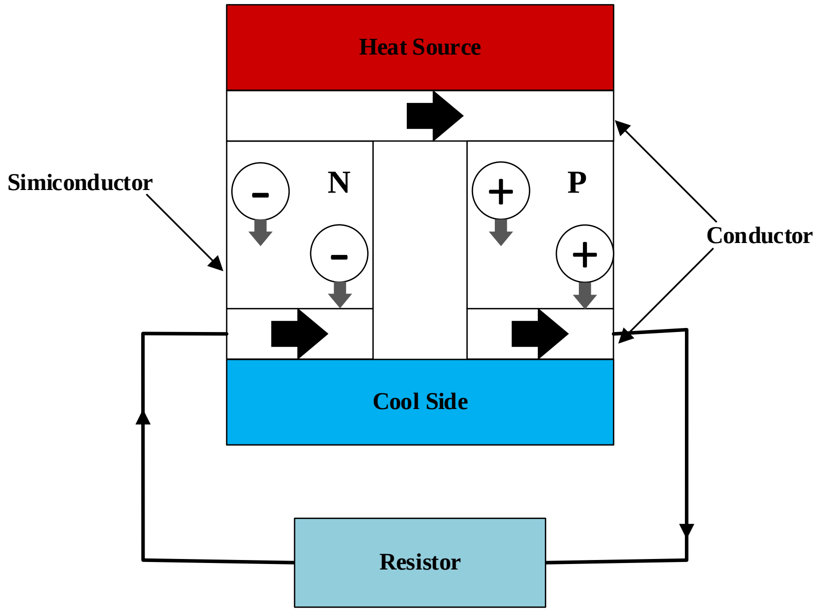

Figure 6.1 Working Principle of Thermoelectric Generator (after Wang et al. 2018)

The principles of the Seebeck effect require that high Seebeck coefficient, low thermal conductivity, and low electrical resistivity are present in order to optimize the conversion efficiency of thermoelectric generator. Minimum loss of energy during heat conduction and joule dissipation is achieved through the low thermal conductivity and electrical resistivity. Thermoelectric semiconductors have typically been used to address the restrictions associated with isotropic metals, whose improvement is limited due to the Wiedemann-Franz law (Uchida *et al.* 2016). The main flaw of this technology is that it possesses a low-efficiency rate. However, it would be possible to enhance the efficiency by using innovative materials in the manufacturing of the TEG.

Hasebe *et al.* (2006) proposed thermoelectric generators using solar thermal energy collected by piping system under the pavement as shown in Figure 6.2. The thermal energy of the hot end of thermoelectric generator (TEG) came from water circulating in the heating pipe, and the cooling pipe carried cool water from an inlet. The results indicated that the output power was about 0.05mW and at an overall system efficiency of 2.05%.

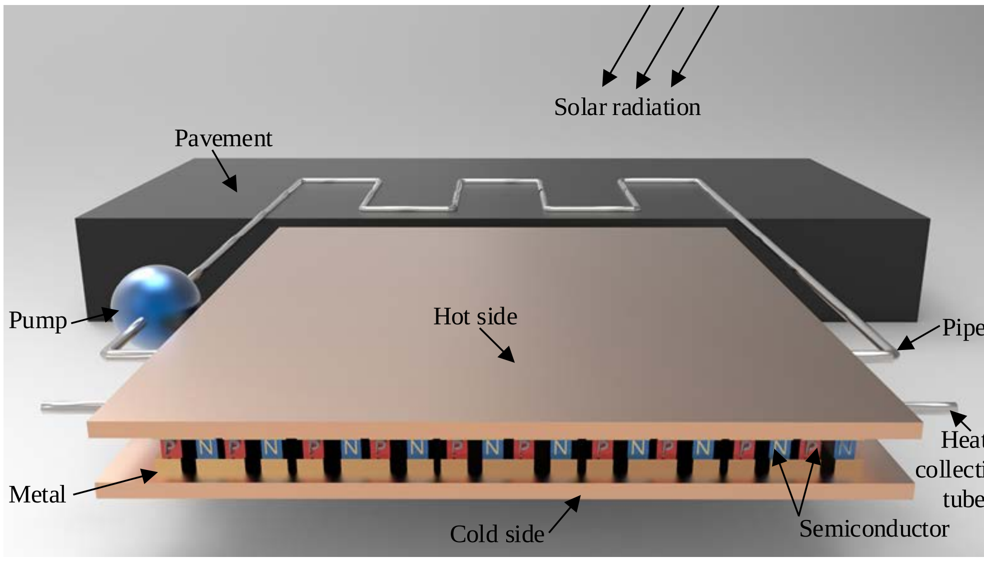

Figure 6.2 Concept of Pipe-Pavement-Thermoelectric Generator System (PP-TEG) (after Wang *et al.* 2018)

6.2.2 Piezoelectric (PE) Energy Harvesting

Piezoelectric materials generate electric charges when subjected to mechanical stresses or change geometric dimensions when an electric field is applied. The working principle of piezoelectric energy harvesting is shown in Figure 6.3. The voltage produced from piezoelectric material varies with time and results in an alternate current (AC) signal, which causes the direct and inverse piezoelectric effect, respectively (Cobbold 2006).

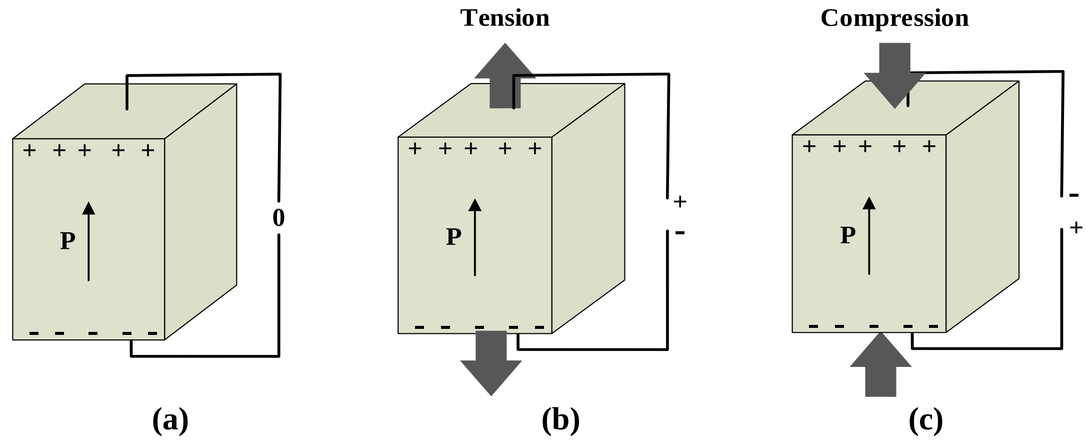

Figure 6.3 Working Principle of piezoelectric effect under (a) zero stress; (b) tension; and (c) compression (Cobbold 2006; Wang et al. 2018)

Piezoelectric materials may be categorized in the following way: single crystalline material (e.g., quartz), piezoceramics (e.g, lead zirconate titanate [PZT]); piezoelectric semiconductors (e.g., ZnO2), polymer (e.g., Polyvinylidene fluoride [PVDF]), piezoelectric composites, and glass ceramics (e.g., Li2Si2O5, Ba2TiSiO6). Despite the fact that piezoelectric materials possess varying piezoelectric and mechanical properties, the most frequent ones are polymers and ceramics. Polymer materials tend to be tender and flexible, whereas ceramics are hard and rigid. Typically, polymers create lower energy than ceramics as a result of different dielectric and piezoelectric features.

There are two key ways of enhancing the amount of electrical energy harvested, the first of which is to apply more stress or strains. The second is to apply the coupling method in a more effective way. There are two types of possible coupling methods, namely the d_{31} mode and the d_{33} method. Their application depends on the poling direction of piezoelectric material in relation to the direction of applied force. If the material is forced to move perpendicular to the poling direction, then the d_{31} mode will be used, whilst the d_{33} mode is used when the applied force is in the same direction as the poling. Anton and Sodano (2007) state that the d_{33} mode creates more effective electromechanical coupling than the d_{31} mode, which is experienced by a majority of piezoelectric materials.

A vast amount of piezoelectric transducer designs have been developed and recommended, for example the multilayer (Heinzmann *et al.* 2002; Uchino 2009), cymbal (Dogan 1994), Moonie (Dogan 1994), bridge (Zhao *et al.* 2010), thin layer unimorph driver and sensor (THUNDER) (Mossi *et al.* 1998), reduced and internally biased oxide wafer (RAINBOW) (Haertling 1991), macro-fiber composite (MFC), and bimorph (Roundy *et al.* 2003). Many factors can impact the energy harvesting capacity of a piezoelectric transducer, including material, external loading and the geometric design of the transducer. In general, the Cymbal and Bridge transducers are preferred configurations for energy harvesting in roadway considering the vehicular load pattern and the stiffness consistency between transducer and pavement materials.

6.3 LEVELIZED COST OF ELECTRICITY (LCOE)

Comparing the potentials of technologies cannot only depend on the electrical energy generated from pavements. In this chapter, the benefits from available systems are evaluated based on the total costs (including annualized capital and yearly operating) divided by total energy service production, computed as $/kWh. LCOE allows the comparison of different technologies (e.g., TEG, PZT) of unequal lifespans, project size, different capital cost, risk, return, and capacities. The indicator of this cost-effectiveness analysis can be termed as a levelized cost of electricity (LCOE). Figure 6.4 shows the main concept of the cost-effectiveness analysis using levelized cost of electricity (LCOE). The levelized cost of electricity (LCOE) is given by:

$$\mathrm{LCOE} = \frac{\text{Sum of Costs over Lifetime}}{\text{Sum of Electrical Energy Produced over Lifetime}} \tag{6.1}$$

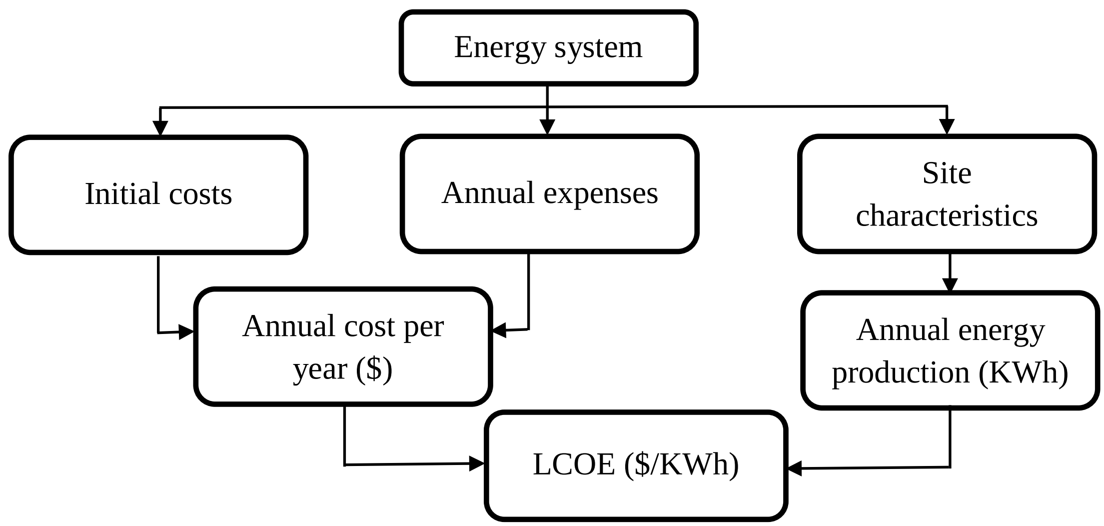

Figure 6.4 Levelized cost of electricity (LCOE) concept

6.4 ESTIMATION OF ELECTRICAL ENERGY GENERATION FROM A PAVEMENT NETWORK

To reveal the potentials of all technologies for harvesting energy from a pavement network, a case study is discussed in this chapter, which uses the New Jersey roadway network as the example for analysis. The case study takes findings from the literature review as inputs to assess and compare the amount of electrical energy that may be collected by some available energy-harvesting technologies from the New Jersey roadway network. Results from the case study are then used in the cost-effectiveness analysis in the next section. The potential of electrical energy generation thermoelectric and piezoelectric (cymbal and novel bridge transducer design) technologies were considered in this chapter.

6.4.1 Thermoelectric Generator (TEG)

6.4.1.1 Network Assumptions

This chapter considers that New Jersey pavement network has one PP-TEG system installed. The PP-TEG system embedded into asphalt pavements which has been proven to efficiently generate electrical energy from solar radiation. A thermoelectric generator containing thermoelectric generator is embedded between two heat tubes to generate power. The first tube is embedded in a meandering arrangement into the surface layer of each segment of the pavement where it can be warmed by heat from the sun. The lower layer, base or subbase layer, of the pavement has a second tube which works as a heat exchanger and uses river water as a cooling agent.

The percentage of thermal energy gathered by the pipe system, the percentage of the heat absorbed by the asphalt, the efficiency of the thermoelectric generator and the amount of solar radiation are all factors which affect the sum of the pipe structure's electrical energy.

The absorption of pavement surfaces was approximated by using the New Jersey GIS road network map, which details different pavement surface material. Bobes-Jesus *et al.* (2013) , Mallick *et al.* (2009) and Engineering-Toolbox (2018) used information on pavement color and material to estimate how much solar radiation was absorbed. Some surfaces which did not offer suitable environments for installing pipes, and which had low solar absorptivity, were given a coefficient of zero. Portland cement concrete pavements were rated at 0.60, and asphalt concrete at 0.85.

Mallick *et al.* (2009), Gao *et al.* (2010) and Bobes-Jesus *et al.* (2013) all conducted research into the efficiency of collecting thermal energy using a pipe structure, reporting differing results. This research will take into account Mallick et al.'s (2009) average findings of 0.15.

Kraemer *et al.* (2011) stated that the efficiency of thermoelectric generators value has lately increased, attributable to the components used, from 4% to approximately 10%. This research assumed that the efficiency of thermoelectric generators is 7 % which is the average maximum efficiency found by Kraemer *et al.* (2011).

Figure 6.5 shows the distribution of electrical energy density from the pipe system (PP-TEG) using the parameter values mentioned previously and solar radiation distribution across the New Jersey road network. An electrical energy output value of 20.11 GWh/day is calculated by multiplying the surface area of the pavement by this electrical energy density.

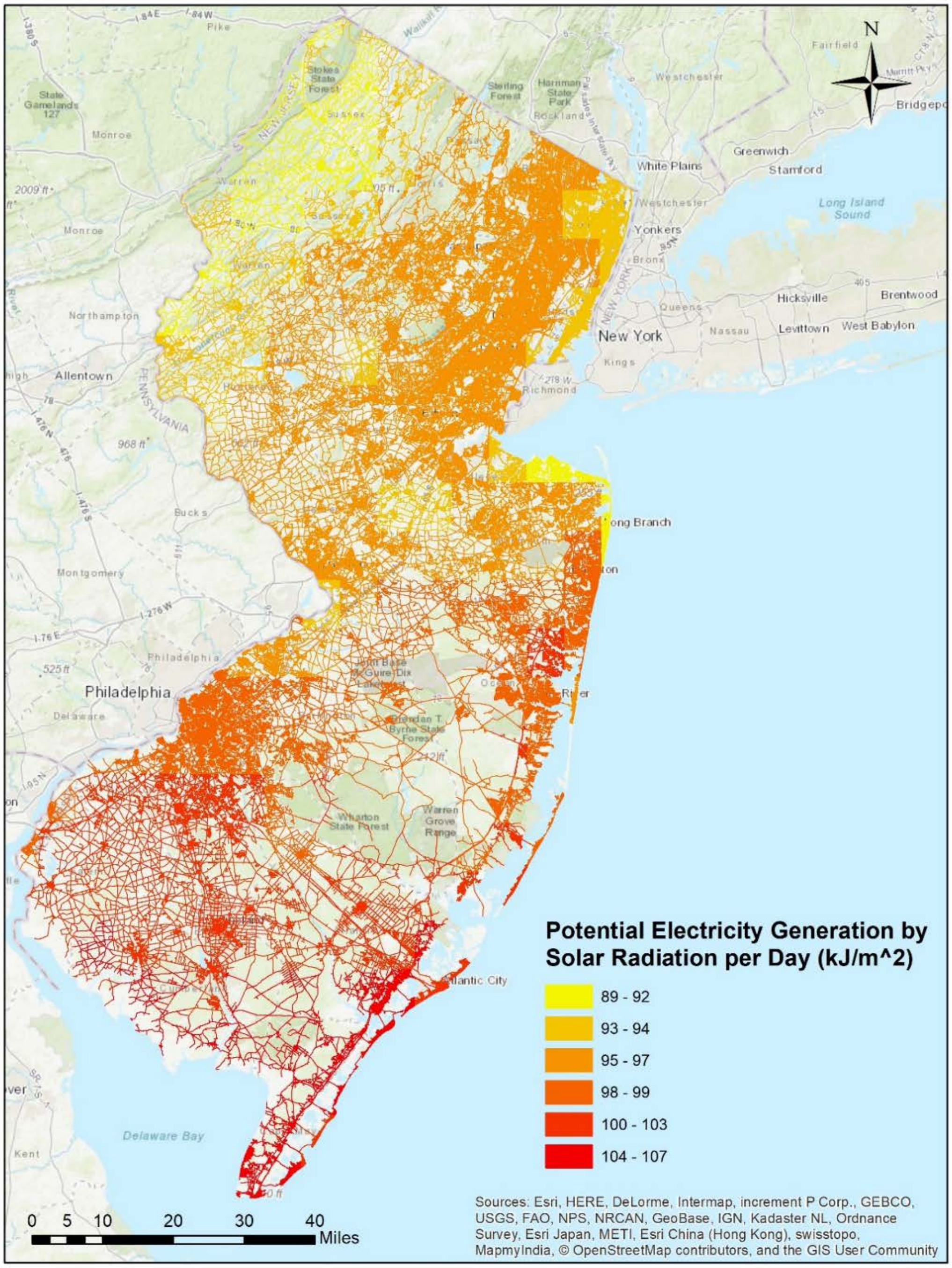

Figure 6.5 Distribution of electrical energy density from the PP-TEG system

6.4.1.2 LCOE Analysis Results

The LCOE from Thermoelectric generator can be expressed as follows;

$$LCOE_{PP-TEG} = \frac{C_{pipe}+C_{pave.}+(C_{main}+C_{pump})\times Y+(C_{module}\times N_{module}+C_{other})/D_{modules}}{W_t\times 365\times Y} \quad (6.2)$$

Where, C_{pipe} =cost of pipe system per m^2 (\$/m^2); $C_{pave.}$ = cost of pavement per m^2 (\$/m^2); C_{main}= cost of maintenance per m^2 per year (\$/m^2/year); C_{pump}= cost of water pump per m^2 per year (\$/m^2/year); C_{module}=cost of each thermoelectric module (\$); C_{other}= cost of other component in each TEG (\$); N_{module}=number of thermoelectric modules in each TEG; $D_{modules}$= distance between two TEGs (m); W_t=energy output from PP-TEG system per m^2 per day (kWh/m^2/day); and Y=service life of PP-TEG system (year).

The study by Yoshitake *et al.* (2010) is used to estimate the information related to total cost of a heating pipe system (C_{pipe} and C_{pump}) and pavement per square meter over their lifetime ($C_{pave\ and}$ C_{main}). This study assumed that the service life of PP-TEG system (Y) is 20 years. Also, based on Hasebe *et al.* (2006) study, the total number of thermoelectric modules (N_{module}) is assumed as 19 modules in each TEG. The cost of each commercial TE module (C_{module}) is assumed as \$30 based on the current market price of TE module. More details on the cost of all PP-TEG system component is listed in Table 6.1.

As shown in Figure 6.5, the energy output from PP-TEG system (W_t) is around 93kJ (0.026 kWh) per square meter per day. Based on the above input data, the LCOE from the PP-TEG system can reach around \$6.88/kWh.

Table 6.1 Cost of all PP-TEG system component (after Guo and Lu 2017)

	Item	Cost ($)
Initial cost of pipe system in pavement ($/m^2) (Yoshitake *et al.* 2010)	Heating pipe system	191.59
	Pavement	94.13
	Other costs	46.24
Running cost of pipe system in pavement ($/m^2/year) (Yoshitake *et al.* 2010)	Water-pump	0.78
	Maintenance	3.34
Thermoelectric generator cost ($) (current market price) (AliExpres 2018; Amazon 2018)	Module cost	30$*19 module
	Other cost	100
	Total cost of TEG	670

6.4.2 Piezoelectric (PE) Technology

6.4.2.1 Network Assumptions

Extensive researches have been carried out to measure the piezoelectric power outputs using various approaches. Analysis and computation factors including the traffic loading pattern, electric rectification design, and the shape and material of the transducer account for the variations in outcomes. Kim *et al.* (2006), Kim *et al.* (2012), and Zhang *et al.* (2015) have consistently collected around 40 mW of instantaneous electric power. Also, the developed energy harvesting module in this dissertation used for comparison purpose. The novel energy harvester module, mentioned in Chapter 5, collects 25-121mW of power at embedded depth of 3 inches below pavement surface. Therefore, these researches were chosen to figure out the power output for the planned PZT system.

A PZT is capable of generating 0.00103 J (2.78×10^{-10} kWh) from every single-wheel load, as approximated by Zhang et al. (2015). A factor of 2, 3 and 4 are used for tandem, tridem and quad axles, respectively. Due to the vehicles' affecting the PZT only where the wheel path, energy density is conveyed in J/m and not J/m^2. Figure 6.6 shows the distribution of electrical energy density (U_A) from the PZT system based on Zhang *et al.* (2015) study, which is worked out as the following;

$$U_A = n \times \int Pd_t \times \sum_{i=1}^{10}(Ni \times \sum_{j=1}^{4}(k_j \times X_j)) \qquad (6.3)$$

Where, n is number of PZTs in one-meter lane length; $\int Pdt$ is the integral of power over time (W) gives the electrical energy produced by every vehicle's load; N_i is the number of truck traffic for class i; k_j is the ratio between number of axles to number of trucks for type j axle load and X_j is the number of axles for type j axle load; I is the number of vehicle class (4 – 13); j is the axle load type (single , tandem, tridem and quad).

The chapter recognized several influencing factors and did not document the number of lanes in the results as traffic was totaled from across all of them. It also identified that 10 PZTs could be included in a 1 m lane since the length of PZT used in Zhang's study was 0.1 m. To avoid further pavement maintenance due taking out the damage modules, this study assumed that the module maintenance done at the same time with regular pavement maintenance. Also, all trucks have same load magnitude on the energy harvester transducer.

The total generated electricity using PZT system can be found by multiplying the energy density distribution matrix approximated in GIS maps by the maximum number of

PZTs. Theoretically, the PZT system developed by Zhang *et al.* (2015) could generate electricity at approximately 3.74 MWh/day.

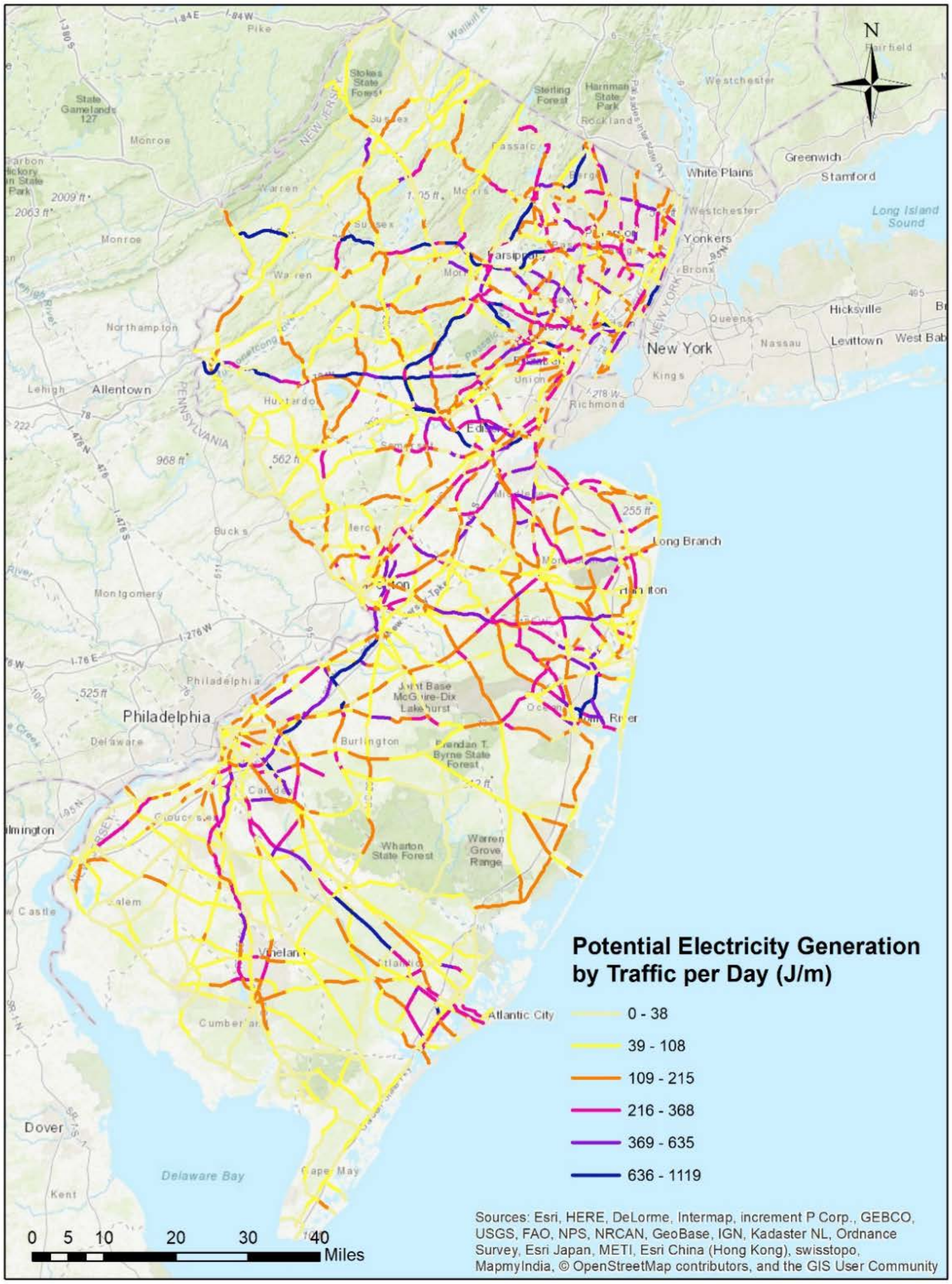

Figure 6.6 Distribution of electrical energy density from the PZT system by Zhang et al. 2015

On the other hand, Figure 6.7 shows the distribution of electrical energy density (U_A) from the PZT system based on the current novel transducer. Equation 6.3 was used to calculate the amount of energy output with the same total number of axles. Two different parameters were changed in Equation 6.3, which are the number of sensors in one-meter length and the power output of energy harvester transducer. Since the length of the energy harvester module that was used in this study is 17.78cm, only five units can be included in one-meter length. Also, it was assumed that the recommended depth of 3 inches below pavement surface and and the average speed of 50mph were used for power calculations. Theoretically, the PZT system developed in this dissertation could generate electricity at approximately 10.01 MWh/day by multiplying the energy density distribution matrix form GIS maps (Figure 6.7) by the maximum number of energy harvester modules.

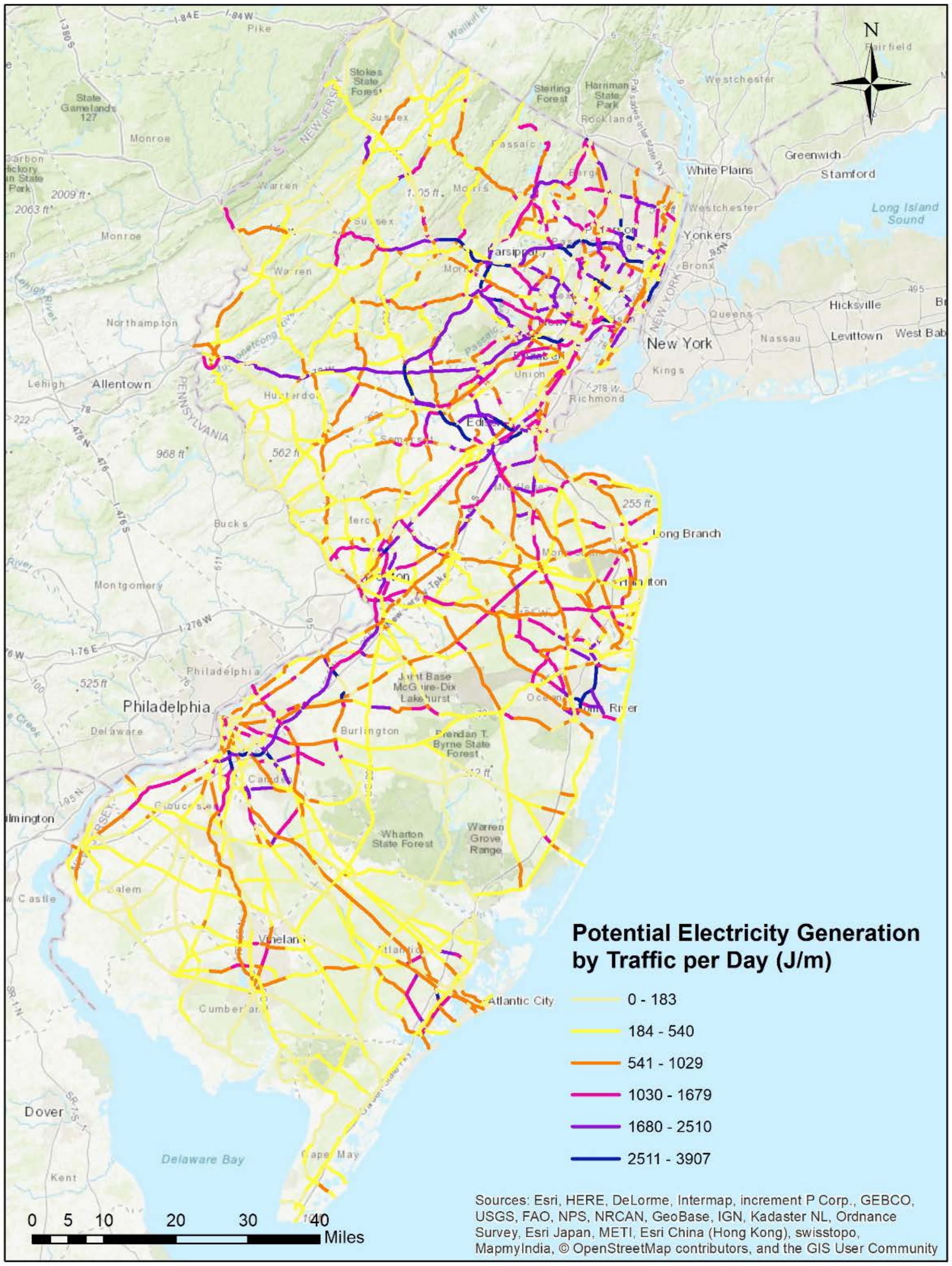

Figure 6.7 Distribution of electrical energy density from the PZT system by Jasim et al. 2017

6.4.2.2 LCOE Analysis Results

The equation of LCOE from piezoelectric system is similar to that from the thermoelectric system, which can be expressed as follows (Moure *et al.* 2016; Xiong 2014):

$$LCOE_{PZT} = \frac{C_{PZT}+C_{inst.}}{W_p \times N \times 365 \times Y} \tag{6.4}$$

Where, C_{PZT}= cost of each PZT units ($); $C_{inst.}$ = cost of installation ($); W_p= energy output from each PZT unit per vehicle (kWh); N= number of vehicle per day; and Y= service life in years.

The study by Moure *et al.* (2016) was used to estimate the material and installation of each PZT. The researchers mentioned that the cost of piezoelectric cymbals is around $1207 per square meter, and the installation cost is $75/m^2. Therefore, the total cost of PZTs in an area of 1609× 0.2m is $412,548 US dollars. Since a total of 482,700 cymbals can be embedded into a 1609 m (1 mile) × 0.2 m area, the total cost of installing each cymbal is around 0.86 cents. Moure *et al.* 2016; Xiong 2014 mentioned that the service life of PZTs is in a range of 5-15 years. For comparison purpose with current energy harvesting module (novel design mentioned in this dissertation), the service life assumed between 2-3 years.

As results, by taking the average value of traffic volume, the LCOE from the PZT system (cymbal design) is varied from $177/kWh to $266/kWh, while the novel design transducer is varied between $36/kWh to $53kWh for 2–3 years' service life.

6.5 ENERGY GENERATION COMPARISON

It can be seen that the PP-TEG system is more cost-effective than the PZT system, unless the PZT system is only paved on the roadway section with very high traffic volume or tunnels where it is impossible to install TEG-PP system. Electrical energy is generated on a greatly lower level by the PZT system, and this may not be enough to justify integration into the present New Jersey road network, contrasting with the pipe system.

For comparison, the LCOE values estimated in the previous section of this chapter are summarized in Table 6.2.

Table 6.2 Inputs for cost-effectiveness analysis of the PZT system

Energy harvesting technology	Service life (Years)	Generate electricity (MWh/day)	LCOE ($/kWh)
Cymbal transducer embedded pavement (Moure *et al.* 2016 and Zhang et al. (2015))	2-3	3.74	177-266
Novel transducer (Jasim et al. 2017)	2-3	10.01	36-53
TEG-PP (Hasebe *et al.* 2006)	2-3 20	20.11×10^3	15-21 6.88

6.6 SUMMARY

For pavement energy harvesting applications, some studies indicated that a pipe system cooperating with a thermoelectric generator (TEG-PP) produce more electric power as compare to piezoelectric transducers (PZTs). This chapter provides the main concept of important energy harvesting technologies in pavements, TEG-PP and PZT, to generate electricity. Then, using the information collected from the literature, a case study is presented based on the New Jersey roadway network, to mathematically assess and compare the potentials of some major energy-harvesting technologies for use in pavements.

CHAPTER 7 FINDINGS, CONCLUSIONS, AND RECOMMENDATIONS

In addition to the laboratory experiments, 3D finite element simulations were performed using the COMSOL commercial finite element modeling program on a single bridge transducer and energy harvester module under static and haversine cyclic load. The results were useful to better understand the behavior of piezoelectric materials under mechanical stresses by comparing the simulations' results to the laboratory results, quantifying the impact on the damage initiation mechanisms due to the applying loads on the energy harvesting module, and also identifying pavement locations that maximize the efficiency of the energy harvester module's output.

8.1 FINDINGS

The main part of this dissertation includes four logically sequential chapters that represent different stages of the research undertaken. The major findings include the following:

8.1.1 Single Transducer Optimization

1) The energy harvesting performance of PZT transducer is affected by PZT material selection, geometry design of transducer, and the external loading. The PZT 5X is preferred in terms of energy output due to the combination of piezoelectric charge constant and piezoelectric voltage constant. The Bridge transducer can produce the higher energy than the Cymbal transducer. As the external loading magnitude increases, the energy output increases nonlinearly.

2) The comparison between analytical solutions and FEA results show that the stress distributions are consistent in general. However, FEA results show high tensile and shear stress concentrations that are responsible for mechanical failure. On the other hand, the discrepancies of energy output between analytical solutions and FEA results are smaller than 5%.

3) It was found that there were no universal relationships that could be observed between geometry parameters and mechanical stresses and energy outputs for the Bridge transducer. The effects of geometry parameters on stress concentration and energy outputs were complicated. The thickness of steel end cap and PZT strip and the cavity height show relatively more significant effects.

4) The new design of Bridge transducer produces about four times energy and energy conversion efficiency as compared to the traditional bridge transducer. This is because layered poling allows that stress is applied in the direction of polarization for each layered segment. The optimized design of Bridge transducer produced an electrical potential of 556V, which could result in 0.743mJ of potential energy (open circuit condition) for a single transducer under 0.7MPa loading.

5) Laboratory testing on energy harvester module showed that simulation results agreed well with the measured power. The maximum output power of 2.1mW was found at a resistive load of 400kΩ under 70kPa at 5Hz. The output power is greater at high resistive loads due to the high impedance of Bridge transducers.

Future research will be conducted to test energy harvester in the roadway under realistic traffic loading.

8.1.2 Piezoelectric Energy Harvester

1) The energy output increased with the increase of loading frequency and load magnitude. This indicates that the energy harvesting performance is affected by vehicle weights, speed, and the embedment location of energy module. On the other hand, the resistive load can be optimized to increase the energy output.
2) The analysis results showed that two different material failure models need be considered in relation to mechanical failure of Bridge transducer, namely tensile and shear failure.
3) The mechanical stresses and fatigue failure of Bridge transducer were significantly affected by the uniform epoxy thickness at the four contact faces between steel cap and PZT strip.
4) The gap design of energy module produced the greater energy output but the fewer fatigue life. The energy harvesting performance and fatigue failure was affected by the selection of cover and base materials of energy module. Therefore, the optimum design of energy module should consider the fabrication of single Bridge transducer and the packaging design of energy module.

8.1.3 Energy Harvesting Module Performance and Fatigue Life

1. The higher the load frequency, the more the output power because it causes shorter load width. Higher vehicle speed produces more power since the piezoelectric materials were excited with higher stress rate.
2. Passing more vehicles from a specific section of a road decreases each cycle of loading. In a particular period of time, higher ADT results in more energy harvesting.
3. Applying higher values of load, more dipoles will be actuated and results in the increase in the output voltage. The need to increase the loading magnitude will match with increasing the output power.
4. The electric power collected from each piezoelectric transducer was limited to within 40-190 mW, which can supply electricity to low-power electronics, such as LED lights or embedded sensors.
5. The maximum power output of the energy harvester module is around 122mW at a vehicle speed of 65mph and 3 inches embedded depth.
6. It is considered that the minimum embedded depth of the energy harvesting module is two inches below pavement surface to ensure that no effects were noticeable at the surface.
7. Embedding the energy harvesting module below three inches from the pavement surface is the best location to maximize both power output and service life.
8. The effect of the pavement temperature on the output power was found to be negligible.

8.1.4 Levelized Cost of Electricity (LCOE)

1. Based on current technologies, a thermoelectric-based pipe system covering the entire New Jersey roadway network may potentially collect 20.11 GWh electrical energy per day, while a piezoelectric transducer system may collect around 3.74 and 10.01MWh of electrical energy per day for cymbal and novel bridge transducer design, respectively.
2. For service life range between 2-3 years, the average LCOE from the PZT system in entire roadway network may range from $177/kWh - $266/kWh for cymbal transducer design based on Zhang et al. (2015) study, $36/kWh - $53/kWh for novel bridge design based on the current dissertation focus and $15/kWh - $21/kWh for TEG-PP systems.

8.2 CONCLUSIONS

The following conclusions are drawn based upon the experimental results and finite modeling simulations, analysis performed in this research study:

1) Among all energy harvesting technologies, most studies found that the mentioned that the peak productivity of photovoltaic technology was much greater than others. However, its energy productivity can be maximized only under direct sunlight during a certain period of a day. The productivity is limited under low illumination conditions, such as during a cloudy day or in a tunnel. Other than photovoltaic technology, under certain conditions, piezoelectric energy harvesting is the most productive one.

2) Different energy harvester designs made of piezoelectric material can be used for stress-based or vibration-based energy harvesting and sensor applications in roadways and bridges. The generated energy output is usually small for individual piezoelectric transducer under one vehicle pass. In order to generate the greater energy, multiple sensor arrays under repeated traffic loading are needed.
3) For energy harvester system embedded in the roadway, it may cause stress concentration depending on the packagingmaterial type, traffic volume and pavement structure. Therefore, investigation is needed to take into account the integrity between energy harvester and road material considering the interaction between pavement structure, traffic loading, and system design. In addition, implementing piezoelectric system on field requires standard specifications in the execution process which has not been established. This is important as to use appropriate management and method to prevent manipulating with road infrastructure and minimize traffic congestion.

8.3 RECOMMENDATIONS FOR FUTURE STUDY

For future research, following recommendations were provided:

1. It is necessary to test the developed energy harvesting module (PEH) in the field to validate the laboratory results. Also, the effect of pavement structure and road type on the output power is required.

2. Developing a statistical model to predict the power output versus stress, loading frequency and temperature is needed to present the physical relationship between the aforementioned variables.
3. The energy harvester module should be able to resist hard environmental factors including dust and water. Testing the module under wet condition (moisture effect) is required in future studies.
4. Additional analysis is required to optimize number and size of piezoelectric bridge transducers inside energy harvesting module based on energy output and economic considerations.
5. Additional analysis is required to optimize the number poling layers, more than seven layers, to increase the efficiency and capacitance of the sensor.
6. Since this research focused on available mechanical energy form roadway, another source of energy with higher mechanical energy is needed for future work such as airports and railways.

REFERENCES

Adu-Osei, A., Little, D., and Lytton, R. (2001). "Cross-anisotropic characterization of unbound granular materials." *Transportation research record: journal of the transportation research board*(1757), 82-91.

Ali, S. F., Friswell, M., and Adhikari, S. (2011). "Analysis of energy harvesters for highway bridges." *Journal of Intelligent Material Systems and Structures*, Vol. 22(No. 16), pp. 1929-1938.

AliExpres (2018). "Thermoelectric Generator Module." <⟨https://www.aliexpress.com/price/thermoelectric-module_price.html⟩>. (03.05.2018, 2018).

Andriopoulou, S. (2012). "A review on energy harvesting from roads." *Independent thesis Advanced level .KTH, School of Architecture and the Built Environment (ABE), Transport Science, Highway and Railway Engineering.*

Anton, S. R., Erturk, A., and Inman, D. J. (2012). "Bending strength of piezoelectric ceramics and single crystals for multifunctional load-bearing applications." *IEEE Transactions on Ultrasonics, Ferroelectrics and Frequency Control*, 59(6), 1085-1092.

Anton, S. R., and Sodano, H. A. (2007). "A review of power harvesting using piezoelectric materials (2003–2006)." *Smart materials and Structures*, 16(3), R1.

Ashley, S. (1995). "Smart skis and other adaptive structures." *Mechanical Engineering-CIME*, 117(11), 76-82.

Auld, B. A. (1981). "Wave propagation and resonance in piezoelectric materials." *The Journal of the Acoustical Society of America*, 70(6), 1577-1585.

Baker, J., Roundy, S., and Wright, P. "Alternative geometries for increasing power density in vibration energy scavenging for wireless sensor networks." *Proc., Proc. 3rd Int. Energy Conversion Engineering Conf.(San Francisco, CA, Aug.)*, 959-970.

Baldwin, J. D., Roswurm, S., Nolan, J., and Holliday, L. (2011). "Energy harvesting on highway bridges." *Final Report FHWA-OK-11-01*(Final Report FHWA-OK-11-01).

Barksdale, R. D. (1971). "Compressive stress pulse times in flexible pavements for use in dynamic testing." *Highway research record*(345).

Basquin, O. "The exponential law of endurance tests." *Proc., Proc. Astm*, 625-630.

Beeby, S. P., Tudor, M. J., and White, N. M. (2006). "Energy harvesting vibration sources for microsystems applications." *Measurement science and technology*, 17(12), R175.

Bennett, J. A. (1946). "Study of the Damaging Effect of Fatigue Stressing on SAE X4130 Steel." *Natl.Bur.Standards (US), Research Paper*, 123-139.

Bhat, S., and Patibandla, R. (2011). *Metal fatigue and basic theoretical models: a review*, INTECH Open Access Publisher.

Bobes-Jesus, V., Pascual-Muñoz, P., Castro-Fresno, D., and Rodriguez-Hernandez, J. (2013). "Asphalt solar collectors: A literature review." *Applied Energy*, 102, 962-970.

Brown, S. F. (1973). "Determination of Young's modulus for bituminous materials in pavement design." *Highway Research Record*(431).

Bryant, R. G. (2007). "Overview of NASA Langley's piezoelectric ceramic packaging technology and applications."

Burmister, D. M. (1945). "The general theory of stresses and displacements in layered systems. I." *Journal of Applied Physics*, 16(2), 89-94.

Campbell, F. C. (2008). *Elements of metallurgy and engineering alloys*, ASM International.

Carcangiu, S., Montisci, A., and Forcinetti, R. (2015). "Numerical Simulation of Wave Propagation." *Ultrasonic Nondestructive Evaluation Systems*, Springer, 17-45.

Cassidy, I. L., Scruggs, J. T., Behrens, S., and Gavin, H. P. (2011). "Design and experimental characterization of an electromagnetic transducer for large-scale vibratory energy harvesting applications." *Journal of Intelligent Material Systems and Structures*, 22(17), 2009-2024.

Chen, C., and Liao, W.-H. "A self-powered, self-sensing magnetorheological damper." *Proc., Mechatronics and Automation (ICMA), 2010 International Conference on*, IEEE, 1364-1369.

Chen, J., Wang, H., and Zhu, H. (2017). "Analytical approach for evaluating temperature field of thermal modified asphalt pavement and urban heat island effect." *Applied Thermal Engineering*, 113, 739-748.

Chen, Y., Zhang, H., Zhang, Y., Li, C., Yang, Q., Zheng, H., and Lü, C. (2016). "Mechanical energy harvesting from road pavements under vehicular load using embedded piezoelectric elements." *Journal of Applied Mechanics*, 83(8), 081001.

Chiarelli, A., Al-Mohammedawi, A., Dawson, A., and García, A. (2017). "Construction and configuration of convection-powered asphalt solar collectors for the reduction of urban temperatures." *International Journal of Thermal Sciences*, 112, 242-251.

Chou, Y. T. (1969). "Stresses and displacements in viscoelastic pavement systems under a moving load."

Christensen, R. (2012). *Theory of viscoelasticity: an introduction*, Elsevier.

Chua, H. G., Kok, B. C., and Goh, H. H. (2014). "Modelling and design analyses of a piezoelectric cymbal transducer (PCT) structure for energy harvesting application." *WIT Transactions on Ecology and the Environment*, 186, 103-114.

Chuang, T.-j., Wang, Z., Hill, M., and White, G. (1996). "Fatigue life predictions of PZT using continuum damage mechanics and finite element methods." *Fracture Mechanics of Ceramics,* Springer, 135-148.

Clark, W. W., and Ramsay, M. J. "Smart material transducers as power sources for MEMS devices." *Proc., International Symposium on Smart Structures and Microsystems, Hong Kong, Oct*, 19-21.

Cobbold, R. S. (2006). *Foundations of biomedical ultrasound*, Oxford University Press.

Coffin Jr, L. F. (1953). "A study of the effects of cyclic thermal stresses on a ductile metal." Knolls Atomic Power Lab.

Cook-Chennault, K. A., Thambi, N., and Sastry, A. M. (2008). "Powering MEMS portable devices—a review of non-regenerative and regenerative power supply systems with special emphasis on piezoelectric energy harvesting systems." *Smart Materials and Structures*, 17(4), 043001.

Corten, H. T., and Dolan, T. J. "Cumulative fatigue damage." *Proc., Proceedings of the international conference on fatigue of metals*, 235.

Daniels, A., Giuliano, A., Zhu, M., and Tiwari, A. "Modeling, validation and design analyses of a piezoelectric cymbal transducer for non-resonant energy harvesting." *Proc., Green Computing and Communications (GreenCom), 2013 IEEE and Internet of Things (iThings/CPSCom), IEEE International Conference on and IEEE Cyber, Physical and Social Computing*, IEEE, 1665-1667.

Datta, U., Dessouky, S., and Papagiannakis, A. "Thermal Energy Harvesting from Asphalt Roadway Pavement." *Proc., International Congress and Exhibition" Sustainable Civil Infrastructures: Innovative Infrastructure Geotechnology"*, Springer, 272-286.

Davidson, J., and Mo, C. (2014). "Recent advances in energy harvesting technologies for structural health monitoring applications." *Smart Materials Research*, 2014.

Dehart, D., and Griffin, S. "Astronautics Laboratory smart structures/skins overview." *Proc., Joint US/Japan Conference on Adaptive Structures*, 3-10.

Dogan, A. (1994). "Flextensional" moonie and Cymbal" Actuators."

Dogan, A., Uchino, K., and Newnham, R. E. (1997). "Composite piezoelectric transducer with truncated conical endcaps" Cymbal"." *Ultrasonics, Ferroelectrics, and Frequency Control, IEEE Transactions on*, 44(3), 597-605.

Dutoit, N. E., Wardle, B. L., and Kim, S.-G. (2005). "Design considerations for MEMS-scale piezoelectric mechanical vibration energy harvesters." *Integrated Ferroelectrics*, Vol. 71(1), pp. 121-160-160.

Edel-Ajulay, J. "Innowattech; Harvesting Energy and Data." *Proc., 1st International symposium the highway to innovation, Tel Aviv*.

El-Hami, M., Glynne-Jones, P., White, N., Hill, M., Beeby, S., James, E., Brown, A., and Ross, J. (2001). "Design and fabrication of a new vibration-based electromechanical power generator." *Sensors and Actuators A: Physical*, 92(1), 335-342.

Elliott, J. F., and Moavenzadeh, F. (1971). "Analysis of stresses and displacements in three-layer viscoelastic systems." *Highway Research Record*(345).

Engineering-Toolbox (2018). "Solar radiation absorbed by various materials." <http://www.engineeringtoolbox.com/solar-radiation-absorbed-materials-d_1568.html>. (01.15, 2018).

Flügge, W. (1975). *Viscoelasticity*.

Freudenthal, A. M., and Heller, R. A. (1959). "On stress interaction in fatigue and a cumulative damage rule." *Journal of the Aerospace Sciences*, 26(7), pp. 431-442.

Fthenakis, V., and Kim, H. C. (2009). "Land use and electricity generation: A life-cycle analysis." *Renewable and Sustainable Energy Reviews*, 13(6), 1465-1474.

Furman, E., Li, G., and Haertling, G. (1994). "An investigation of the resonance properties of rainbow devices." *Ferroelectrics*, 160(1), 357-369.

Gao, Q., Huang, Y., Li, M., Liu, Y., and Yan, Y. (2010). "Experimental study of slab solar collection on the hydronic system of road." *Solar energy*, 84(12), 2096-2102.

Gillespie, T. D. (1993). *Effects of heavy-vehicle characteristics on pavement response and performance*, Transportation Research Board.

Goldfarb, M., and Jones, L. D. (1999). "On the efficiency of electric power generation with piezoelectric ceramic." *Journal of Dynamic Systems, Measurement, and Control*, 121(3), 566-571.

Goldsmid, H. J. (2016). *Introduction to thermoelectricity*, Springer.

Gonçalves, V. O., Pardini, L. C., and Ancelotti Jr, A. C. "Fatigue under Shear Stress by Using the Iosipescu Method for Carbon/Epoxy Composites." *Proc., Advanced Engineering Forum*, Trans Tech Publ, 22-28.

Gonzalez, J. L., Rubio, A., and Moll, F. "A prospect on the use of piezoelectric effect to supply power to wearable electronic devices." *Proc., Proceedings of the International Conference on Materials Engineering Resources (ICMR)*, 202-206.

Guldentops, G., Nejad, A. M., Vuye, C., and Rahbar, N. (2016). "Performance of a pavement solar energy collector: Model development and validation." *Applied Energy*, 163, 180-189.

Guo, L., and Lu, Q. (2017). "Modeling a new energy harvesting pavement system with experimental verification." *Applied Energy*.

Guo, L., and Lu, Q. (2017). "Potentials of piezoelectric and thermoelectric technologies for harvesting energy from pavements." *Renewable and Sustainable Energy Reviews*, 72, 761-773.

Ha, S. K., Keilers, C., and Chang, F.-K. (1992). "Finite element analysis of composite structures containing distributed piezoceramic sensors and actuators." *AIAA Journal*, 30(3), 772-780.

Haertling, G. "Compositional study of PLZT Rainbow ceramics for piezo actuators." *Proc., Applications of Ferroelectrics, 1994. ISAF'94., Proceedings of the Ninth IEEE International Symposium on*, IEEE, 313-318.

Hasebe, M., Kamikawa, Y., and Meiarashi, S. "Thermoelectric generators using solar thermal energy in heated road pavement." *Proc., 2006 25th International Conference on Thermoelectrics*, IEEE, 697-700.

Hashin, Z., and Rotem, A. (1978). "A cumulative damage theory of fatigue failure." *Materials Science and Engineering*, 34(2), 147-160.

Heinzmann, A., Hennig, E., Kolle, B., Kopsch, D., Richter, S., Schwotzer, H., and Wehrsdorfer, E. "Properties of PZT Multilayer Actuators." *Proc., Actuator 2002: Eighth International Conference on New Actuators*.

Heinzmann, A., Hennig, E., Kolle, B., Kopsch, D., Richter, S., Schwotzer, H., and Wehrsdorfer, E. "Properties of PZT multilayer actuators." *Proc., 8th International Conference on New Actuators, Bremen, Germany*.

Hendrowati, W., Guntur, H. L., and Sutantra, I. N. (2012). "Design, modeling and analysis of implementing a multilayer piezoelectric vibration energy harvesting mechanism in the vehicle suspension." *Engineering*, 4(11), 728.

Hicks, R. G., and Monismith, C. L. (1971). "Factors influencing the resilient response of granular materials." *Highway research record*(345).

High, J. W., and Wilkie, W. K. (2003). "Method of fabricating NASA-standard macro-fiber composite piezoelectric actuators."

Hill, D., Agarwal, A., and Tong, N. (2013). "Assessment of piezoelectric materials for roadway energy harvesting." *DNV KEMA, California Energy Commission, California*.

Huang, Y. H. (1973). "Stresses and strains in viscoelastic multilayer systems subjected to moving loads." *Highway research record*(457), pp. 60-71.

Huang, Y. H. (1993). *Pavement analysis and design*, Prentice Hall, Upper Saddle River, NJ.

Hurlebaus, S. (2002). "A contribution to structural health monitoring using elastic waves." Inst. A für Mechanik.

Ilyas, M. A., and Swingler, J. (2015). "Piezoelectric energy harvesting from raindrop impacts." *Energy*, 90, 796-806.

Jasim, A., Wang, H., Yesner, G., Safari, A., and Maher, A. (2017). "Optimized design of layered bridge transducer for piezoelectric energy harvesting from roadway." *Energy*, 141, 1133-1145.

Jeon, Y. B., Sood, R., Jeong, J. H., and Kim, S. G. (2005). "MEMS power generator with transverse mode thin film PZT." *Sensors and Actuators A: Physical*, 122(1), 16-22.

Jung, I., Shin, Y.-H., Kim, S., Choi, J.-y., and Kang, C.-Y. (2017). "Flexible piezoelectric polymer-based energy harvesting system for roadway applications." *Applied Energy*, 197, 222-229.

Kamel, T. M. (2007). "Poling and switching of PZT ceramics: field and grain size effects." Eindhoven University of Technology.

Kang-Won, W., and Correia, A. J. (2010). "A pilot study for investigation of novel methods to harvest solar energy from asphalt pavements." *A final report for Korea Institute of Construction Technology (KICT).*

Kasyap, A., Lim, J., Johnson, D., Horowitz, S., Nishida, T., Ngo, K., Sheplak, M., and Cattafesta, L. "Energy reclamation from a vibrating piezoceramic composite beam." *Proc., Proceedings of 9th International Congress on Sound and Vibration*, 36-43.

Kim, C.-I., Kim, K.-B., Jeon, J.-H., Jeong, Y.-H., Cho, J.-H., Paik, J.-H., Kang, I.-S., Lee, M.-Y., Choi, B.-J., and Cho, Y.-B. (2012). "Development and Evaluation of the Road Energy Harvester Using Piezoelectric Cantilevers." *Journal of the Korean Institute of Electrical and Electronic Material Engineers*, 25(7), 511-515.

Kim, H., Jang, E., Kim, D., Hwang, L., and Yoo, J. (2009). "Thickness–Vibration-Mode Multilayer Piezoelectric Transformer for DC-DC Converter Application." *Integrated Ferroelectrics*, 107(1), 12-23.

Kim, H., Priya, S., and Uchino, K. (2006). "Modeling of piezoelectric energy harvesting using cymbal transducers." *Japanese journal of applied physics*, 45(7R), 5836.

Kim, H. S., Kim, J.-H., and Kim, J. (2011). "A review of piezoelectric energy harvesting based on vibration." *International Journal of precision engineering and manufacturing*, 12(6), pp. 1129-1141.

Kim, H. W., Batra, A., Priya, S., Uchino, K., Markley, D., Newnham, R. E., and Hofmann, H. F. (2004). "Energy harvesting using a piezoelectric “cymbal” transducer in dynamic environment." *Japanese journal of applied physics*, 43(9R), 6178.

Kim, H. W., Priya, S., Uchino, K., and Newnham, R. E. (2005). "Piezoelectric energy harvesting under high pre-stressed cyclic vibrations." *Journal of Electroceramics*, 15(1), 27-34.

Kommers, J. B. "The effect of overstress in fatigue on the endurance life of steel." *Proc., PROCEEDINGS-AMERICAN SOCIETY FOR TESTING AND MATERIALS*, AMER SOC TESTING MATERIALS 100 BARR HARBOR DR, W CONSHOHOCKEN, PA 19428-2959, 532-541.

Kraemer, D., Poudel, B., Feng, H.-P., Caylor, J. C., Yu, B., Yan, X., Ma, Y., Wang, X., Wang, D., and Muto, A. (2011). "High-performance flat-panel solar thermoelectric generators with high thermal concentration." *Nature materials*, 10(7), 532.

Kwon, J., Tutumluer, E., and Al-Qadi, I. L. (2009). "Validated mechanistic model for geogrid base reinforced flexible pavements." *Journal of Transportation Engineering*, 135(12), 915-926.

Leinonen, M., Palosaari, J., Juuti, J., and Jantunen, H. (2014). "Combined electrical and electromechanical simulations of a piezoelectric cymbal harvester for energy harvesting from walking." *Journal of Intelligent Material Systems and Structures*, 25(4), 391-400.

Lesieutre, G. A., Hofmann, H., and Ottmann, G. "Structural damping due to piezoelectric energy harvesting." *Proc., 13th International Conference on Adaptive Structures and Technologies*, 368-377.

Li, H., Tian, C., and Deng, Z. D. (2014). "Energy harvesting from low frequency applications using piezoelectric materials." *Applied Physics Reviews*, 1(4), 041301.

Lin, M., and Chang, F. K. "Development of smart layer for built-in diagnostics for composite structures." *Proc., Thirteenth Technical Conference of the American Society for Composites*.

Loos, M., Yang, J., Feke, D., and Manas-Zloczower, I. (2012). "Enhanced fatigue life of carbon nanotube-reinforced epoxy composites." *Polymer Engineering & Science*, 52(9), 1882-1887.

Loulizi, A., Al-Qadi, I., Lahouar, S., and Freeman, T. (2002). "Measurement of vertical compressive stress pulse in flexible pavements: representation for dynamic loading tests." *Transportation Research Record: Journal of the Transportation Research Board*(1816), 125-136.

Mallick, R. B., Chen, B.-L., and Bhowmick, S. (2009). "Harvesting energy from asphalt pavements and reducing the heat island effect." *International Journal of Sustainable Engineering*, 2(3), 214-228.

Manson, S. S. (1954). "Behavior of materials under conditions of thermal stress."

Manson, S. S. (1966). "Interfaces between fatigue, creep, and fracture." *International Journal of Fracture Mechanics*, 2(1), 327-327.

Marco, S. M., and Starkey, W. L. (1954). "A concept of fatigue damage." *Trans.ASME*, 76(4), 627-632.

Masad, S., Little, D., and Masad, E. (2006). "Analysis of flexible pavement response and performance using isotropic and anisotropic material properties." *Journal of Transportation Engineering*, 132(4), 342-349.

McLean, D. B. (1974). *Permanent deformation characteristics of asphalt concrete*, University of California, Berkeley.

Miclea, C., Tanasoiu, C., Amarande, L., Miclea, C., Plavitu, C., Cioangher, M., Trupina, L., Miclea, C., and David, C. (2007). "Effect of temperature on the main piezoelectric parameters of a soft PZT ceramic." *Rom. J. Inf. Sci. Technol*, 10(3), 243-250.

Miner, M. A. (1945). "Cumulative damage in fatigue." *Journal of applied mechanics*, 12(3), 159-164.

Mo, C., Arnold, D., Kinsel, W. C., and Clark, W. W. (2013). "Modeling and experimental validation of unimorph piezoelectric cymbal design in energy harvesting." *Journal of Intelligent Material Systems and Structures*, 24(7), 828-836.

Mossi, K. M., Selby, G. V., and Bryant, R. G. (1998). "Thin-layer composite unimorph ferroelectric driver and sensor properties." *Materials Letters*, 35(1), 39-49.

Moulthrop, J., and Witczak, M. W. (2011). "A Performance-Related Specification for Hot Mixed Asphalt. NCHRP Report 704." *Transportation Research Board, Washington, DC, USA.*

Moure, A., Izquierdo Rodríguez, M. A., Rueda, S. H., Gonzalo, A., Rubio-Marcos, F., Cuadros, D. U., Pérez-Lepe, A., and Fernández, J. F. (2016). "Feasible integration in asphalt of piezoelectric cymbals for vibration energy harvesting." *Energy Conversion and Management*, 112, 246-253.

Nordmann, T., and Clavadetscher, L. (2004). "PV on noise barriers." *Progress in Photovoltaics: Research and Applications*, 12(6), 485-495.

Nordmann, T., Froelich, A., Goetzberger, A., Kleiss, G., Hille, G., Reise, C., Wiemken, E., van Dijk, V., Betcke, J., and Pearsall, N. "The potential of PV noise barrier technology in Europe." *Proc., 16th European Photovoltaic Solar Energy Conference and Exhibition*, 1-5.

Oh, J.-H., Lytton, R. L., and Fernando, E. G. (2006). "Modeling of pavement response using nonlinear cross-anisotropy approach." *Journal of Transportation Engineering*, 132(6), 458-468.

Okayasu, M., Odagiri, N., and Mizuno, M. (2009). "Damage characteristics of lead zirconate titanate piezoelectric ceramic during cyclic loading." *International Journal of Fatigue*, 31(8-9), 1434-1441.

Okayasu, M., Ozeki, G., and Mizuno, M. (2010). "Fatigue failure characteristics of lead zirconate titanate piezoelectric ceramics." *Journal of the European Ceramic Society*, 30(3), 713-725.

Pacca, S., and Horvath, A. (2002). "Greenhouse gas emissions from building and operating electric power plants in the Upper Colorado River Basin." *Environmental Science & Technology*, 36(14), 3194-3200.

Palmgren, A. (1924). "Die lebensdauer von kugellagern." *Zeitschrift des Vereins Deutscher Ingenieure*, 68(14), 339-341.

Pan, M.-J., and Yoshikawa, S. (1996). "Design factors in multilayer actuators." *Mechanical Engineering*, 118(4), 74.

Papagiannakis, A. T., Dessouky, S., Montoya, A., and Roshani, H. (2016). "Energy Harvesting from Roadways." *Procedia Computer Science*, 83, pp. 758-765.

Park, S.-W., and Lytton, R. L. (2004). "Effect of stress-dependent modulus and Poisson's ratio on structural responses in thin asphalt pavements." *Journal of Transportation Engineering*, 130(3), 387-394.

Pascual-Muñoz, P., Castro-Fresno, D., Serrano-Bravo, P., and Alonso-Estébanez, A. (2013). "Thermal and hydraulic analysis of multilayered asphalt pavements as active solar collectors." *Applied Energy*, 111, pp. 324-332.

Peigney, M., and Siegert, D. (2013). "Piezoelectric energy harvesting from traffic-induced bridge vibrations." *Smart Materials and Structures*, 22(9), 095019.

Phillips, T. (2009). *Dynamo-Electric Machinery; a Manual for Students of Electrotechnics*, BiblioBazaar, LLC.

Pinkerton, J. L., and Moses, R. W. (1997). "A feasibility study to control airfoil shape using THUNDER."

Priya, S. (2007). "Advances in energy harvesting using low profile piezoelectric transducers." *Journal of Electroceramics*, 19(1), 167-184.

Priya, S., and Inman, D. J. (2009). *Energy harvesting technologies*, Springer.

Richart, F., and Newmark, N. "An hypothesis for the determination of cumulative damage in fatigue." *Proc., Selected Papers By Nathan M. Newmark: Civil Engineering Classics*, ASCE, 279-312.

Roshani, H., Dessouky, S., Montoya, A., and Papagiannakis, A. T. (2016). "Energy harvesting from asphalt pavement roadways vehicle-induced stresses: A feasibility study." *Applied Energy*, 182, 210-218.

Roshani, H., Jagtap, P., Dessouky, S., Montoya, A., and Papagiannakis, A. (2017). "Theoretical and Experimental Evaluation of Two Roadway Piezoelectric-Based Energy Harvesting Prototypes." *Journal of Materials in Civil Engineering*, 30(2), 04017264.

Roundy, S. (2005). "On the effectiveness of vibration-based energy harvesting." *Journal of Intelligent Material Systems and Structures*, 16(10), 809-823.

Roundy, S., Wright, P. K., and Rabaey, J. (2003). "A study of low level vibrations as a power source for wireless sensor nodes." *Computer Communications*, 26(11), 1131-1144.

Saadeghvaziri, M. (1993). "Finite element analysis of highway bridges subjected to moving loads." *Computers & structures*, 49(5), 837-842.

Sardini, E., and Serpelloni, M. (2011). "An efficient electromagnetic power harvesting device for low-frequency applications." *Sensors and Actuators A: Physical*, 172(2), 475-482.

Sazonov, E., Haodong, L., Curry, D., and Pillay, P. (2009). "Self-Powered Sensors for Monitoring of Highway Bridges." *IEEE Sensors Journal*, 9(11), 1422-1429.

Seyhan, U., Tutumluer, E., and Yesilyurt, H. (2005). "Anisotropic aggregate base inputs for mechanistic pavement analysis considering effects of moving wheel loads." *Journal of Materials in Civil Engineering*, 17(5), 505-512.

Shaopeng, W., Mingyu, C., and Jizhe, Z. (2011). "Laboratory investigation into thermal response of asphalt pavements as solar collector by application of small-scale slabs." *Applied Thermal Engineering*, 31(10), 1582-1587.

Shigley, J. E. (2011). *Shigley's mechanical engineering design*, Tata McGraw-Hill Education.

Siochi, E. J., Young, P. R., and Bryant, R. G. (1995). "Effect of molecular weight on the properties of a soluble polyimide." *Materials Challenge: Diversification and the Future.*, 40, 11-18.

Smoker, J., Nouh, M., Aldraihem, O., and Baz, A. (2012). "Energy harvesting from a standing wave thermoacoustic-piezoelectric resonator." *Journal of Applied Physics*, 111(10), 104901.

Sodano, H. A., Inman, D. J., and Park, G. (2004). "A review of power harvesting from vibration using piezoelectric materials." *Shock and Vibration Digest*, 36(3), pp. 197-206.

Song, Y., Yang, C. H., Hong, S. K., Hwang, S. J., Kim, J. H., Choi, J. Y., Ryu, S. K., and Sung, T. H. (2016). "Road energy harvester designed as a macro-power source using the piezoelectric effect." *International Journal of Hydrogen Energy*, 41(29), 12563-12568.

Sridharan, N., and Mallik, A. K. (1979). "Numerical analysis of vibration of beams subjected to moving loads." *Journal of Sound and Vibration*, 65(1), 147-150.

Standards Committee of the IEEE Ultrasonics, F., and Frequency Control Society, (1987). "An american national standard: IEEE standard on piezoelectricity”."

Sugawara, Y., Onitsuka, K., Yoshikawa, S., Xu, Q., Newnham, R. E., and Uchino, K. (1992). "Metal–ceramic composite actuators." *Journal of the American Ceramic Society*, 75(4), 996-998.

Swallow, L. M., Luo, J. K., Siores, E., Patel, I., and Dodds, D. (2008). "A piezoelectric fibre composite based energy harvesting device for potential wearable applications." *Smart Materials and Structures*, 17(2), 025017.

System, W. (2005). "Fatigue aspects of epoxies and epoxy/wood composites.", W. System, ed.

Szary, P. J. (2009). *Development and evaluation of piezoelectric ceramic-polymer composite sensors for weigh-in-motion applications*, RUTGERS THE STATE UNIVERSITY OF NEW JERSEY-NEW BRUNSWICK.

Thompson, M. R., and Robnett, Q. L. (1976). "Resilient properties of subgrade soils."

Truitt, A., and Mahmoodi, S. N. "Piezoelectric Energy Harvesting Through Fluid Excitation." *Proc., ASME 2012 Conference on Smart Materials, Adaptive Structures and Intelligent Systems*, American Society of Mechanical Engineers, 785-792.

Tutumluer, E. (1995). "Predicting behavior of flexible pavements with granular bases." Georgia Institute of Technology.

Tutumluer, E. "State of the art: Anisotropic characterization of unbound aggregate layers in flexible pavements." *Proc., Proceedings of the Symposium on Pavement Mechanics and Materials at the Inaugural International Conference of the Engineering Mechanics Institute*.

Tutumluer, E., Little, D., and Kim, S.-H. (2003). "Validated model for predicting field performance of aggregate base courses." *Transportation Research Record: Journal of the Transportation Research Board*(1837), 41-49.

Tutumluer, E., and Seyhan, U. (1999). "Laboratory determination of anisotropic aggregate resilient moduli using an innovative test device." *Transportation Research Record: Journal of the Transportation Research Board*(1687), 13-21.

Tutumluer, E., and Thompson, M. (1997). "Anisotropic modeling of granular bases in flexible pavements." *Transportation Research Record: Journal of the Transportation Research Board*(1577), 18-26.

Tzou, H., and Ye, R. (1996). "Analysis of piezoelastic structures with laminated piezoelectric triangle shell elements." *AIAA journal*, 34(1), 110-115.

Uchida, K.-i., Adachi, H., Kikkawa, T., Kirihara, A., Ishida, M., Yorozu, S., Maekawa, S., and Saitoh, E. (2016). "Thermoelectric generation based on spin Seebeck effects."

Uchino, K. (2009). *Ferroelectric Devices 2nd Edition*, CRC press.

Ugural, A. (1999). *Stresses in plates and shells*, McGraw-Hill.

Uzan, J. (1992). "Resilient characterization of pavement materials." *International Journal for Numerical and Analytical Methods in Geomechanics*, 16(6), 453-459.

Voigt, T., Ritter, H., and Schiller, J. "Utilizing solar power in wireless sensor networks." *Proc., Local Computer Networks, 2003. LCN'03. Proceedings. 28th Annual IEEE International Conference on*, IEEE, pp. 416-422.

Wang, H. (2013). "Accurate Determination of Equivalent Modulus of Nonlinear Anisotropic Granular Base Layer." *International Journal of Pavement Research and Technology*, 6(4), 313-318.

Wang, H., and Al-Qadi, I. (2009). "Combined Effect of Moving Wheel Loading and Three-Dimensional Contact Stresses on Perpetual Pavement Responses." *Transportation Research Record: Journal of the Transportation Research Board*, 2095, 53-61.

Wang, H., Al-Qadi, I., Portas, S., and Coni, M. (2013). "Three-Dimensional Finite Element Modeling of Instrumented Airport Runway Pavement Responses." *Transportation Research Record: Journal of the Transportation Research Board*, 2367, 76-83.

Wang, H., Jasim, A., and Chen, X. (2018). "Energy harvesting technologies in roadway and bridge for different applications–A comprehensive review." *Applied Energy*, 212, 1083-1094.

Wang, H., and Li, M. (2016). "Comparative Study of Asphalt Pavement Responses under FWD and Moving Vehicular Loading." *Journal of Transportation Engineering*, 142(12), 04016069.

Wang, H., Li, M., and Garg, N. (2015). "Airfield Flexible Pavement Responses Under Heavy Aircraft and High Tire Pressure Loading." *Transportation Research Record: Journal of the Transportation Research Board*(2501), 31-39.

Wang, P.-H., Dai, X.-H., Fang, D.-M., and Zhao, X.-L. (2007). "Design, fabrication and performance of a new vibration-based electromagnetic micro power generator." *Microelectronics Journal*, 38(12), 1175-1180.

Wang, W., Cao, J., Bowen, C. R., Zhou, S., and Lin, J. (2017). "Optimum resistance analysis and experimental verification of nonlinear piezoelectric energy harvesting from human motions." *Energy*, 118, 221-230.

Wang, Z. L. (2008). "Energy harvesting for self-powered nanosystems." *Nano Research*, 1(1), 1-8.

Wilkie, W. K., Bryant, R. G., High, J. W., Fox, R. L., Hellbaum, R. F., Jalink Jr, A., Little, B. D., and Mirick, P. H. "Low-cost piezocomposite actuator for structural control applications." *Proc., SPIE's 7th Annual International Symposium on Smart Structures and Materials*, International Society for Optics and Photonics, 323-334.

Williams, C., and Yates, R. B. (1996). "Analysis of a micro-electric generator for microsystems." *sensors and actuators A: Physical*, 52(1), 8-11.

Wilson, J. F., and Barbas, S. T. (1980). "Responses of continuous, elastically supported beam guideways to transit loads." *Journal of Dynamic Systems, Measurement, and Control*, 102(4), 247-254.

Wischke, M., Masur, M., Kröner, M., and Woias, P. (2011). "Vibration harvesting in traffic tunnels to power wireless sensor nodes." *Smart Materials and Structures*, 20(8), 085014.

Wu, G.-X., and Yu, B. (2012). "Thermal energy harvesting system to harvest thermal energy across pavement structure." *International Journal of Pavement Research and Technology*, 5(5), 311-316.

Wu, G., and Yu, X. "Thermal energy harvesting across pavement structure." *Proc., Transportation Research Board 91st Annual Meeting*.

Xiang, H. J., Wang, J. J., Shi, Z. F., and Zhang, Z. W. (2013). "Theoretical analysis of piezoelectric energy harvesting from traffic induced deformation of pavements." *Smart Materials and Structures*, 22(9), 095024.

Xie, X., and Wang, Q. (2015). "Energy harvesting from a vehicle suspension system." *Energy*, 86, 385-392.

Xie, X. D., Wang, Q., and Wang, S. J. (2015). "Energy harvesting from high-rise buildings by a piezoelectric harvester device." *Energy*, 93, 1345-1352.

Xiong, H.-C., Wang, L.-B., Wang, D., and Druta, C. (2012). "Piezoelectric energy harvesting from traffic induced deformation of pavements." *International Journal of Pavement Research and Technology*, Vol. 5(5), pp. 333337.

Xiong, H. (2014). "Piezoelectric Energy Harvesting on Public Roadways." Ph.D Dissertation, Virginia Polytechnic Institute and State University, VA.

Xiong, H., and Wang, L. (2016). "Piezoelectric energy harvester for public roadway: On-site installation and evaluation." *Applied Energy*, 174, 101-107.

Xu, H., and Tan, Y. (2015). "Modeling and operation strategy of pavement snow melting systems utilizing low-temperature heating fluids." *Energy*, 80, 666-676.

Xu, Q. C., Yoshikawa, S., Belsick, J. R., and Newnham, R. E. (1991). "Piezoelectric composites with high sensitivity and high capacitance for use at high pressures." *IEEE transactions on ultrasonics, ferroelectrics, and frequency control*, 38(6), 634-639.

Yang, H., Wang, L., Hou, Y., Guo, M., Ye, Z., Tong, X., and Wang, D. (2017). "Development in Stacked-Array-Type Piezoelectric Energy Harvester in Asphalt Pavement." *Journal of Materials in Civil Engineering*, 29(11), 04017224.

Yang, J. (2004). *An introduction to the theory of piezoelectricity*, Springer Science & Business Media.

Yesner, G., Kuciej, M., Safari, A., Jasim, A., Wang, H., and Maher, A. "Piezoelectric energy harvesting using a novel cymbal transducer design." *Proc., Applications of Ferroelectrics, European Conference on Application of Polar Dielectrics, and Piezoelectric Force Microscopy Workshop (ISAF/ECAPD/PFM), 2016 Joint IEEE International Symposium on the*, IEEE, 1-4.

Yesner, G., Safari, A., Jasim, A., Wang, H., Basily, B., and Maher, A. "Evaluation of a novel piezoelectric bridge transducer." *Proc., Applications of Ferroelectric (ISAF)/International Workshop on Acoustic Transduction Materials and Devices (IWATMD)/Piezoresponse Force Microscopy (PFM), 2017 Joint IEEE International Symposium on the,* IEEE, 113-115.

Yildiz, F., and Coogler, K. L. (2017). "Low Power Energy Harvesting with a Thermoelectric Generator through an Air Conditioning Condenser." *Journal of Engineering Technology*, 34(1), 8.

Yin, H., Solaimanian, M., Kumar, T., and Stoffels, S. (2007). "The effect of loading time on flexible pavement dynamic response: a finite element analysis." *Mechanics of Time-Dependent Materials*, 11(3), 265-288.

Yoshitake, I., Yasumura, N., Syobuzako, M., and Scanlon, A. (2010). "Pipe heating system with underground water tank for snow thawing and ice prevention on roads and bridge decks." *Journal of Cold Regions Engineering*, 25(2), 71-86.

Yuan, J.-b., Shan, X.-b., Xie, T., and Chen, W.-s. (2009). "Energy harvesting with a slotted-cymbal transducer." *Journal of Zhejiang University SCIENCE A*, 10(8), 1187-1190.

Zaghloul, S. M., and White, T. (1993). "Use of a three-dimensional, dynamic finite element program for analysis of flexible pavement."

Zhang, S., Shrout, T., Nagata, H., Hiruma, Y., and Takenaka, T. (2007). "IEEE Trans. Ultrason. Ferroelectr. Freq. Control."

Zhang, Y., Cai, S. C., and Deng, L. (2014). "Piezoelectric-based energy harvesting in bridge systems." *Journal of intelligent material systems and structures*, 25(12), 1414-1428.

Zhang, Z., Xiang, H., and Shi, Z. (2015). "Modeling on piezoelectric energy harvesting from pavements under traffic loads." *Journal of Intelligent Material Systems and Structures*, Vol. 1, pp. 1-12.

Zhang, Z., Zhang, X., Rasim, Y., Wang, C., Du, B., and Yuan, Y. (2016). "Design, modelling and practical tests on a high-voltage kinetic energy harvesting (EH) system for a renewable road tunnel based on linear alternators." *Applied Energy*, 164, 152-161.

Zhao, D. (2013). "Waste thermal energy harvesting from a convection-driven Rijke–Zhao thermo-acoustic-piezo system." *Energy conversion and management*, 66, 87-97.

Zhao, D., and Chew, Y. (2012). "Energy harvesting from a convection-driven Rijke-Zhao thermoacoustic engine." *Journal of Applied Physics*, 112(11), 114507.

Zhao, D., Ji, C., Li, S., and Li, J. (2014). "Thermodynamic measurement and analysis of dual-temperature thermoacoustic oscillations for energy harvesting application." *Energy*, 65, 517-526.

Zhao, H., Ling, J., and Yu, J. (2012). "A comparative analysis of piezoelectric transducers for harvesting energy from asphalt pavement." *Journal of the Ceramic Society of Japan*, 120(1404), 317-323.

Zhao, H., Qin, L., and Ling, J. (2015). "Test and Analysis of Bridge Transducers for Harvesting Energy from Asphalt Pavement." *International Journal of Transportation Science and Technology*, 4(1), 17-28.

Zhao, H., Yu, J., and Ling, J. (2010). "Finite element analysis of Cymbal piezoelectric transducers for harvesting energy from asphalt pavement." *Journal of the Ceramic Society of Japan*, 118(1382), 909-915.

Zheng, Z., and Zhang, R. (2014). "Implementation of a Viscoelastic Material Model to Simulate Relaxation in Glass Transition."

Zienkiewicz, O. C., and Taylor, R. L. (2000). *The finite element method: solid mechanics*, Butterworth-heinemann.

Zuo, L., Scully, B., Shestani, J., and Zhou, Y. (2010). "Design and characterization of an electromagnetic energy harvester for vehicle suspensions." *Smart Materials and Structures*, 19(4), 045003.